5-2007

Participation of mouse DNA polymerases iota, eta, and rev1 in translesion synthesis of carcinogen induced DNA adducts and carcinogenesis.

Chad Aaron Dumstorf 1977-
University of Louisville

Follow this and additional works at: https://ir.library.louisville.edu/etd

PARTICIPATION OF MOUSE DNA POLYMERASES IOTA, ETA, AND REV1 IN TRANSLESION SYNTHESIS OF CARCINOGEN INDUCED DNA ADDUCTS AND CARCINOGENESIS

By

Chad Aaron Dumstorf
B.G.S., Indiana University
M.S., University of Louisville

A Dissertation
Submitted to the Faculty of the
Graduate School of the University of Louisville
In Partial Fulfillment of the Requirements
for the Degree of

Doctor of Philosophy

Department of Pharmacology and Toxicology
University of Louisville
Louisville, Kentucky

May 2007

PARTICIPATION OF MOUSE DNA POLYMERASES IOTA, ETA, AND REV1 IN

TRANSLESION SYNTHESIS OF CARCINOGEN INDUCED DNA ADDUCTS

AND CARCINOGENSIS

By

Chad Aaron Dumstorf

B.G.S., Indiana University

M.S., University of Louisville

A Dissertation Approved on

March 21, 2007

By the following Dissertation Committee:

William Glenn McGregor, M.D.
(Dissertation Director)

Ramesh Gupta, Ph.D.

Jason Chesney M.D., Ph.D.

Haribabu Bodduluri, Ph.D.

Wolfgang Zacharias, Ph.D.

DEDICATION

This dissertation is dedicated to my wonderful children

Amber Lynn Dumstorf

and

Colten Aaron Dumstorf.

ACKNOWLEDGEMENTS

ABSTRACT

PARTICIPATION OF MOUSE DNA POLYMERASES IOTA, ETA, AND REV1 IN

TRANSLESION SYNTHESIS OF CARCINOGEN INDUCED DNA ADDUCTS

AND CARCINOGENESIS

Chad Aaron Dumstorf

March 21, 2007

Recent advances in understanding the molecular mechanisms of mutagenesis indicate that most mutations are dependent on the activity of translesion synthesis DNA polymerases. The impact of reducing the level of these polymerases on mutagenesis and carcinogenesis in mouse models is poorly defined. Using knock out strategies we were able to remove polymerase eta (pol η), and polymerase iota (pol ι) and pol eta/pol iota from the mouse and lower REV1 in the mouse lung. This dissertation reports the changes in UV-induced carcinogenesis and mutagenesis that were observed.

Mutagenesis data in pol iota deficient cells clearly indicate pol iota as a mutagenic TLS polymerase in UV lesion bypass. Pol iota removal effectively lowered the mutational frequency in both pol eta null and wild-type backgrounds.

Unexpectedly, after *Hprt* mutant screening, pol eta and pol iota deficient cells were found to participate in UV lesion bypass in a strand-specific manner. This suggests that not only does bypass of photoproducts occur but occurs in an asymmetrical fashion, with preference of polymerases for leading or lagging strand.

To examine the hypothesis that reducing the mutagenic load will reduce the incidence of cancer, we examined how pol iota status contributes to carcinogenesis. Despite the fact that pol iota was mutagenic in bypass of UV induced lesions, its removal accelerated cancer formation in the pol eta null background. The mechanisms behind this tumor suppressor function remain elusive, but indicate pol iota may have additional cellular roles in conjunction with its polymerase activity.

Examining the hypothesis that reducing the mutagenic load will reduce the incidence of cancer, we developed strategies to reduce REV1 in mouse models of lung carcinogenesis. Endogenous REV1 mRNA in the lung was effectively lowered with the use of gene delivery of REV1 targeting ribozyme. This reduction was found to effectively decrease the multiplicity of B[a]P-induced lung tumors. This reduction did not affect the size or types of tumors induced suggesting inhibition of cancer formation occurred at the initiation step. Collectively, these data yield insight into the molecular mechanisms of mutagenesis that induce cancer formation.

TABLE OF CONTENTS

LIST OF FIGURES

LIST OF TABLES

CHAPTER I

INTRODUCTION

DNA DAMAGE

Genomic stability is central to the survival of cells, both prokaryotic and eukaryotic. The loss of such stability is fundamental for evolution and is most easily appreciated in single-cell organisms. It is more difficult to understand why multicellular organisms have maintained mechanisms that result in alterations in the primary sequence of DNA, since such alterations are thought to underlie cancer and a wide variety of diseases associated with aging. Never the less, these molecular pathways, collectively called DNA damage tolerance, have been highly conserved. The chemical stability of DNA has been recognized for decades, but the cellular DNA of living organisms is continually subjected to many DNA damaging agents, which must be bypassed if the cell is to survive. In this context, "bypass" refers to the completion of replication of genomes that contain helix-distorting lesions such as those induced by the environmentally relevant carcinogens ultraviolet (UV) radiation and benzo[a]pyrene (B[a]P). It is now recognized that the principal mechanism underlying mutagenesis is the direct replication of DNA that contains non-instructive bases as a result of

adduction with these carcinogens. These agents, whether exogenous or endogenous, damage DNA, induce mutations, and cause cancer. This dissertation specifically focuses on the bypass of bulky helix distorting lesions induced by the aforementioned agents. This bypass, termed translesion synthesis (TLS), is responsible for both error free and mutagenic bypass of these lesions. The studies covered in this dissertation yield new insight into the polymerases responsible for inducing mutations after UV and B[a]P exposure and how manipulating these polymerases effects cancer formation.

ULTRAVIOLET LIGHT

UV light is generally segregated into three varying wavelengths UV-A (long wave UV with a ~380 to ~315nm wavelength), UV-B (medium wave with a ~315 to ~280nm wavelength), and UV-C (short wave UV that ranges less than 280nm). Absorption of UV light produces two predominant types of DNA damage, cyclobutane pyrimidine dimers (CPD) and 6-4 pyrimidine-pyrimidone photoproducts (6-4PP). The structure for CPD and 6-4PP are shown in Figure 1a-b. Both of these helix-disturbing lesions can be induced by the complete spectrum of UV light (~380nm-100nm), albeit to varying extents[1].

The production of CPD's and 6-4PP's from UV-A wavelength absorption is considered relatively minor. Despite low levels of photoproduct formation this wavelength probably contributes to carcinogenesis. It has been postulated that the formation of oxidative free radicals, rather than photoproduct production, is the most damaging aspect of UV-A exposure[2]. Longer wavelengths such as

2

those in the UV-A and UV-B region are long enough to pass through the ozone and reach the earth's surface. Since UV-B also passes to the earths surface and is energetic enough to form considerable amounts of CPD and 6-4PP photoproducts, it is considered the most biologically significant source of UV damage[3]. The more energetic short-wave UV-C radiation is the most damaging to DNA, but generally does not penetrate the ozone thus preventing it from reaching the Earth's surface. Nevertheless, the dosimetry and resulting adduct load following UV-C exposure has been well-established after over 40 years of use in DNA repair and mutagenesis studies. Therefore, UV-C is commonly used in the laboratory to induce DNA photoproducts for biological studies[4]. UV-C may also be produced in occupational settings, such as welding, and may possibly contribute to skin cancer in exposed populations[5].

CPD form as a result of covalent linkages between adjacent pyrimidine bases in the form of a four carbon (cyclobutane) ring, as illustrated in Figure 1a. CPD may occur between any two pyrimidines (i.e. 5' T<>T, 5' T<>C, 5' C<>T, or 5' C<>C)[6]. The occurrence of the type of pyrimidine dimer formed is sequence dependent with 5' T<>T being the most common CPD and 5' C<>C the least[7]. Unlike CPD, 6-4PP occur primarily between 5' T<>C, 5' C<>C, and less frequently at 5' T<>T with little formation between 5' C<>T[8]. This linkage, as illustrated in Figure 1b, is a covalent bond between the C6 position of the 5' pyrimidine and the C4 position of the 3' pyrimidine.

The frequency of photoproduct formation is greater for both CPD and 6-4PP at shorter wavelengths. Though it is possible that the ratio of CPD to 6-4PP

production varies with wavelength, it is generally considered that regardless of wavelength, CPD occur 4 – 5 times more frequently than 6-4 photoproducts[9,10]. Because the proportion and type of CPD and 6-4PP are relatively stable for UV-B or UV-C, the decision for which wavelength to use for biological experimentation is subject to the nature of a particular experiment. Because of this, the experiments covered in this dissertation involve UV irradiation of both cells and mice at different wavelengths. UV-C with a sharp 254 nm emission is used for cell culture irradiation and UV-B with a peak at 302 nm is used for animal irradiation.

1a)

1b)
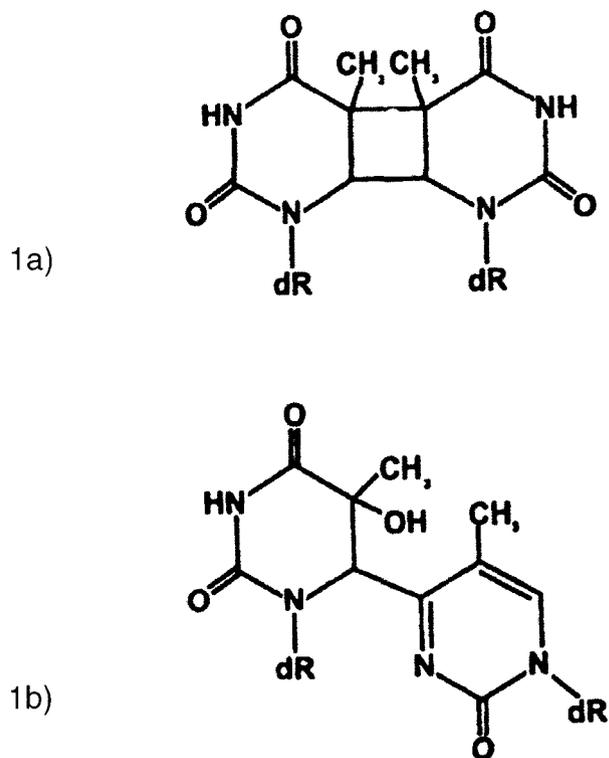
Figure 1. Major UV light induced photoproducts 1a) Absorption of ultraviolet (UV) light produces two predominant types of UV light induced adducts. a) T<>T cyclobutane pyrimidine dimer (CPD) b) pyrimidine (6-4) pyrimidone photoproduct (6-4PP).

Benzo[a]pyrene (B[a]P) is a natural byproduct and is ubiquitously distributed throughout the environment through the combustion of organic matter. B[a]P is readily absorbed via the gastrointestinal (GI) tract, lung and skin. The compound is activated and detoxified primarily in the liver although other organs such as the lung, skin, GI, and placenta can contribute significantly to these processes[11-13]. B[a]P and many other polycyclic aromatic hydrocarbons (PAH) are activated to intermediates that covalently bind to DNA as a result of endogenous cytochrome P450 metabolism[14]. B[a]P in its unmodified form is a hydrophobic planar shaped molecule (Figure 2a).

In order for B[a]P to bind DNA it must undergo cytochrome P450 enzymatic reactions that create a variety of phenols, dihydrodiols, and electrophilic epoxides. While the principle mutagen is debated, it is widely accepted that (±) *anti* diol-epoxides (BPDE) (Figure 2b) react at N^2-dG in DNA (Figure 2c) to give four stereoisomers. More specifically the (+)-*anti*-BPDE reacts with DNA via *trans*- and *cis*- configurations to give [+ta]- and [+ca]-B[a]P–N^2-dG. Similarly (–)-*anti*-BPDE gives [–ta]- and [–ca]-B[a]P–N^2-dG adducts (Figure 2d)[15]. While all four of the steroisomers can cause mutations, principally G-T transversions, the [+ta]-B[a]P–N^2-dG produces the dominant adduct[16].

B[a]P is given to animals used in this dissertation to primarily induce murine lung tumors. Activation to its carcinogenic potential is therefore based on the animals' own metabolic pathways. In contrast, the human fibroblasts used in the cell culture assays referenced throughout this dissertation lack the capacity

for B[a]P activation. These cell culture based assays therefore require the use of the active metabolite BPDE.

B[a]P

2a)

BPDE

2b)

[+ta]-B[a]P-N²-dG

2c)

[+ca]-B[a]P-N²-dG

[-ta]-B[a]P-N²-dG

[-ca]-B[a]P-N²-dG

2d)
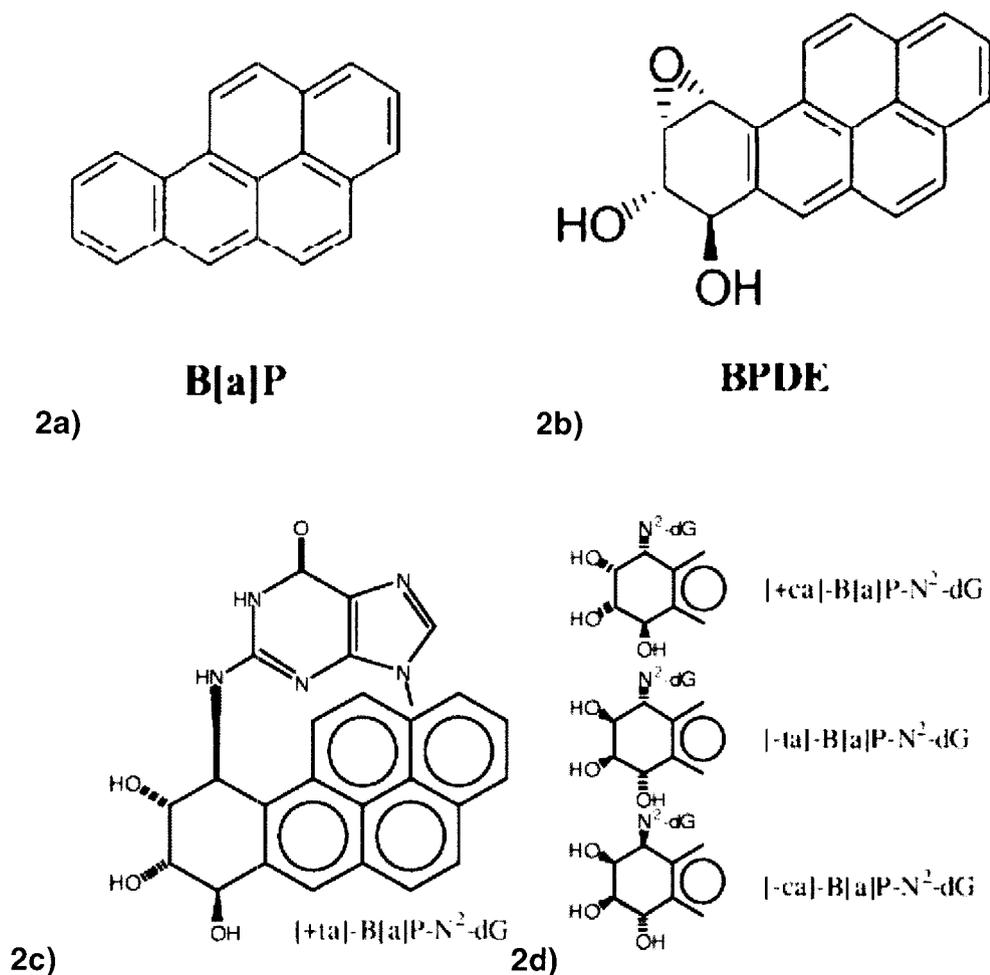
Figure 2. Illustrations of the polycyclic aromatic hydrocarbon benzo[a]pyrene (B[a]P), its electrophilic metabolite, and major DNA adduct. 2a) B[a]P 2b) one known metabolite benzo[a]pyrene-7,8-diol-9,10-epoxide (BPDE), and 2c) DNA adduct formed on the N2 position of guanine. 2d) Structures of the four stereoisomers of N^2-dG adducts: [+ta]-, [+ca]-, [− ta]- and [− ca]-B[a]P–N^2-dG.

POLYMERASE STALLING

Environmental DNA-damaging agents such as UV-light and B[a]P can produce damage to nucleotides (lesions) which can block transcription and replication complexes. Inhibition of such fundamental DNA transactions may have detrimental results, such as the induction of mutations or cell death. Therefore, cells have evolved efficient mechanisms for the recognition of helix-distorting lesions. Arguably the most versatile system for recognizing and removing such lesions, including those induced by UV or B[a]P, is nucleotide excision repair. Lesions on a base in the transcribed strand of an active gene have a high propensity to block the RNA polymerase complex. Such polymerase stalling induces cell-cycle arrest, and possibly apoptosis, in a p53-dependent manner[17]. In addition, the stalled complex acts as damage-recognition sensor to signal the excision repair apparatus via the Cockaynes syndrome A and B (CSA/B) proteins. CSA/B signals the basal transcription complex TFIIH to the stalled polymerase, by mechanisms that are not fully understood. However, the RNA polymerase is generally considered to "back up" in order to expose the lesion. The helicase activity inherent in TFIIH unwinds the DNA, allowing the scaffolding protein XPA to gain access to the lesion and RPA to coat single-strand DNA. Subsequent steps include endonuclease activity by XPG 3' to the lesion and XPF-ERCC1 5' to the lesion in an ordered series of reactions. This results in a 26-29 base oligonucleotide gap containing the lesion. The gap is filled in by the replicative DNA polymerase complex and sealed with a ligase. The high fidelity of this complex ensures that this process is error-free[18].

Lesions in non-transcribed regions are repaired by global genomic pathways, which differ from transcription-coupled repair (TCR) only in the manner of lesion recognition. It is known that CPD are initially recognized by XPE and then this complex attracts the XPC-HHR23B complex. Lesions that distort the helix to a greater extent, such as 6-4 PP and BPDE-induced adducts, are directly recognized by XPC-HHR23B. The subsequent steps proceed as in TCR.

If the cell enters S-phase with residual (unrepaired) DNA damage, which can occur if the damage is induced close to the onset of S-phase or if the cells cannot remove the damage as a result of DNA repair defects, the DNA polymerase may be blocked[19]. Current data indicate that cells may use at least two complementary pathways to continue replication across the damage. These pathways are collectively called "damage tolerance", since the damage is tolerated rather than removed. These were first identified in the budding yeast *S. cerevisiae*, and are within the RAD6 epistasis group. Recent data have begun to elucidate the molecular mechanisms underlying this pathway, and indicate a remarkable conservation of these mechanisms in higher eukaryotes. One pathway, called "damage avoidance", copies undamaged DNA with the same sequence as the original template. This can occur by using the sister chromatid sequence or by "copy-choice" template switching in which the nascent strand templated by the undamaged strand is used as the template. Both mechanisms are recombinational in nature are considered to be error-free. An alternative mechanism, termed translesion synthesis (TLS) uses accessory polymerases in lieu of normal replication polymerases to bypass the damage. Unlike "damage

avoidance", these polymerases switch places with normal replication machinery and continue to use the damaged strand as a template. Because the damage remains, the bypass may result in error free or error prone incorporation of nucleotides across the lesion. TLS is summarized at the end of this chapter (Figure 3).

The RAD6-dependant damage tolerance pathway is central to both of these "damage tolerance" pathways. Though the exact mechanism cells use to decide whether TLS or "damage avoidance" is employed remains controversial, there are some well-characterized components. The RAD6 gene encodes the ubiquitin conjugating enzyme (Ubc or E2) that is required along with RAD18 (UBL or E3) for damage tolerance to occur[20]. Cysteine-88, located in the RAD6 enzyme active site, is required for its ubiquitin conjugating activity[21]. Upon replication fork stalling, the RAD6-RAD18 complex binds to the DNA through a chromatin associated RING finger motif[22]. This complex mono-ubiquitinates the proliferating nuclear cell antigen (PCNA) at lysine-164 (K164) which signals the recruitment of a variety of accessory DNA polymerases[23].

Current data indicate that the "damage avoidance" pathway also requires the further poly-ubiquitination of the conjugate at lysine-63 (K63)[24]. This multi-ubiquitination allows the recruitment of MMS2, UBC13, and RAD5 which are required for "damage avoidance" to occur[23]. With the stalling of replication machinery and the poly-ubiquitination of PCNA there are at least two mechanisms for the "damage avoidance" pathway. While both mechanisms result in error free replication, the differences lie in where the information for non-

damaged sequence template arises. The first proposed mechanism uses an allelic copy as a template. The other mechanism employs the use of the newly synthesized sister strand[25]. Regardless of the mechanism, data indicate that loss of MMS2 ubiquitin conjugating enzyme-like protein (required for the poly-ubiquitin chain) in *S. cervisiae* increases the mutagenic effect of UV light and spontaneous mutations. Although much more controversial in higher eukaryotic cells, such cells have homologs to the polyubiquitination machinery, and knockdown of MMS2 results in less recombination and more mutants induced by UV. Available data support a role for polyubiquitination in recombination-mediated damage avoidance[26-28].

Current models hypothesize that mono- or polyubiquitination of PCNA is the molecular switch that determines whether the cell will undergo damage avoidance (polyubiquitination) or TLS (monoubiquitination)[29]. This process is further complicated by studies that indicate PCNA may also be conjugated by small ubiquitin-like modifier (SUMO) UBC9 at K164[30]. While poorly understood, data indicate that the attachment of SUMO (sumoylation) to PCNA is an event that occurs to recruit the helicase Srs2 to the site of damage[31]. This recruitment effectively prevents recombination during S phase and apparently shifts the cell away from damage avoidance and into TLS[32,33]. While this mechanism likely plays an extremely important role in damage tolerance, the purpose of sumoylation is still poorly defined. In any case, these PCNA modifications have been shown to affect DNA damage resistance and support the notion that the

alternative modes of modification of PCNA act as molecular switches to enable alternative functions in lesion bypass.

The second option employed by cells is termed translesion synthesis (TLS). TLS also occurs at stalled replication forks, but unlike "damage avoidance" occurs when PCNA is either monoubiquitinated or as recent data indicates perhaps sumoylated[23]. TLS enables the cell to avoid apoptosis through the recruitment of specialized DNA polymerases. These polymerases generally have less stringent base pairing requirements and are able to accommodate the lesion into their active site. These low fidelity polymerases are well adapted to replicate across helix distorting lesion in such a way that the outcome may result in mutagenic or error free bypass of lesion. While the exact sequence of events that occurs in TLS is still being elucidated, much of what is currently known is through individual polymerase and protein analysis. Three major TLS proteins are the subject matter of the studies covered in this dissertation and a general discussion of their history and significance in TLS is given in the following section.

Y-FAMILY POLYMERASES

Y-family polymerases are a functionally diverse group of DNA polymerases that are characterized by their low fidelity of replication and ability to efficiently bypass a variety of helix distorting DNA lesions. Originally named the UmuC/DinB/Rev1/Rad30 super-family, these polymerases share similar amino acid sequence homology to themselves and little homology to other polymerase families[34]. These polymerases lack proofreading capabilities and appear to exhibit great diversity among themselves in lesion specificity, rate of nucleotide incorporation, and extension of mismatched primer-termini. Data suggest many of these are able to participate in lesion bypass past adducts that typically impede normal replication machinery but the extent to which it occurs is poorly understood[35]. These polymerases have traditionally been labeled error-prone translesion polymerases, most likely due to their low fidelity characteristics, but may also function in an error-free manner across these lesions[36,37].

TLS is generally performed by one or another of the Y-family polymerases with one extremely important exception. DNA polymerase zeta (pol zeta/ pol ζ), which is a member of the B-family of polymerases, together with the replicative polymerases α, δ, and ε, is required for TLS to occur. Pol zeta is composed of two subunits encoded by the *REV3* and *REV7* genes[38]. REV3 is the catalytic subunit of pol zeta and results in embryonic lethality when abolished in mice[39,40]. Despite the embryonic lethality that occurs with REV3 knockout strategies, insights into pol zeta function in higher eukaryotes have been gained using antisense-mediated strategies in cell culture and in mice. Mice that express

antisense to mREV3 endogenous RNA transcripts, which do not have completely abolished REV3 protein, are viable. These mice also have a decreased frequency and highly aberrant spectrum of UV-induced mutations at the *hypoxanthine-guanine phosphoribosyltransferase (Hprt)* locus indicating a fundamental role for pol zeta in TLS[39]. Additionally, these knockdown mice have reduced levels of B cells and impaired development of high-affinity memory B cells perhaps suggesting an additional function in somatic hypermutation[41,42]. Pol zeta is also capable, unlike other polymerases implicated in TLS, to efficiently extend past DNA damaged induced lesions[43]. Since most Y-family polymerases inefficiently incorporate nucleotides after lesion bypass, pol zeta has been proposed to be responsible for finishing the bypass before normal replication resumes. Additionally, human REV3 (hREV3) has been shown to be essential for error prone translesion synthesis past UV or BPDE-induced lesions in human fibroblasts[44]. These data collectively indicate a primary function for pol zeta in extension past the lesion once the damage is bypassed[45].

Y-family TLS polymerases REV1 and pol eta are homologous in yeast and higher eukaryotes. In contrast, the latter cells have two additional, distinct homologs termed pol iota and pol kappa[46]. These polymerases are capable of accepting various DNA lesions into their active sites and are able to replicate across helix distorting lesions that would normally impede replication machinery. However, the cellular roles of each member of this superfamily are unknown[34]. The studies in this dissertation were designed to examine the relative importance of these enzymes in the bypass of structurally diverse lesions in the context of

intact cells and to determine if members of this family are potential targets for cancer chemoprevention.

POLYMERASE ETA

Polymerase eta (pol eta/ pol η) is the best characterized enzyme in the Y family and absence of the enzyme results in the skin cancer-prone xeroderma pigmentosum variant (XP-V) syndrome. Xeroderma pigmentosum (XP) patients are noted for the predisposition to sunlight induced skin cancer. XP is subdivided into seven subclasses called complementation groups, labeled XP-A through XP-G. Theses complementation groups (XP-A to XP-G) are known to exhibit a deficiency in the rate of excision repair of UV induced DNA damage, which contributes to their cancer predisposition. In addition to these seven complementation groups, there is one additional group termed XP-V. These patients are considered variant due to exhibiting similar clinical symptoms and cancer predisposition, but unlike the other complementation groups have normal excision repair after DNA damage from UV light[47]. Human fibroblasts derived from the XP-V patients have a moderately increased sensitivity to the cytotoxic effects of UV-light but are extremely hypermutable when exposed to UV, despite having normal NER[47]. These cells also have a higher rate of transformation to anchorage independence after UV[48].

It had been suspected for some time that the XP-V gene encoded a protein that was involved in error-prone DNA replication, but the defective gene product was not identified as a DNA polymerase until 1999[36]. These studies used

primer extension assays past a site-specific CPD, and isolated a homolog of the yeast Rad30 protein in XP-V cell extracts[49] that was found to be capable of bypassing T-T CPD. In addition, eight mutations were found in the hRad30 gene in human XP-V cell lines, with seven resulting in severely truncated hRad30 protein[50]. Earlier studies also indicate that XP-V cells are less likely to incorporate dAMP or dGMP opposite the pyrimidine photoproduct, and preferentially induce unusual CG to AT mutations arising from photoproducts in the leading strand template[51,52]. Collectively these studies support the conclusion that pol eta is a tumor suppressor, and the absence of the enzyme results in the cancer-prone XP-V syndrome.

The mechanism of tumor suppression by pol eta appears to be its remarkable ability to efficiently incorporate AA across TT dimers with nearly the same efficiency and processivity as undamaged template[53,54]. This is presumed to result from accommodation of the photoproduct within its open active site. However, pol eta is unable to successfully complete bypass of 6-4PP photoproducts, although it can preferentially incorporate a G opposite the 3'T of the adduct[55]. Thus pol eta has evolved to specifically bypass the most common lesion induced by UV, namely CPD between adjacent thymidine bases. It is presumed that the hypermutability of XP-V cells after exposure to UV results from the mutagenic bypass of the lesion by another, error-prone polymerase.

The question of the specificity of pol eta with respect to UV is controversial. Early studies indicated that XP-V cells were not abnormally sensitive to BPDE[56], but recent data indicate that mutagenic responses to BPDE

17

are *reduced* in such cells (Burke and McGregor, unpublished). In primer extension assays using purified enzyme, pol eta is error prone when it bypasses a BPDE adduct, preferentially inserting dAMP across from the adduct. Such insertion would be consistent with the observed GC to TA transversions induced by BPDE in cells. In addition to CPD bypass, pol eta efficiently bypasses DNA damage[57-60] from other adducts. Pol eta has been shown to be able to efficiently and accurately replicate through 8-oxoguanine (8-oxoG) lesions by inserting a C across from the lesion[61]. *In vitro*, such bypass has the same efficiency as that of an undamaged G. However, the relevance of these *in vitro* studies with purified enzyme to intact cells is not resolved.

The evidence implicating pol eta in the error-free TLS is convincing. However, the polymerase or polymerases responsible for UV induced mutations in XP-V, and by extension in wild-type cells, are unknown. The increased UV-induced mutagenesis associated with pol eta deficiency indicates that mutagenic bypass of UV photoproducts can be catalyzed by other polymerases. Two Y-family polymerases have been hypothesized to assume lesion bypass in the absence of pol eta. One candidate is pol zeta, which can bypass a thymine-thymine dimer *in vitro*[62], and is required for a large proportion of UV mutagenesis in both yeast and mammalian cells. Another candidate is pol iota, which physically interacts with pol eta and co-localizes with pol eta at replication foci following UV irradiation[63]. Chapter II examines the hypothesis that pol iota is directly responsible for inducing mutations after UV exposure especially in pol eta-deficient cells.

POLYMERASE IOTA

Polymerase iota (pol ι) is a Y-family polymerase encoded by the RAD30B gene. Its shares homology to pol eta and is known to exist in many species including drosophila and mammals, but it is not found in yeast. Pol iota has been shown to have varying roles in species dependent *in vitro* lesion bypass assays. Specifically, *in vitro* evidence suggests that pol iota bypasses *cis-syn* TT dimers in drosophilia but the human enzyme does so with lower efficiency[64,65]. Authors have speculated that pol iota arose as a duplication of pol eta, but may have evolved more specialized properties in evolutionary time frames.

There have been conflicting reports on the exact abilities of pol iota to bypass various lesions *in vitro*. For instance, some early studies indicate pol iota as having limited insertion across CPD, while others report complete lesion bypass[66]. It is possible these differences may be a result of pol iota's fidelity being template and sequence dependent[66]. While numerous primer extension assays indicate pol iota does perform misinsertion of nucleotides across various lesions[67], there still is no concrete evidence suggesting a cellular role in TLS.

Two hypotheses have been promulgated regarding the outcome of putative UV photoproduct bypass by pol iota. One suggests that bypass should be mutagenic due to pol iota-catalyzed misinsertion of nucleotides opposite photoproducts[67,68]. Pol iota is renowned for high rates of misinsertion of nucleotides opposite template pyrimidines during DNA synthesis *in vitro*[64,66,69]. However, a study of UV-induced mutagenesis in a shuttle vector replicated in cultured 293T cells, in which pol iota expression was decreased using siRNA

concluded that pol iota has no significant role in UV lesion bypass and mutagenesis[57]. A second hypothesis is that pol iota bypass could be antimutagenic for UV-induced C to T transition mutations. This derives from an undisputed pol iota preference for inserting dGMP opposite template T[70] leading to the suggestion that synthesis by pol iota could be antimutagenic via insertion of dGMP opposite lesions resulting from deamination of cystosine. Indeed, cytosines in dipyrimidine photoproducts readily deaminate[71] and pol iota readily inserts dGMP opposite template uracil in cyclobutane pyrimidine dimmers (CPD)[72].

Additionally, it has been hypothesized that polymerase iota may serve other biological roles outside of TLS. Its pattern of nucleotide misincorporation resembles that which occurs in somatic hypermutation[69]. Studies in pol iota-deficient mice however show normal immunoglobulin hypermutation though this could be attributed to other low fidelity polymerases assuming its role when absent[73]. Pol iota has also been suggested to participate in a specialized form of base excision repair (BER) *in vivo*. This hypothesis is supported largely because it possesses a unique 5'- deoxyribose phosphate lyase activity and is catalytically more active in gap filling than some types of primer extension[70,74].

Pol iota has been implicated in tumor suppression. The mouse *Pol iota* gene is on chromosome 18 and within the *Par2* (pulmonary adenoma resistance 2) locus that is a major determinant of susceptibility to urethane-induced pulmonary adenomas. Interestingly, two strains of mice with differing lung tumor susceptibility differ in *Pol iota* gene status by 25 nucleotides and 10 amino acids,

and the two enzymes have altered substrate specificity, suggesting that pol iota is a modifier of lung tumorigenesis[75]. More recently, the defective *Pol iota* allele in the 129X1/Sv mouse strain that contains the nonsense mutation in the coding sequence has been associated with susceptibility to urethane-induced lung tumors[76]. These data do not indicate whether the tumor suppressor activity is related to the polymerase function or to a separate function that is not currently identified. A precedent exists for the latter possibility in the case of REV1, the polymerase activity of which is dispensable for and distinct from its role in mutagenesis.

The function of pol iota in a cellular context has remained extremely controversial. The experiments described in Chapter II were designed to examine our hypothesis that pol iota is involved in the mutagenic bypass of UV photoproducts in cells. Additionally, these studies explore the possibility that TLS is accomplished by multiple polymerases that act preferentially to bypass photoproducts on the leading or lagging strand template. Finally, these studies are also used to determine pol iota participation in UV induced skin cancer in both pol eta-proficient and pol eta-deficient mice.

REV1

It is apparent that virtually all mutations induced by bulky DNA adducts are dependent on the activity of DNA polymerase zeta acting in concert with another DNA polymerase encoded by the *REV1* gene[77], which encodes the REV1 DNA polymerase. Together, these proteins are required for the generation of 95% to 98% of UV-induced base pair substitutions in yeast[78,79]. In yeast the protein is required for mutagenic TLS past adducts induced in the DNA by a variety of mutagens[80-83]. *In vitro* studies of the purified protein derived from yeast and human sources indicate that REV1 is a deoxycytidyl transferase and incorporates dCMP across from a noninstructive abasic site[84]. Further studies indicated that REV1 is also capable of incorporating C across from a template dG, dT, dA, and dC with preferential insertion across from dG[85]. REV1 uses a unique mechanism to accomplish this insertion by allowing the incoming dCTP to pair with an arginine in the active site rather than the template base[80].

Despite this intriguing mechanism, the catalytic activity of REV1 appears to be dispensable for TLS. It has been known for some time that the yeast *rev1-1* mutant results from a mutation in REV1 that abolishes the dCMP transferaase catalytic activity. Nevertheless, this mutant is proficient for UV mutagenesis. These data support the conclusion that REV1 plays a structural role in TLS that is distinct from its catalytic activity[83]. Indeed, REV1 has an N-terminal BRCT region and a C-terminal "interacting domain" that have variously been implicated in protein-protein interactions and in mutagenesis[86-89]. REV1 has been shown to

physically interact with the Pol zeta subunit REV7 and with the other members of the Y-family[85,90-92] through a ~100 amino acid C-terminal region in REV1 that binds these TLS polymerases. Activity of these polymerases while bound to REV1 was normal, as determined by *in vitro* primer extensions assays[93]. These interactions, including the association of REV1 with replication foci, may be mediated by ubiquitin. It has been hypothesized that the ubiquitination of PCNA is a molecular switch that facilitates TLS[94]. REV1 contains ubiquitin-binding motifs (UBMs) located at the C terminus of the protein and these motifs have been shown to be required for association of REV1 with replication foci [95]. These data are consistent with current models that REV1 serves as a scaffolding protein to tether error-prone polymerases to the site of stalled DNA replication forks[96]. Whatever the mechanism, data strongly implicate REV1 in mutagenic TLS[97]. What remains completely unknown and untested is the role REV1 has in carcinogensis. Although the somatic mutation hypothesis of cancer would predict that inhibition of the involvement of REV1 in mutagenic bypass would lower the incidence of cancer after DNA damage, the actual consequences are completely unknown and constitute the focus of Chapter III.
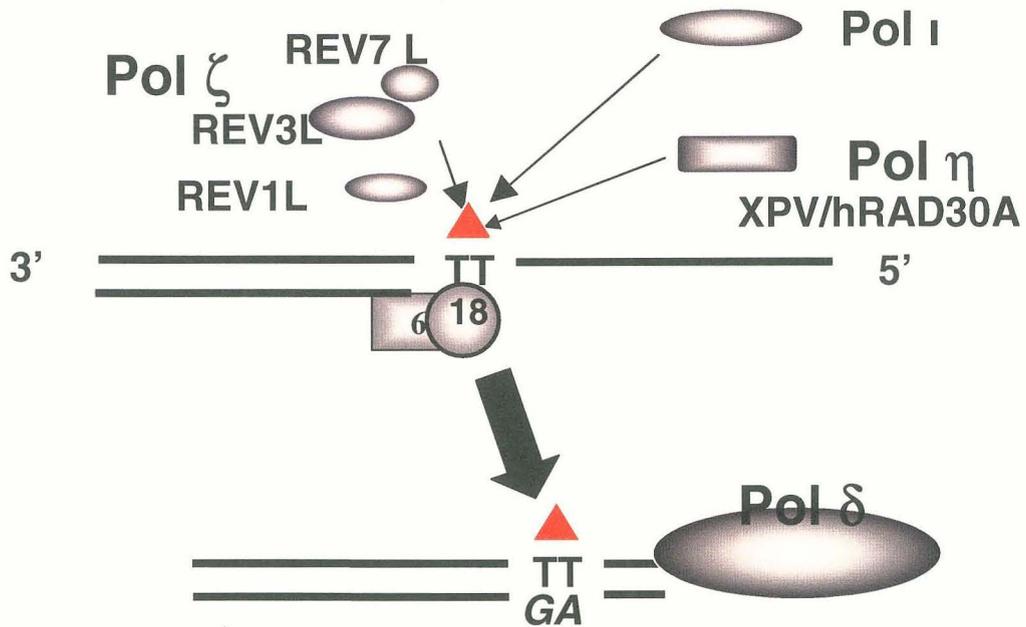
Figure 3. Translesion synthesis. After DNA damage, polymerase δ stalls on the DNA lesion (not illustrated). Current data indicate that RAD6/ RAD18 monoubiquitinate PCNA which signals the recruitment of polymerase η, ι, κ, and REV1. These polymerases insert nucleotides directly across from the lesion, most likely in a lesion or sequence dependant fashion. Polymerase ζ then, in a semi-processive manner, extends the mispair. This forms a template-primer that is fully extendable by polymerase δ to continue replication[98].

CHAPTER II

PARTICIPATION OF MOUSE DNA POLYMERASE IOTA IN STRAND-BIASED MUTAGENIC BYPASS OF UV PHOTOPRODUCTS AND SUPPRESSION OF SKIN CANCER

SUMMARY

As indicated earlier, DNA polymerase iota is a conserved Y family enzyme that is able to bypass replication-blocking lesions *in vitro*. However, its role in TLS in intact cells is unknown and remains highly controversial. We hypothesized that this enzyme is responsible for mutagenic bypass of photoproducts, and that this activity is responsible for the extreme hypermutability of cells that lack pol eta. To test this, we compared UV-induced mutagenesis in primary fibroblasts derived from wild-type mice to mice lacking functional pol iota, pol eta, or both. A deficiency in mouse DNA polymerase eta greatly enhanced UV-induced *Hprt* mutant frequencies. This enhanced UV-induced mutagenesis was strongly diminished in cells deficient in pol iota. Pol iota deficiency also reduced UV induced mutagenesis in wild-type cells. These data conclusively indicate that pol iota participates in the bypass of UV photoproducts in cells. Sequence analysis of *Hprt* mutants derived from each of the four genotypes indicated that the lack of

DNA polymerase eta resulted in a dramatic increase in mutations that were targeted by putative photoproducts in the leading strand template. Further, these mutations were principally CG to AT transversions. This spectrum completely recapitulates that found in human XPV cells. The lack of pol iota did not alter the kinds of mutations in either the wild-type or pol eta-deficient background, but there was a highly significant reduction in mutations that were targeted by putative photoproducts in the lagging strand template. These data support the hypothesis that pol eta is specialized for the *error-free* bypass of photoproducts on the leading strand template. In the absence of this enzyme, these photoproducts are bypassed by pol iota in a mutagenic fashion. Further, pol iota is specialized for *error-prone* bypass of photoproducts in the leading strand template. The reduced frequency of UV-induced mutants in cells lacking pol iota would predict that these mice would have a reduced incidence of UV-induced skin cancer. We UV irradiated and compared the UV-induced skin cancer susceptibility of wild-type mice to mice lacking functional pol eta, pol iota, or both. Pol iota deficiency alone had no effect on cancer susceptibility in mice with functional pol eta. Unexpectedly, however, UV-induced skin tumors in pol iota-deficient mice developed four weeks *earlier* in mice concomitantly deficient in pol eta. Collectively, these data reveal functions for pol iota in bypassing UV photoproducts. Additionally, these data indicate that pol iota acts as a tumor suppressor by a mechanism that is presumably distinct from is TLS functions.

MATERIALS AND METHODS

GENERATION OF DOUBLE KNOCKOUT MICE

In an earlier study[99] an ES cell line derived from pol ι-deficient 129 mice was used to generate pol eta knockout mice. In that study[99] chimeric mice were bred with B6 mice to produce F1 pol eta heterozygotes that were then intercrossed to generate the F2 mice. The present study began by PCR-genotyping 595 F2 mice twelve of which were pol eta +/-/ pol iota -/-. These mice were intercrossed to generate the double homozygous mice studied here.

GENERATION AND GROWTH OF PRIMARY EAR FIBROBLASTS

Primary fibroblasts derived from ear punches were grown at 37° under hypoxic conditions (2-3% O_2, 5% CO_2). These conditions were previously reported to increase the number of population doublings and lengthen the time before senescense of primary murine cells[100]. Nitrogen gas was used to sustain hypoxic conditions in the incubators using an oxygen control module (Biospherix, Ltd., PROOX model 110). Cells were maintained in MEM-α (Cambrex Bio Science Walkersville, MD) supplemented with 10% FBS (Hyclone Laboratories, Logan, UT), 2mM glutamine, nonessential amino acids (Mediatech, Inc. Herndon, VA), penicillin (100 units/ml), streptomycin (100 µg/ml) for all assays with the exception of the 6-thioguanine (6-TG) screening, which utilized DMEM (Mediatech, Inc. Herndon, VA).

CYTOTOXIC AND MUTAGENIC EFFECTS OF UV IRRADIATION

Fibroblasts were assayed for cytotoxic and mutagenic responses to UV$_{254nm}$ radiation at early passages (6-8 population doublings) after primary cultures were established. The UV source was a Spectroline germicidal lamp that emits short wave UV with a peak emission at 254nm. The energy emitted by the light was quantified using an International Light model IL1700 radiometer and a sensor fitted with a 254nm filter and W diffuser. The height of the light was adjusted to deliver 0.1-0.2 J/m^2/sec at the level of the cells.

A series of independent populations (1.5 x 10^6 cells each, plated on 150-mm-diameter plates) were treated with UV$_{254nm}$ at fluences of 0-12 J/m^2 for pol eta +/+ cells or 0-6 J/m^2 for pol iota -/- cells. Prior to UV exposure, the culture medium was aspirated and the cells were washed with PBS (pH 7.4). Sufficient dishes were used to ensure at least 1.0 x 10^6 surviving cells. Each dish was allowed 3-5 days of growth before trypsinization and passage of 1.5 x 10^6 cells. After 8-9 days of post-irradiation expression, 0.5-1.0 x 10^6 cells were selected for 6-thioguanine (6-TG) resistance (TG^r) as described below. Cytotoxic responses to radiation were established by plating the cells at cloning density and measuring colony forming ability. The media of cells exposed at cloning density were replaced with fresh medium after 24 hours and 7 days post-irradiation and stained at ~14 days. Colony forming ability was also determined at the time of TG^r selection by plating the cells at cloning density in nonselective medium. This value was used to correct the observed frequency of mutants. After 14 - 20 days, TG^r clones were isolated in RNase free PBS for *Hprt* coding region amplification

(described below). After colony isolation, plates were stained for missed colonies and mutant frequency was determined, defined as the number of observed TG^r clones per 10^6 clonable cells (corrected for cloning efficiency). The significance of differences in frequencies between polymerase genotypes was calculated using the Fisher's exact test.

AMPLIFICATION AND SEQUENCING OF HPRT CDNA

Isolation of TG^r clones, reverse transcriptase-PCR (RT-PCR) of the coding region of the *Hprt* gene, and sequence analysis of the PCR products was done as described below. After the 8 - 10 day expression period dishes were visually inspected in a dark room under flashlight for apparent (macroscopic) thioguanine resistant (TG^r) colonies. Individual clones were circled before aspirating the media washing the dish with sterile PBS (pH 7.4). A dry sterile cotton swab was used to dry around the resistant colony before addition of 10 µl of trypsine. A micropipette was then used to pull the colony from the dish. Pulled colonies were put into a sterile 50 µl microfuge tube filled with 500 µl sterile PBS (pH 7.4) to dilute trypsin. The cells were pelleted by centrifugation at 15,000 x g for 10 minutes at 4°C and samples frozen at -80°C (for later amplification of the *Hprt* coding region). Dishes were then stained and total colonies counted to determine mutant frequency. Amplification of *Hprt* cDNA from small clones was adapted from Yang *et al*[101]. The cells were either directly processed or frozen at -80 °C before cDNA preparation. While on ice the cells were lysed by adding 10 µl of Reverse Transcription (RT) lysis buffer containing1X Superscript III RT buffer

(Invitrogen Corp), 2 units/ µl RNASE OUT (Invitrogen Corp), 25 ng/ µl Oligo dT (20 mer, Integrated DNA Technologies), 10 mM DTT, 500 µM dNTPs (Invitrogen Corp), 10 units/ µl Superscript III RT (Invitrogen Corp), 2.5% NP-40, H_2O to 10 µl. The resuspended cell pellet was transferred to a 200 µl PCR tube and incubated for 50 minutes at 50°C. The reverse transcription (RT) reaction was terminated by heating to 70 °C for 10 minutes. Amplification was performed through two rounds of PCR using inner and outer sets of primers. First round PCR reaction mix contained 5 µl cDNA, 1X PCR buffer (Invitrogen Corp), 1.5 mM $MgCl_2$ (Invitrogen Corp), 200 µM dNTPs (Invitrogen Corp), 0.2 µM outer primer A (Integrated DNA Technologies GGC TTC CTC CTC AGA CCG CT), 0.2 µM outer primer B (Integrated DNA Technologies ACA TCA ACA GGA CTC CTC GT), 2 units Platinum Taq polymerase (Invitrogen Corp), H^2O to 50 µl. Using a Stratagene Robocycler the reaction was held at 94 °C for 3 minutes, then 30 cycles of 94 °C for 30 seconds, 57 °C for 30 seconds, 72 °C for 1 minute, and final extention using 72 °C for 10 minutes. Second round PCR mix contained 1 µl of 1st round product, 1X PCR buffer (Invitrogen Corp), 1.5 mM $MgCl_2$ (Invitrogen Corp), 200 µM dNTPs (Invitrogen Corp), 0.2 µM inner primer 3 (Integrated DNA Technologies TTT TGC CGC GAG CCG ACC GG), 0.2 µM inner primer 4 (Integrated DNA Technologies ATT TGC AGA TTC AAC TTG CG), 2 units Platinum Taq polymerase (Invitrogen Corp), H_2O to 50 µl. Second round PCR Program using Stratagene Robocycler consisted of 94 °C for 3 minutes followed by 20 cycles of 94 °C for 30 seconds, 57 °C for 30 seconds, 72 °C for 1 minute and final extension of 72 °C for 10 minutes. The final product was analyzed using

5 µl of 2nd round product on 1% agarose prior to sequencing. The sequence of both DNA strands was determined by automated DNA sequencing. For sequencing dRhodamine dye terminator chemistry (Applied Biosystems) was used along with the same inner primer 3 (Integrated DNA Technologies TTT TGC CGC GAG CCG ACC GG), and primer 4 (Integrated DNA Technologies ATT TGC AGA TTC AAC TTG CG) used during second round PCR.

IRRADIATION OF MICE

Eight to twelve week old mice were used for UV irradiation. All of the mice were litter-mates and had their backs shaved once a week during the UV irradiation period. Mice were irradiated with UV-B light. The UV source was a bank of two UV-B lamps (Blak-Ray lamp Model XX-15M, Ultraviolet Products, Inc., Upland, CA 91786, USA) that emit wavelengths in the 280-370 nm range, with a peak at 302 nm. UV-B flux was measured by a UVX digital radiometer (Model UVX-31, Ultraviolet Products, Inc., Upland, CA). UV irradiation was terminated upon initial observation of tumor formation.

HISTOLOGICAL ANALYSIS OF MOUSE TISSUE AND SKIN TUMORS

Mice were sacrificed via CO_2 inhalation for whole body tumor and tissue analysis. Tissue and tumors were isolated and fixed in Bouin's solution. The tissue was later stained with haematoxylin and eosin (H&E) stain and examined.

RESULTS

GENERATION OF MICE AND PRIMARY FIBROBLASTS

Mice with homozygous deficiencies in pol iota and pol eta were generated by mating F2 pol eta +/-/ pol iota -/- mice. The progeny included 23 pol eta +/+/ pol iota -/- mice, 48 pol eta +/-/ pol iota -/- mice, and 30 pol eta -/-/ pol iota -/- mice. The multiple progeny indicates that mice deficient in both pol eta and pol iota develop normally and are viable. These mice were used to examine whether pol iota has a role in response to irradiation with UV light. At the same time mice were being irradiated to examine the susceptibility of the mice to UV light-induced skin cancer (see below), primary fibroblasts were isolated from ear biopsies. Primary fibroblasts were successfully derived from wild-type mice and mice deficient in pol eta only, pol iota only and both pol eta and pol iota (Table 1). Different cell line numbers/letters indicate the fibroblast originated from separate mice.

Primary cells grew well in normal cell culture media (as described in the Materials and Methods section). Growing the primary fibroblast in hypoxic conditions lengthened the time before senescence with senescence typically occurring around 20 population doublings and/or five cryogenic freezes. Individual fibroblasts were examined for UV light-induced cytotoxicity and mutagenesis.

Mouse Strain/ Cell Line	Background
129 (83)	Pol iota +/+ Pol eta +/+
129 (35d)	Pol iota +/+ Pol eta +/+
129 (47)	Pol iota +/+ Pol eta +/+
129 (70)	Pol iota -/- Pol eta +/+
129 (69)	Pol iota -/- Pol eta +/+
129 (75d)	Pol iota +/+ Pol eta -/-
129 (34d)	Pol iota +/+ Pol eta -/-
129 (48)	Pol iota +/+ Pol eta -/-
129 (71)	Pol iota -/- Pol eta -/-
129 (73)	Pol iota -/- Pol eta -/-

Table 1. Fibroblast Cell Lines. Cell lines that were successfully derived from wild-type mice and mice deficient in pol eta only, pol iota only, and both pol eta and pol iota. Different cell line numbers/ letters indicate the fibroblast originated from separate mice.

SURVIVAL OF PRIMARY MOUSE FIBROBLASTS FOLLOWING UV IRRADIATION

The influence of mouse genotype on survival of primary dermal fibroblasts after irradiation with UV_{254nm} was measured by colony forming ability (Figure 4). Cells deficient in pol eta alone were moderately sensitive to killing by UV irradiation at a dose 2.8 J/ m^2 resulting in 37% survival (D_{37}) (Figure 4). In either the pol eta deficient or pol eta proficient background, cells deficient in pol iota were more sensitive to UV-induced cytotoxicity (Figure 4, filled squares and diamonds). Statistical significance of the reduced survival of pol iota deficient cells was determined by polynomial regression analysis, with the best fit provided by cubic polynomials. This analysis revealed that the percent survival for pol eta +/+ pol iota -/- cells was significantly lower than for pol eta +/+ pol iota +/+ cells (p = 0.018). This analysis also showed that the percent survival for pol eta -/- pol iota -/- cells was significantly lower than for pol eta -/- pol iota +/+ cells (p = 0.001).
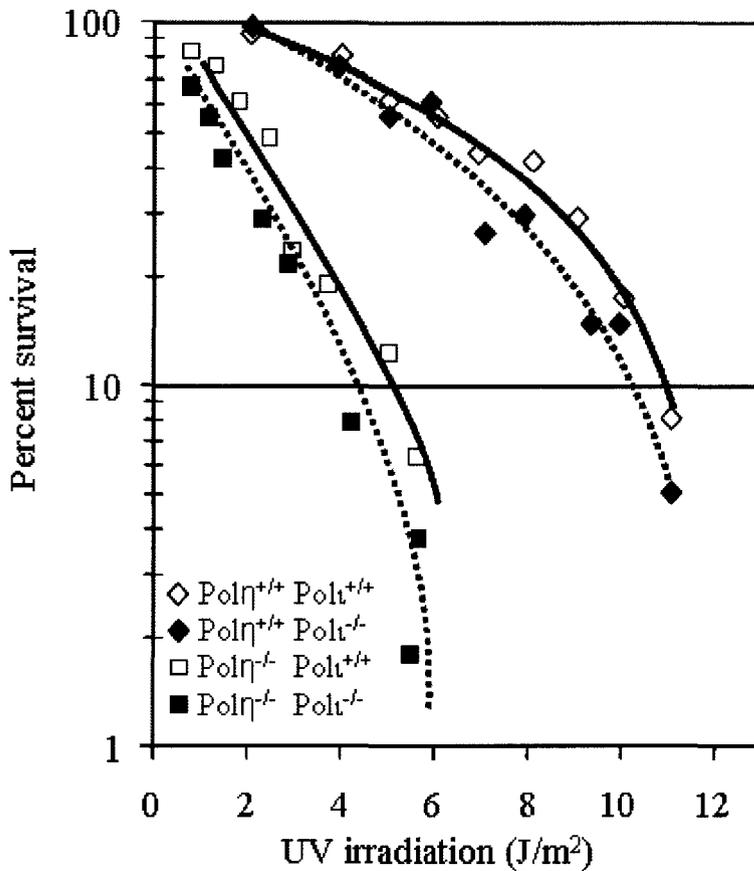
Figure 4. Survival of primary mouse fibroblasts following UV irradiation.
The influence of mouse genotype on survival of primary dermal fibroblasts after irradiation with UV_{254nm} was measured by colony forming ability, as described in Methods. The fluence required to reduce the survival of pole eta (pol η) +/+ pol iota (pol ι) +/+ cells to 37% of the unirradiated control (D_{37}) was 8 J/m². This was reduced to ~2.8 J/m² in the cells derived from pol eta (pol η) -/- pol iota (pol ι) +/+. Statistical significance of the reduced survival of pol iota deficient cells was determined by polynomial regression analysis, with the best fit provided by cubic polynomials. This analysis revealed that the percent survival for pol eta +/+ pol iota -/- cells was significantly lower than for pol eta +/+ pol iota +/+ cells (p = 0.018). This analysis also showed that the percent survival for pol eta -/- pol iota -/- cells was significantly lower than for pol eta -/- pol iota +/+ cells (p = 0.001).

UV LIGHT-INDUCED MUTAGENESIS AT THE HPRT LOCUS IN PRIMARY MOUSE FIBROBLASTS

The hypoxanthine-guanine phosphoribosyl transferase (*Hprt*) gene is a useful target for studying somatic mutations. This target gene is located on the X-chromosome and encodes the *Hprt* protein[102]. *Hprt* exists in low levels in all somatic tissue constituting .005-.01% of total mRNA[103]. This protein's activity is required for the phosphoribosylation of hypoxanthine and guanine and its enzymatic activity is part of the salvage pathway for purine nucleic acid biosynthesis. This enzyme is also responsible for the phosphoribosylation of purine analogs such as 8-azaguanine and 6-thioguanine (6-TG) which enables them to be incorporated into DNA[104]. Thus, when one of these purine analogs is present in cell culture medium, the cells incorporate these analogs into their DNA. This incorporation severely taxes DNA mismatch repair systems causing cell death. If however, mutations are present in the *Hprt* gene, which abolish functional enzyme, the cells do not incorporate the analog into the DNA and survive.

This purine salvage pathway provides an efficient mechanism to study induced mutations in the *Hprt* gene through the selection of purine analog mutants[105]. While any of the purine analogs may be used to select for *Hprt* mutations, issues such as concentration, lack of efficacy, and selection time has lead 6-TG to become the standard in *Hprt* mutant selection[106]. The studies covered in this dissertation utilize 6-thioguanine as the purine analog for selection, the mutants of which are indicated as thioguanine resistant (TG^r).

Table 2 reports individual experiments after irradiation of cells plated on three 150 mm-diameter dishes at a density of 10^4 cells/ dish. These results

indicate the percent survival, number of mutants observed, percent survival, number of cells selected for and mutant frequencies for three different doses. Mutation frequency results are summarized and compared in Figure 5.

Compared to wild-type fibroblasts (Figure. 5, open diamonds), a deficiency in mouse pol eta alone resulted in increased UV irradiation-induced mutagenesis at the endogenous *Hprt* locus (Figure. 5, open squares). Interestingly, in pol eta-deficient cells in which pol iota was also deficient, the mutant frequency was also reduced (Figure. 5, closed squares), implicating pol iota in mutagenic TLS when pol eta is absent. Even when pol eta is proficient, pol iota deficiency reduced UV induced mutagenesis (Figure 5, compare open to closed diamonds), again implicating mouse pol iota in bypass of UV photoproducts. The fact that the UV-induced mutant frequency in cells that are deficient in both pol eta and pol iota (Figure 5, filled boxes) is higher than the spontaneous mutant frequency ($\sim 10^{-5}$) indicates that a third polymerase performs mutagenic bypass of photoproducts.

	Cell Line	UV (J/m²)	Percent Survival	TG^r Clones Observed	Cells Selected x 10^6	Mutants Per 10^6 Clonable Cells	Mutants Per 10^6 Clonable Cells minus Background
Iota +/+ Eta +/+	47	0	100	2	.5	12	107±18
		7	50	88	4.5	119	
	83	0	100	60	.5	255	245
		8	27	230	1	500	
	35d	0	100	4	.5	17	198
		9	10	86	1	215	
Iota -/- Eta +/+	70	0	100	0	.5	0	42±12
		7	32	53	3.5	42	
	69	0	100	0	.5	0	31
		8	17	13	1	31	
	69	0	100	3	.5	26	67±13
		9	10	41	2	93	
Iota +/+ Eta -/-	75d	0	100	0	.5	0	86
		2.5	71	33	1	86	
	34d	0	100	6	.5	33	69
		3	40	43	1	102	
	48	0	100	0	.5	0	830±78
		3.8	25	805	2.5	830	
Iota -/- Eta -/-	73	0	100	0	.5	0	78±22
		2.5	46	59	2	78	
	73	0	100	0	.5	0	239
		3	15	32	1	239	
	71	0	100	0	.5	0	245±17
		4	13	107	1.5	245	

Table 2. Mutant frequencies of individual cell lines after exposure to 254nm UV light. Cells were plated on three 150 mm-diameter dishes at a density of 10^4 cells/dish to determine mutant frequency at three varying dose, column 3. Cells were also plated at cloning density to determine survival, column 4. Column 5 list total mutant clones observed. Total mutant corrected for cloning efficiency (not listed) yields the number mutants per 10^6 clonable cells is listed in column 5. Column 6 list mutants per 10^6 clonable cells after subtracting background.
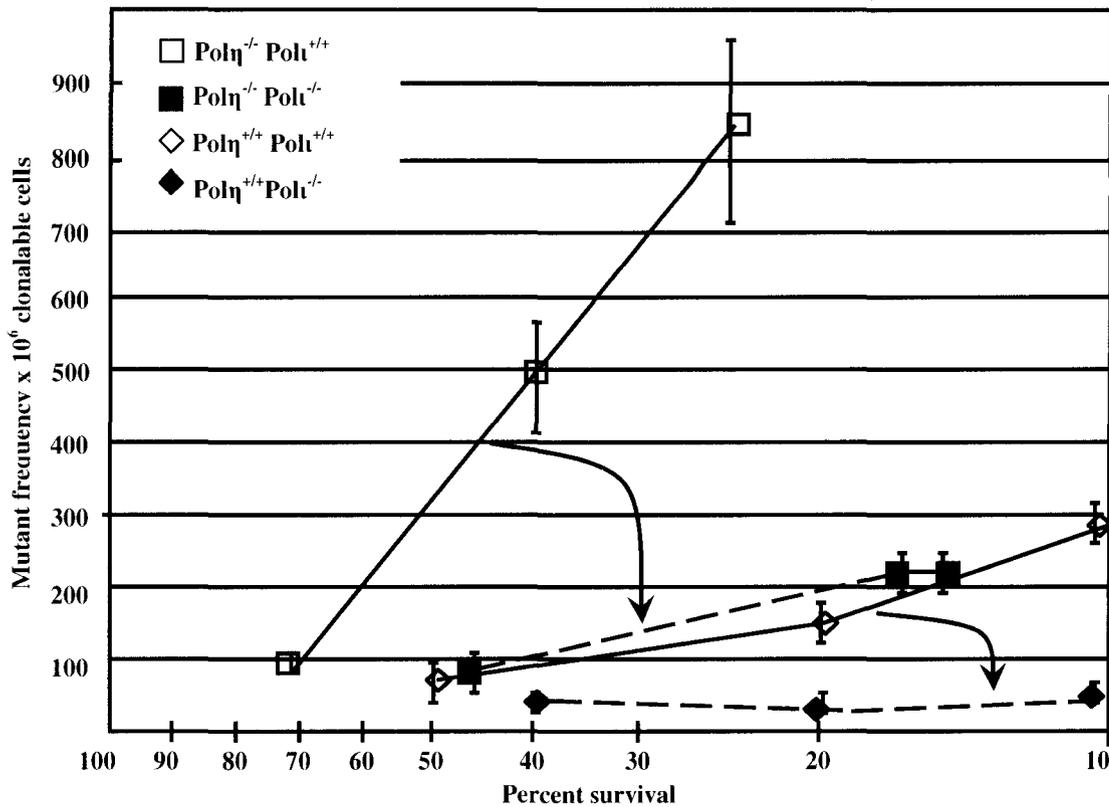
Figure 5. Frequency of thioguanine-resistant (TG^r) clones as a function of survival after UV-irradiation. Cells were plated on three 150 mm-diameter dishes at a density of 10^4 cells/cm^2 to determine mutant frequency, or at cloning density to determine survival. After attachment, plates were irradiated with UV fluences determined from the data in Figure 4 that were estimated to give an expected survival of 20- 40%. The actual survival in the mutagenesis experiments were determined as in Figure 4 and are plotted on the X-axis. The corresponding mutant frequency at each survival is plotted on the Y-axis. Each point represents the mean of three independent dishes at the indicated survival, plus or minus 1 standard deviation. Mutant frequency is defined as the number of TG^r clones per million clonable cells. Each data point represents at least two independent experiments in which 2-4 x 10^6 surviving cells were selected after UV irradiation and an 8-9 day expression period. The data have been corrected for cloning efficiency on the day of selection and the spontaneous background mutant frequency (10^{-5}) has been subtracted. The arrows indicate the reduction in mutant frequency when pol ι is disrupted in the pol eta-deficient background (larger arrow) and in the pol eta-proficient background (smaller arrow).

SPECIFICITY OF UV-INDUCED MUTAGENESIS

To discover the types and locations of pol iota-dependent UV-induced mutations, we sequenced independent UV-induced *Hprt* mutants derived from cells of each of the four genotypes. The results are summarized in Table 3 and presented in detail as Tables 4, 5, 6, and 7 at the end of the chapter. In all four instances, we analyzed mutant clones for exposures that resulted in ~37% survival for that genotype (Figure 5).

To further understand the strand specificity of UV-induced mutagenesis we determined the strand containing the dipryimidine sequence in the case of each targeted base substitution. The proportion of mutations that arose from putative photoproducts in either strand was multiplied by the mutant frequency induced at the D_{37} for each of the four genotypes. This data is summarized as presented in Figure 6.

WILD-TYPE CELLS

Among 36 *Hprt* mutant clones from wild-type cells, 31 base pair substitutions were found (Table 3 and Table 4 at the end of the chapter). Twenty-seven substitutions occurred at dipyrimidines, indicating that dipyrimidine photoproducts are responsible for the majority of the UV-induced mutations. Interestingly, 22 of the 27 substitutions are inferred to result from bypass of a dipyrimidine photoproduct on the non-transcribed strand (Table 4). This represents a 4.5 fold bias in favor of mutations templated at dipyrimidines on the

non-transcribed strand compared to the transcribed strand (Figure 6, 49×10^{-6} versus 11×10^{-6}, p <0.0001).

POL ETA-DEFICIENT CELLS

A deficiency in mouse pol eta alone resulted in an ~7-fold increase in induced mutant frequency (Table 3, compare 80×10^{-6} to 550×10^{-6}). Sequence analysis of UV-induced *Hprt* mutants in pol eta-deficient fibroblasts (Table 3 and Table 5 at the end of the chapter) revealed increased frequencies for several types of single base substitutions (up to 40-fold for T-A to C-G substitutions), for tandem double base substitutions (>10-fold) and for exon deletions (20 fold). The exon deletions could result from splicing abnormalities caused by mutations in splice donor or acceptor sites. Most substitutions were at dipyrimidines (Table 5). However, the bias in favor of mutations templated at dipyrimidines in the nontranscribed strand was reduced from 4.5-fold in wild-type cells to 2.9 fold in pol eta-deficient cells (Figure 6, 290×10^{-6} versus 100×10^{-6}). This is consistent with an earlier study using XP variant cells[99]. This study also shows that pol eta is acting to preferentially bypass photoproducts in the transcribed strand. Of notable importance is the high proportion of CG to AT tranversions, 78% (7/9) of which arose from dipyrimidines on the transcribed strand.

In the present study of asynchronously growing mouse cells lacking pol eta, similar frequencies and proportions of transitions and transversions were observed following UV irradiation, and the frequency of C to T transitions was 100×10^{-6} (Table 3). The data reported here in mouse cells has some

discrepancies with that presented in human XP varient lines[52]. In particular, in that study when XP variant cells deficient in pol eta[52] were irradiated at the beginning of S-phase the UV-induced substitutions included 13 transitions and 17 transversions. The calculated frequency of C to T transitions was 130 x 10^{-6}. However, when the XP variant cells were irradiated in the G_1 phase to allow time for repair before replication, transversions exceeded transitions by 11:4, and the calculated frequency of UV-induced C to T transitions was only 18 x 10^{-6}. The differences between our study in mouse cells and human XP variant cells irradiated in the G_1 could partially be related to the relationship between repair and replication. It could also or additionally be a result of the amount of time available for deamination of cytosine-containing photoproducts to occur. The later is particular noteworthy since rodent cells have a reduced level of global nucleotide excision repair compared to human cells.

POL IOTA-DEFICIENT CELLS

Fibroblasts deficient in pol iota have UV-induced total mutant frequencies and base substitution frequencies that are more than 2-fold lower than for wild-type cells. This decrease observed in pol iota deficient cells almost brings the mutation frequency to background levels. Specifically, wild-type cells after UV irradiation at D_{37} have a mutational frequency of 80 mutants per 10^{-6} clonable cells. Pol iota removal lowered this frequency to 32 mutants per 10^{-6} clonable cells (see Table 3, compare columns 1 and 3). These differences are extremely significant resulting in a p value of <0.0001.

Among 18 base substitutions (Table 6, at the end of the chapter), 14 were at dipyrimidines as listed in column three (Table 3). Notably, the dipyrimidine was on the non-transcribed strand for 10 of these, such that the non-transcribed to transcribed strand bias was 2.4-fold (Figure 6., 17×10^{-6} versus 7×10^{-6}, $p = 0.064$). This is less than the 4.5-fold bias observed in wild-type cells. This decrease in strand bias after UV irradiation suggests that some of the strand bias observed in wild-type cells is a result of pol iota. Specifically pol iota is working preferentially on the non-transcribed (leading) strand in an error prone fashion.

CELLS DEFICIENT IN BOTH POL ETA AND POL IOTA

Fibroblasts deficient in pol eta and pol iota had UV-induced mutant frequencies (Table 3, column 4), that in comparison to cells deficient in pol eta alone (Table 3, column 2), were reduced for all mutations. Additional reduction was also observed for total substitutions, transitions, transversions, tandem double base substitutions and exon deletions. These 4- to 5-fold differences are significant with a p value of ≤0.05. Among 15 substitutions at dipyrimidines, seven are inferred to result from bypass of a lesion on the non-transcribed strand and eight are inferred to result from bypass of a lesion on the transcribed strand (Table 7). The fact that deficiency in both pol eta and pol iota eliminated the strand bias 41×10^{-6} on the non-transcribed strand versus 46×10^{-6} on the transcribed strand (Figure 6), suggests that this bias depends on both polymerases. Also noteworthy is that the UV-induced mutant frequency of fibroblasts deficient in both pol eta and pol iota is 120×10^{-6} (Table 3, column 4), this is much higher than the spontaneous mutant frequency in un-irradiated cells

(1 x 10^{-5}). This is direct evidence that even in cells lack po eta and pol iota there is an elevated mutation frequency after UV irradiation and this indicates that at least one other polymerase performs mutagenic TLS across these lesions.

	pol η +/+ pol ι +/+	pol η -/- pol ι +/+	pol η +/+ pol ι -/-	pol η -/- pol ι -/-
	Frequency $(x\ 10^{-6})$	Frequency $(x\ 10^{-6})$	Frequency $(x\ 10^{-6})$	Frequency $(x\ 10^{-6})$
Total mutation frequency[b]	80 [36][c]	550 [48][c]	32 [19][c]	120 [20][c]
Frameshifts	4 (2)[d]	23 (2)	≤2 (0)	6 (1)
Large deletions[e]	4 (2)	92 (8)	2 (1)	29 (5)
Large insertions	2 (1)	≤11 (0)	≤2 (0)	≤6 (0)
Base substitutions at dipyrimidine sites	60 (27)	390 (34)	24 (14)	87 (15[f])
Tandems	≤2 (0)	23 (2)	5 (3)	6 (1)
Transitions	31 (14)	180 (16)	8 (5)	41 (7)
C•G → T•A	29 (13)	100 (9)	8 (5)	23 (4[f])
T•A → C•G	2 (1)	80 (7)	≤2 (0)	17 (3[f])
Transversions	29 (13)	180 (16)	10 (6)	41 (7)
C•G → A•T	4 (2)	100 (9)	2 (1)	23 (4[f])
C•G → G•C	≤2 (0)	11 (1)	≤2 (0)	≤6 (0)
T•A → A•T	13 (6)	57 (5)	8 (5)	17 (3[f])
T•A → G•C	11 (5)	11 (1)	≤2 (0)	≤6 (0)

Table 3. UV-induced *Hprt* mutation frequencies in mouse primary fibroblasts [a]Frequency measurements were determined for at least 6 independent assays and using primary fibroblasts isolated from at least 2 independent mice. [b]Mutation frequencies were determined at UV exposures resulting in 37% cell survival. [c]Numbers in brackets are the number of independent mutants sequenced (Tables 4-7). [d]Numbers in parentheses are the number of independent mutations observed (Tables 4-7). [e]Large deletions are primarily deletions of exons (Tables 4-7). [f]Three mutants contained multiple mutations separated by more than 100 nucleotides (see Supplemental Tables 7).

45
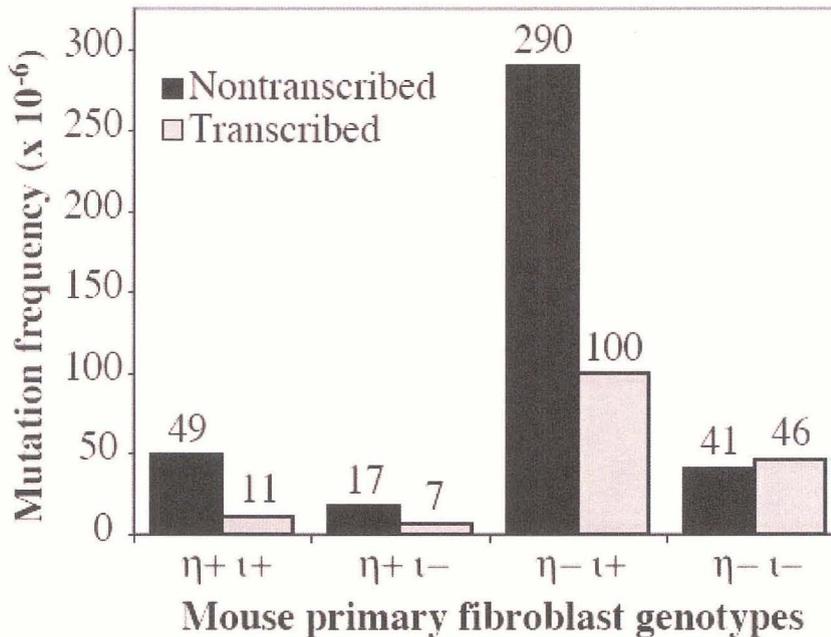
Figure 6. Strand specificity of UV-induced mutagenesis. The strand containing the dipryimidine sequence was determined in the case of each targeted base substitution. The proportion of mutations that arose from putative photoproducts in either strand was multiplied by the mutant frequency induced at the D_{37} for each of the four genotypes as presented in Figure 5. Non-transcribed to transcribed strand bias was lower for pol ι deficient cells compared to wildtype 2.4-fold This is less than the 4.5-fold bias observed in wild-type cells. Non-transcribed strand was additional reduced from 4.5-fold in wild-type cells to 2.9-fold in pol η-deficient cells. Double knockout eliminated strand bias suggesting that strand bias depends on both polymerases.

SUSCEPTIBILITY OF POL ETA AND POL IOTA DOUBLE KNOCKOUT MICE TO UV-INDUCED SKIN CARCINOMA

To determine the susceptibility of pol eta [-/-] / pol iota [-/-] mutant mice to UV light-induced skin carcinoma, sets of littermates were shaved on part of their backs once a week, UV irradiated three times a week at 3.75 kJ/m^2. These mice were examined for skin tumors each week. Irradiation was for 20 weeks and was discontinued when the first skin tumor was observed. Twelve pol eta -/- / pol iota -/- mutant mice, 13 pol eta +/- / pol iota -/- mutant mice and nine pol eta +/+ / pol iota -/- mutant mice were treated and examined. These results were then compared to those reported earlier for wild-type and pol iota -/- mutant mice[99]. Similar to results with wild-type mice, (Figure 7, open squares) none of the 13 pol eta +/- / pol iota -/- mutant mice or the nine pol eta +/+ / Pol iota -/- mutant mice developed skin tumors over the 20 week course of irradiation (data not shown). Similar to results with the pol eta [-/-] mutant mice [99] the irradiated ears of the pol eta -/- / pol iota -/- mutant mice became darker, curved and atrophied, while littermate controls (e.g., pol eta +/+ / pol iota -/- mice) did not show such abnormalities or develop skin tumors even after 30 weeks of exposure. More importantly, UV-induced skin tumors developed in the double knockout pol eta -/- / pol iota -/- mice starting at week 8 of irradiation. All 12 mice developed skin tumors by week 13 (Figure 7, open circles). This data shows that time for tumor formation in pol eta -/- / pol iota -/- is earlier than for pol eta knockout mice. Specifically, the first UV induced skin tumors in pol eta null mice at week 12 (compared to 8 in pol eta -/- / pol iota -/-) of irradiation and the last at week 18

47

(compared to 13 of pol eta -/- / pol iota -/-) (Figure 7, open diamonds), reproduced from[99]. This pol iota dependent difference in time to skin tumor formation is statistically significant, with low p values as determined by three different statistical tests, a log rank test (p value = <0.0001), a t-test (p value = <0.0001) and a Mann-Whitney test (p value = <0.0002). Histological analysis of skin tumors (data not shown) revealed phenotypes in double knockout mice that were indistinguishable from those of the pol eta null knockouts. Both developed tumors that formed from squamous cell carcinoma *in situ* and advanced to invasive carcinomas. Thus, loss of pol iota increases the susceptibility of pol eta deficient mice to UV induced skin cancer, with no detectable change in the tumor developmental pathway.
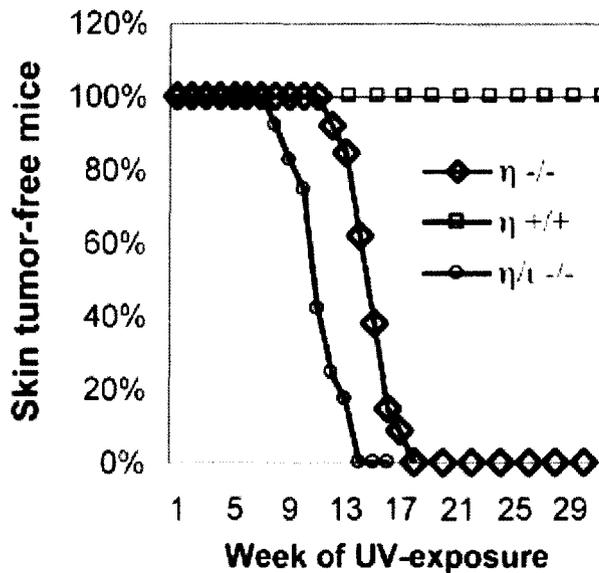
Figure 7. UV light-induced skin cancer in mice. Mice were shaved once per week and irradiated three times per week with 3.5 kJ/m^2, for twenty weeks or until the first skin tumor arose. Mice were inspected weekly for the development of skin tumors. Results with 12 pol eta (pol η) $^{-/-}$ / pol iota (pol ι) $^{-/-}$ mice (open circles) are compared with results previously reported[99] for 14 wild-type mice (open squares) and 12 homozygous pol eta knockout mice (open diamonds), eight of which were pol iota $^{+/+}$ and four of which were pol iota $^{+/-}$. We also irradiated 13 pol eta $^{+/-}$ / pol iota $^{-/-}$ mice and nine pol eta $^{+/+}$ / pol iota $^{-/-}$ mice, none of which developed skin tumors after 20 weeks of irradiation (not plotted). In fact, the latter mice did not develop skin tumors after more than 41 weeks.

DISCUSSION

This study provides new insights into the biological function of pol iota and has several implications regarding TLS and the mutagenic and carcinogenic effects of UV radiation.

POL IOTA PARTICIPATES IN TRANSLESION DNA SYNTHESIS

As expected based on results with human cells[52,107,108] and mouse embryonic fibroblasts[99], primary fibroblasts deficient in mouse pol eta alone are moderately sensitive to killing by UV irradiation compared to wild-type cells (Figure 4). Also, as expected based on results with *XPV* cells lacking functional pol eta[52], a deficiency in mouse pol iota strongly enhances UV light-induced mutagenesis at the endogenous *Hprt* locus (Figure 5). This is the starting point for the novel observation that UV mutagenesis in pol eta deficient cells is suppressed by inactivation of pol iota (Figure 5, Table 3). This suggests that pol iota participates in mutagenic bypass of UV photoproducts when pol eta is deficient. The fact that pol iota deficiency also suppresses UV-induced mutagenesis in pol eta proficient cells (Figure 5, Table 3) suggests that TLS is a normal function of pol iota, not only a replacement function when another TLS enzyme is missing.

The interpretation that pol iota can conduct mutagenic photoproduct bypass in mouse cells is consistent with earlier biochemical studies suggesting that pol iota contributes to enhanced UV mutagenesis in pol eta deficient XPV cells[68].

Our results however differ from a recent study in which pol iota expression in cultured 293T cells was decreased using siRNA[57]. In that study, decreased pol iota expression had no effect on UV-induced mutagenesis. In that study mutagenesis was detected using the *supF* gene present on an extrachromosomal shuttle vector and lead to the conclusion that that pol iota has no significant role in UV lesion bypass and mutagenesis. Experimental differences between that study and the ones presented here could account for the different conclusions. These differences include the reporter (a gene in a shuttle vector versus an endogenous chromosomal gene) used to monitor mutagenesis and possible incomplete silencing of pol iota in 293T cells.

The extent to which pol iota contributes to bypass of UV light induced lesions may partly depend on the type of photoproduct. Although pol eta bypasses *cis-syn* thymine-thymine dimers, it cannot bypass or insert nucleotides opposite the two distorted bases of a 6-4 photoproduct. In contrast, pol iota inserts nucleotides opposite 6-4 photoproducts. Because pol iota does not extend the resulting primer termini, other polymerases, e.g., pol kappa (pol κ) or pol zeta (pol ζ), have been suggested to perform that task. Thus pol iota's role may sometimes be subservient to pol eta, perhaps explaining why pol iota's affect on UV mutagenesis is about 2-fold lower when pol eta is present (Table 3). Perhaps pol iota predominantly inserts nucleotides opposite photoproducts not efficiently bypassed by pol eta. While that could occur at the replication fork, it may also possibly occur during filling of gaps left in the DNA after the fork has moved on[109]. However, when pol eta is missing, pol iota may assume a

somewhat larger role in bypassing UV photoproducts, consistent with a 5-fold mutagenic decrease when pol eta is absent (Table 3). Moreover, the details of TLS by pol iota could differ in the presence or absence of pol eta because the two enzymes physically interact and because pol iota localization to foci in UV irradiated human cells is reduced in pol eta-deficient cells[110] These ideas, and the identity of the photoproducts responsible for mutagenesis, could be tested by combining the pol eta and pol iota defects studied here with mice defective in global and transcription-coupled nucleotide excision repair, or with mice that express photolyases that selectively remove cyclobutane pyrimidine dimers or 6-4 photoproducts[111].

The specificity of strand bias in Table 3 implies that pol iota contributes to multiple types of UV-induced base substitutions. The pol iota-dependent substitution specificity in Table 3 is generally consistent with the insertion specificity of pol iota. Pol iota has been shown to preferentially misinserts dNTPs opposite template pyrimidines[66]. The exception may be the high rate of C to T transitions that could result from incorporation of dAMP opposite a damaged pyrimidine (Table 3). UV-induced C to T transitions may primarily result from "correct" insertion of dAMP opposite uracil that results from deamination of cystosine in photoproducts[112]. Based on that idea, the ability of pol iota to preferentially insert dGMP opposite U could theoretically be antimutagenic for cytosine deamination in general[70] and/ or during TLS of photoproducts[113] That hypothesis is not supported by our observations. The data presented here rather

52

support that pol iota promotes rather than suppresses UV-dependent mutagenesis for C to T transitions (Table 3).

POL ETA AND POL IOTA PARTICIPATE IN STRAND-SPECIFIC DNA TRANSACTIONS

In wild-type cells or cells deficient in pol eta alone or pol iota alone, there is a bias for UV-induced base substitutions at dipyrimidines on the non-transcribed DNA strand (Figure 6). This bias may reflect removal of photoproducts from the transcribed strand by transcription-coupled nucleotide excision repair, since such repair is known to alter the mutation spectrum[107,114]. Relative to wild-type cells, the strand bias is slightly reduced when pol eta or pol iota is deficient, and is eliminated when both enzymes are deficient (Figure 6). This suggests that both polymerases contribute to modulating mutagenic bypass of UV photoproducts in a strand-specific manner. The strand biases could be related to differences in leading versus lagging strand replication enzymology (see below), transcription, or perhaps a more prominent role in bypassing a subset of photoproducts that remain in the non-transcribed strand for a longer time.

STRAND BIAS FOR UV-INDUCED C-G TO A-T TRANSVERSIONS

The exception to the non-transcribed strand bias is that the majority of C-G to A-T substitutions are inferred to result from lesions in the transcribed strand. This observation in mouse cells is similar to results in XP variant cells[52]. In human cells, a chromosomal origin of replication is located 3′ to exon 1 of *Hprt*[115] implying that the transcribed strand of *Hprt* is replicated as the leading strand

template. That interpretation is consistent with studies of replication in extracts of XP variant cells, which generates a high proportion of C-G to A-T substitutions arising from replication of photoproducts on the leading strand template[51]. By extrapolation, the C-G to A-T substitutions in the present study may result from leading strand replication, leading to the further speculation that the non-transcribed strand bias discussed above could reflect TLS during replication of the lagging strand template. In addition to CPDs and 6-4 photoproducts, UV irradiation also generates oxidative damage to DNA. Thus, oxidative lesions like 8-oxo-guanine may contribute to the G-C to T-A transversions observed in irradiated fibroblasts, and possibly to the skin cancer. However, this may be unlikely since monobasic forms of DNA damage induced by the wavelengths used in the present study occur at less than 1% of the frequency of dipyrimidine photoproducts[116]. Interestingly, the CG to AT transversions on the transcribed strand largely originate when pol eta is deficient, suggesting that they are made by a different TLS polymerase, such as pol iota (Table 6, in pol eta deficient cells) or perhaps pol zeta or pol kappa (Table 7, double deficient-cells).

PARTICIPATION OF AT LEAST ONE OTHER POLYMERASE IN BYPASS OF UV PHOTOPRODUCTS

The observation that the UV-induced mutant frequency in cells deficient in both pol eta and pol iota (Table 3), is much higher than the spontaneous mutant frequency of un-irradiated cells indicates that at least one other polymerase performs mutagenic TLS. One candidate is pol zeta. Notably, yeast pol zeta has

recently been shown to efficiently bypass UV photoproducts when assisted by accessory proteins[117]. This polymerase, despite belonging to the B-family, which mostly contains high fidelity replicative polymerases remarkably copies undamaged templates with low fidelity[118].

POL IOTA HAS A FUNCTION IN DELAYING THE ONSET OF UV LIGHT-INDUCED SKIN CANCER

There are well known correlations between increased mutagenesis and increased carcinogenesis, and there is considerable evidence to support the hypothesis that a mutator phenotype promotes multistage carcinogenesis[119]. Thus, it was unexpected to observe that UV light-induced skin cancer is suppressed by pol iota (Figure 7), even though pol iota appears to contribute to mutagenic bypass of photoproducts (Figure 5 and Table 3). Several hypotheses can be considered. It could simply be that mutagenesis at the *Hprt* locus in primary fibroblasts does not reflect rate-limiting mutations in the cell types and/ or genes most relevant to development of skin tumors in mice. Against this are similar measurements of mutagenesis at the *Hprt* locus in pol eta-deficient *XPV* fibroblasts that do demonstrate elevated UV-induced mutant frequencies that correlate with elevated susceptibility to skin cancer. It could be that the function of pol iota that suppresses skin cancer is simply to bypass lesions, regardless of whether this is performed in an accurate or mutagenic fashion. Alternatively, pol iota could modulate cancer susceptibility via a function other than TLS. Recent studies have reported that polymerases implicated in TLS also participate in

recombination[120,121], in nucleotide excision repair[122], and in checkpoint response to UV irradiation[123]. If pol iota were to have similar roles in the absence of pol eta, then loss of function could increase susceptibility to skin cancer. In fact, loss of either TLS or checkpoint control due to pol iota deficiency might logically be anticipated to result in increased UV-induced cytotoxicity, Because the cytotoxic effect is not drastically increased could indicate that some photoproducts are initially tolerated and later bypassed by a different polymerase to yield delayed mutagenesis[124,125]. Another possibility is that pol iota may play an important role in development of normal immunity, such that a pol iota deficiency would compromise immune suppression of skin cancer and lead to increased susceptibility. Against this possibility are reports that class switch recombination and somatic hypermutation of immunoglobulin genes appear to be normal in 129-derived strains of mice[73,126]. Finally, it is formally possible that some cells in the double knockout mice may retain pol iota activity. As mentioned in the introduction, *129* mice are homozygous for a spontaneous C to A mutation in exon 2 that creates a nonsense codon in the *Pol iota* gene at Ser27, such that the protein should be truncated[73]. Indeed, no pol iota protein was detected by Western blotting of testis extracts of 129 mice using an antibody raised against the COOH terminus of murine pol iota that recognizes full-length or mis-spliced variants of pol iota[73]. However, a recent study[127] has reported that crude extracts of brain cells from 129/J mice (but not extracts of other 129/J cells) have the ability to insert dGMP opposite template T in an oligonucleotide primer-template. The authors claim that this misinsertion activity is due to pol iota, rather than any

of the other DNA polymerases that can insert dGMP opposite T, and they further speculate that brain cells of 129 mice contain alternatively-spliced pol iota that retains catalytic activity.

The observation that pol iota delays onset of skin cancer in pol eta deficient mice (Figure 7) is consistent with other studies suggesting a role for mouse pol iota in tumor suppression. The mouse *Pol iota* gene is on chromosome 18 and within the *Par2* (pulmonary adenoma resistance 2) locus that is a major determinant of susceptibility to urethane-induced pulmonary adenomas. Interestingly, two strains of mice with differing lung tumor susceptibility differ in *Pol iota* gene status by 25 nucleotides and 10 amino acids, and the two enzymes have altered substrate specificity, suggesting that pol iota is a modifier of lung tumorigenesis[128]. More recently, the defective *Pol iota* allele in the 129X1/Sv mouse strain that harbors the nonsense mutation in the coding sequence has been associated with susceptibility to urethane-induced lung tumors[129].

Table 4. UV-induced mutations at the Hprt locus in primary fibroblasts derived from Pol eta [+/+] Pol iota [+/+] mice.

Mutant	Mutation	Position	Surrounding sequence[a]	Amino acid changed	Strand with affected dipyrimidine
Dipyrimidine Base Substitutions					
Mutations involving cytosine					
WT7	C•G → T•A	74	ATA CCT AAT	Pro → Leu	Nontranscribed
WT15	C•G → T•A	74	ATA CCT AAT	Pro → Leu	Nontranscribed
WT3	C•G → T•A	74	ATA CCT AAT	Pro → Leu	Nontranscribed
WT19	C•G → T•A	113	ATT CCT CAT	Pro → Leu	Nontranscribed
WT1	C•G → T•A	145	AGA CTT GCT	Leu → Phe	Nontranscribed
WT18	C•G → T•A	145	AGA CTT GCT	Leu → Phe	Nontranscribed
WT512	C•G → T•A	145	AGA CTT GCT	Leu → Phe	Nontranscribed
WT412	C•G → T•A	151	GCT CGA GAT	Arg → STOP	Nontranscribed
WT4	C•G → T•A	209	AAG GGG GGC	Gly → Glu	Transcribed
WT14	C•G → T•A	508	TCT CGA AGT	Arg → STOP	Nontranscribed
WT22	C•G → T•A	550	ATT CCA GAC	Pro → Ser	Nontranscribed
WT112	C•G → T•A	550	ATT CCA GAC	Pro → Ser	Nontranscribed
WT15	C•G → T•A	601	AGG GAT TTG	Asp → Asn	Transcribed
WT40	C•G → A•T	134	GAC AGG ACT	Arg → Met	Transcribed
WT35	C•G → A•T	379	ACT GGA AAG	Gly → STOP	Transcribed
Mutations involving thymidine					
WT44	T•A → C•G	194	GCC CTC TGT	Leu → Pro	Nontranscribed
WT6	T•A → A•T	125	CTG ATT ATG	Ile → Asn	Nontranscribed
WT51	T•A → A•T	125	CTG ATT ATG	Ile → Asn	Nontranscribed
WT7	T•A → A•T	125	CTG ATT ATG	Ile → Asn	Nontranscribed
WT28	T•A → A•T	245	TAC ATT AAA	Ile → Asn	Nontranscribed
WT8	T•A → A•T	245	TAC ATT AAA	Ile → Asn	Nontranscribed
WT532	T•A → A•T	410	ATA ATT GAC	Ile → Asn	Nontranscribed
WT213	T•A → G•C	194	GCC CTC TGT	Leu → Arg	Nontranscribed
WT512	T•A → G•C	194	GCC CTC TGT	Leu → Arg	Nontranscribed
WT10	T•A → G•C	424	AAA ACA ATG	Thr → Pro	Transcribed
WT71	T•A → G•C	449	CTG GTT AAG	Val → Gly	Nontranscribed
WT510	T•A → G•C	449	CTG GTT AAG	Val → Gly	Nontranscribed

Mutant	Mutation	Position	Surrounding sequence[a]	Amino acid changed	Strand with affected dipyrimidine
Nontandem double base substitutions					
WT2	C•G → T•A	113	ATT CCT CAT	Pro → Leu	
	C•G → A•T	115		His → Asn	
WT12	C•G → T•A	113	CCT CAT GGA	Pro → Leu	
	C•G → A•T	118		Gly → STOP	
Nondipyrimidine base substitutions					
WT31[b]	C•G → A•T	157	GAT GTC ATG	Val → Phe	
WT43	T•A → A•T	1	GTC ATG CCG	START → Leu	
Frameshifts					
WT83	+T	372 – 374	ACT TTA ACT		
WT11	+T	655	AAA GCC TAA	STOP → Leu	
Exon deletions					
WT96		Exon 2-3			
WT171		Exon 7			
Large insertion					
WT243	+67 bases	403,404			

[a]Sequences of the non-transcribed (coding) strand
[b]Ccomplex photoproducts have been suggested to occur at ACA sequences.

Table 5. UV-induced mutations at the Hprt locus in primary fibroblasts derived from Pol eta [-/-] Pol iota [+/+] mice.

Mutant	Mutation	Position	Surrounding sequence[a]	Amino acid changed	Strand with affected dipyrimidine
Dipyrimidine Base Substitutions					
Mutations involving cytosine					
H6	C•G → T•A	74	ATA CCT AAT	Pro → Leu	Nontranscribed
H3	C•G → T•A	74	ATA CCT AAT	Pro → Leu	Nontranscribed
H31	C•G → T•A	464	AGC CCC AAA	Pro → Leu	Nontranscribed
H5	C•G → T•A	464	AGC CCC AAA	Pro → Leu	Nontranscribed
H29	C•G → T•A	464	AGC CCC AAA	Pro → Leu	Nontranscribed
H12	C•G → T•A	544	TTT GAA ATT	Glu → Lys	Transcribed
H2	C•G → T•A	551	ATT CCA GAC	Pro → Leu	Nontranscribed
H15	C•G → T•A	551	ATT CCA GAC	Pro → Leu	Nontranscribed
H9	C•G → T•A	551	ATT CCA GAC	Pro → Leu	Nontranscribed
H62	C•G → A•T	329	CAG TCA ACG	Ser → STOP	Nontranscribed
H18	C•G → A•T	329	CAG TCA ACG	Ser → STOP	Nontranscribed
H16	C•G → A•T	355	GGT GGA GAT	Gly → STOP	Transcribed
H13	C•G → A•T	400	GTT GAA GAT	Glu → STOP	Transcribed
H1	C•G → A•T	580	CTT GAC TAT	Asp → Tyr	Transcribed
H17	C•G → A•T	589	AAT GAG TAC	Glu → STOP	Transcribed
H23	C•G → A•T	601	AGG GAT TTG	Asp → Tyr	Transcribed
H21	C•G → A•T	606	GAT TTG AAT	Leu → Phe	Transcribed
H14	C•G → A•T	634	ACT GGA AAA	Gly → STOP	Transcribed
H19	C•G → G•C	550	ATT CCA GAC	Pro → Ala	Nontranscribed

Mutant	Mutation	Position	Surrounding sequence[a]	Amino acid changed	Strand with affected dipyrimidine
H23	T•A → A•T	214	GGC TAT AAG	Tyr → Asn	Nontranscribed
H24	T•A → A•T	389	AAT GTC TTG	Val → Asp	Nontranscribed
H71	T•A → A•T	389	AAT GTC TTG	Val → Asp	Nontranscribed
H85	T•A → A•T	437	ACT TTG CTT	Leu → STOP	Nontranscribed
H45	T•A → A•T	543	GGA TTT GAA	Phe → Leu	Nontranscribed
H76	T•A → C•G	203	GTG CTC AAG	Leu → Pro	Nontranscribed
H90	T•A → C•G	203	GTG CTC AAG	Leu → Pro	Nontranscribed
H53	T•A → C•G	254	GCA CTG AAT	Leu → Pro	Nontranscribed
H84	T•A → C•G	392	GTC TTG ATT	Leu → Ser	Nontranscribed

Mutant	Mutation	Position	Surrounding sequence[a]	Amino acid changed	Strand with affected dipyrimidine
H26	T•A → C•G	404	GAA G<u>AT</u> ATA	Asp → Gly	Transcribed
H78	T•A → C•G	437	ACT T<u>TG</u> CTT	Leu → Ser	Nontranscribed
H30	T•A → C•G	542	GGA T<u>TT</u> GAA	Phe → Ser	Nontranscribed
H2	T•A → G•C	655	AAA GCC <u>T</u>AA	STOP→ Glu	Nontranscribed
Tandem dipyrimidine base substitutions					
H81	C•G → T•A	112			
	C•G → T•A	113	ATT <u>CC</u>T CAT	Pro → Phe	Nontranscribed
H20	C•G → T•A	112			
	C•G → T•A	113	ATT <u>CC</u>T CAT	Pro → Phe	Nontranscribed
Nondipyrimidine base substitutions					
H7[b]	C•G → A•T	617	GTT T<u>GT</u> GTC	Cys → Phe	
H22[b]	T•A → A•T	109	TTT <u>AT</u>T CCT	Ile → Phe	
H27[b]	T•A → G•C	584	GAC T<u>AT</u> AAT	Tyr → Ser	
H91[b]	T•A → G•C	584	GAC T<u>AT</u> AAT	Tyr → Ser	
Frameshift mutations					
H99	+T	578 – 579	GCC C<u>TT</u> GAC	Asp → STOP	
H37	−TA	520, 521	GGA <u>TA</u>C AGG		
Exon deletions					
H25		Exon 2			
H10		Exon 2			
H8		Exon 2-3			
H60		Exon 2-5			
H68		Exon 2-7			
Deletions					
H11[c]		Δ403 – 456			
H4[c]		Δ404 – 448			
H93[d]		Δ533 – 553			

[a]Sequences of the non-transcribed (coding) strand
[b]Ccomplex photoproducts have been suggested to occur at ACA and TGT sequences.
[c]Presumed cryptic splice acceptor within exon 6
[d]Presumed cryptic splice acceptor within exon 8

Table 6. UV-induced mutations at the Hprt locus in primary fibroblasts derived from Pol eta [+/+] Pol iota [-/-] mice.

Mutant	Mutation	Position	Surrounding sequence[a]	Amino acid changed	Strand with affected dipyrimidine
Dipyrimidine Base Substitutions					
Mutations involving cytosine					
I2	C•G → T•A	113	ATT CCT CAT	Pro → His	Nontranscribed
I1	C•G → T•A	209	AAG GGG GGC	Gly → Glu	Transcribed
I5	C•G → T•A	325	GAT CAG TCA	Gln → STOP	Nontranscribed
I42	C•G → T•A	463	AGC CCC AAA	Pro → Ser	Nontranscribed
I62	C•G → T•A	544	TTT GAA ATT	Glu → Lys	Transcribed
I32	C•G → A•T	634	ACT GGA AAA	Gly → STOP	Nontranscribed
Mutations involving thymidine					
I24	T•A → A•T	64	TTG TTT TGT	Phe → Ile	Nontranscribed
I28	T•A → A•T	64	TTG TTT TGT	Phe → Ile	Nontranscribed
I79	T•A → A•T	125	CTG ATT ATG	Ile → Asn	Nontranscribed
I17	T•A → A•T	245	TAC ATT AAA	Ile → Asn	Nontranscribed
I6	T•A → A•T	247	AAT AAA GCA	Lys → STOP	Transcribed
Tandem dipyrimidine base substitutions					
I14	C•G → T•A	171	ATG GGA GGC	Met → Ile	Transcribed
	C•G → T•A	172		Gly → Arg	
I22	C•G → A•T	112	ATT CCT CAT	Pro → Ile	Nontranscribed
	C•G → T•A	113		Pro → Ile	
I12	T•A → A•T	389	AAT GTC TTG	Val → Asp	Nontranscribed
	C•G → T•A	390		Val → Asp	
Nontandem double base substitutions					
I8	C•G → A•T	589	AAT GAG TAC	Glu → STOP	
	C•G → T•A	591		Glu → STOP	
I91	C•G → T•A	599	TTC AGG GAT	Arg → Lys	
	C•G → T•A	601		Asp → Asn	

62

Mutant	Mutation	Position	Surrounding sequence[a]	Amino acid changed	Strand with affected dipyrimidine
Nondipyrimidine base substitutions					
I3[b]	C•G → A•T	397	ATT <u>G</u>TT GAA	Val → Phe	
I161	C•G → A•T	482	GTT G<u>C</u>A AGC	Ala → Glu	
Exon deletions					
I412			Exon 2-3		

[a]Sequences of the non-transcribed (coding) strand
[b]Ccomplex photoproducts have been suggested to occur at ACA sequences.

Table 7. UV-induced mutations at the Hprt locus in primary fibroblasts derived from Pol eta [-/-] Pol iota [-/-] mice.

Mutant	Mutation	Position	Surrounding sequence[a]	Amino acid changed	Strand with affected dipyrimidine
Dipyrimidine Base Substitutions					
Mutations involving cytosine					
HI761[b]	C•G → T•A	34	AGC <u>G</u>AT GAT	Asp → Asn	Transcribed
HI757	C•G → T•A	325	GAT C<u>A</u>G TCA	Gln → STOP	Nontranscribed
HI7	C•G → T•A	464	AGC C<u>C</u>C AAA	Pro → Leu	Nontranscribed
HI759[b]	C•G → T•A	493	CTG <u>G</u>TG AAA	Val → Met	Transcribed
HI81	C•G → A•T	538	GTT <u>G</u>GA TTT	Gly → STOP	Transcribed
HI61	C•G → A•T	606	GAT TT<u>G</u> AAT	Leu → Phe	Transcribed
HI759[b]	C•G → A•T	606	GAT TT<u>G</u> AAT	Leu → Phe	Transcribed
HI761[b]	C•G → A•T	606	GAT TT<u>G</u> AAT	Leu → Phe	Transcribed
Mutations involving thymidine					
HI76	T•A → C•G	146	AGA C<u>T</u>T GCT	Leu → Pro	Nontranscribed
HI761[b]	T•A → C•G	203	GTG C<u>T</u>C AAG	Leu → Pro	Nontranscribed
HI10[b]	T•A → C•G	194	GCC C<u>T</u>C TGT	Leu → Pro	Nontranscribed
HI4	T•A → A•T	247	ATT <u>A</u>AA GCA	Lys → STOP	Transcribed
HI11	T•A → A•T	543	GGA TT<u>T</u> GAA	Phe → Leu	Nontranscribed
HI10[b]	T•A → A•T	656	GCC T<u>A</u>A GAT	STOP → Leu	Transcribed
Tandem dipyrimidine base substitutions					
HI63	C•G → T•A	112	ATT <u>CC</u>T CAT	Pro → Phe	Nontranscribed
		113			
Tandem non-dipyrimidine base substitutions					
HI86	T•A → G•C	516	AGT GT<u>T</u> GGA	Val → Val	
	C•G → A•T	517	AGT GT<u>T</u> GGA	Gly → STOP	

Mutant	Mutation	Position	Surrounding sequence[a]	Amino acid changed	Strand with affected dipyrimidine
Nondipyrimidine base substitutions					
HI2[c]	C•G → A•T	617	GTT T<u>G</u>T GTC	Cys → Phe	
HI759[b,c]	C•G → T•A	243	GAT TA<u>C</u> ATT	Tyr → Tyr	
HI62[c]	T•A → A•T	109	TTT <u>A</u>TT CCT	Ile → Phe	
Frameshifts					
HI6	ΔA	451,452	GTT <u>AA</u>G CAG		
Exon deletions					
HI83		Exon 2-3			
HI32		Exon3			
HI114		Exon 4			
HI9		Exon 5			
HI82		Exon 8			

[a] Sequences of the nontranscribed (coding strand)
[b] Mutants containing multiple dimer sites at greater than 150 nucleotides apart
[c] Ccomplex photoproducts have been suggested to occur at ACA and TGT sequences.

CHAPTER III

REV1 INHIBITION REDUCES THE INCIDENCE OF MURINE LUNG

TUMORS

SUMMARY

REV1 is a Y-family polymerase that has catalytic and structural functions

that implicate it in translesion replication across pre-mutagenic lesions in

Saccharomyces cerevisae[45], mouse[93] and human cells[130]. The studies covered

within this chapter test the hypothesis that a reduction in the mutagenic load,

through REV1 inhibition, will reduce the incidence of cancer. To test this

hypothesis, vectors that express a ribozyme inhibitory RNA against REV1 were

created. One vector was designed to target the nucleus (Rz407pU6) and the

other the cytoplasm (Rz407pN2A). These vectors were complexed with the

cationic polymer polyethylenimine (PEI) and tested for their ability to reduce

REV1 mRNA in cell culture. Of the two vectors, the nuclear vector (Rz407pU6)

clearly showed reduced levels in REV1 mRNA after transfection in NIH 3T3 cells.

To reduce REV1 in the murine lung the Rz407pU6 vector was delivered via non-

invasive PEI/ transgene aerosol therapy. This strategy is widely employed as an

effective non-viral transgene delivery method and is noted as having low

cytotoxicity, direct pulmonary transgene delivery, and long transgene expression. To determine REV1 mRNA levels in the mouse lung, after PEI/Rz407pU6 delivery, laser capture microdissection (LCM) was used in conjunction with real-time RT-PCR. Isolation of bronchial epithelial cells (BEC) from the lung tissue in conjunction with real-time RT-PCR indicated REV1 mRNA levels were reduced by at least 50% in the bronchial epithelium.

Ribozyme-mediated REV1 inhibition was used either before or after subjecting A/J mice through a carcinogen (B[a]P-induced) lung tumor model[131,132]. After monitoring the mice for an extended period of time, mice were analyzed for tumor burden via micro-positron emission tomography (microPET) using the common tracer, [F-18]-fluorodeoxyglucose (FDG). Mice were scanned at 12, 16, and 20 weeks with no obvious tumor formation observed. Tumors were known to be present in 20 week-old mice by physical dissection and visualization of the lung. MicroPET imaging either lacked the resolution or the tumors were not metabolically active enough, opposed to surrounding tissue, to support further microPET scanning. MicroPET screening was therefore abandoned and tumor burden, individual tumor size, and tumor location were elucidated via lung dissection after experiment termination.

After ~28 weeks post carcinogen injection, there was a statistically significant (p value <.02) reduction in tumor multiplicity in animals that received aerosolized PEI/Rz407pU6 complex before carcinogen treatment. This reduction was observed only in animals that received Rz407pU6 24 and 48 hours before B[a]P injection. Mice receiving the PEI/Rz407pU6 complex developed

approximately 3.4 tumors per lung compared to approximately 6.4 in mice receiving B[a]P alone. In addition to having a lower tumor multiplicity, REV1 inhibition prevented tumor formation in 27% of the carcinogen treatment group. Tumor size or classification was not affected by treatment. Additionally, when REV1 reduction occurred ~4 weeks post-carcinogen administration, no statistically significant effects in tumor number, size, or mice mortality were observed.

We deduce that the inhibition of tumor development seen with REV1 inhibition is directly related to a reduction in the total number of mutations resulting from REV1-dependant mutagenic bypass of B[a]P lesions. The data presented here collectively support the use of noninvasive aerosolized PEI gene therapy and the use of ribozyme inhibitory RNAs in the chemoprevention of lung disease. Furthermore these studies show REV1 as having a primary function in TLS and indicate targeting mutagenic TLS polymerases can be an effective chemoprevention strategy to reduce the incidence of cancer.

MATERIALS AND METHODS

RIBOZYME DESIGN AND RECOMBINANT PLASMID CONSTRUCT

Hammerhead ribozymes were designed according to established structural and sequence principles, maintaining the conserved catalytic core and variable target-specific 5'- and 3'-arms[133-135]. A GUC cleavage sites at position 407 on the mouse REV1 mRNA (homologous to position 618 on the human REV1 mRNA) was chosen based on potentially accessible loop structures of the mouse REV1 mRNA, as modeled with the MFOLD program [136]. BLAST search determined that the targeted sequence for mouse REV1 around the GUC cleavage site has no homology to any other murine REV RNAs and is unique to the mouse REV1 target gene (Figure 8). The pLNSX-based retroviral vector pN2A-tRNA (gift of Dr. H. Kobayashi, Univ. of Tokyo, Japan) modified with a Pol III-tRNA gene ribozyme expression cassette is used for ribozyme expression (Figure 9). This promoter system directs the fused tRNA-ribozyme transcripts into the cytoplasm, the natural cellular compartment for tRNAs[137-141]. Alternatively, the ribozyme was cloned into pU6+27 vector containing a human U6 snrp RNA promoter/5'-stem-loop/3'-terminator element (gift of Dr. D. Engelke)[142].

Custom-synthesized DNA oligonucleotides coding for ribozymes were annealed and cloned between Sac II and Mlu I sites of the expression cassette in pN2A-tRNA and the Sal I and Xba I sites of the expression cassette in pU6+27, generating the ribozyme clones Rz407pN2A and Rz407pU6 respectively. Thus, the cloned ribozyme inserts are transcribed from the constitutive Pol III tRNA and

U6 promoters. The sequences coding for ribozymes were as follows; the underlined regions correspond to the catalytic ribozyme core; the bold and italic regions to restriction site ends.

Rz407 pN2A upper strand:

5' ***GG***TGCAGCC<u>CTGATGAGTCCGTGAGGACGAAAC</u>GGCTTGGTGT***A*** 3'

Rz407 pN2A lower strand:

5'***CGCGT***ACACCAAGCC<u>GTTTCGTCCTCACGGACTCATCAG</u>GGCTGCA***CCG***
C 3'

Rz407pU6 upper strand:

5' ***TCGAC***TGCAGCC<u>CTGATGAGTCCGTGAGGACGAAAC</u>GGCTTGGTGT***T*** 3'

 Rz407pU6lower strand:

5' ***CTAGA***ACACCAAGCC<u>GTTTCGTCCTCACGGACTCATCAG</u>GGCTGCA***G*** 3'

The presence of ribozyme inserts in clones were confirmed by sequencing and PCR. Large scale (16L) endotoxin free plasmid production was performed by Bayou Biolabs, LA.

```
5'    A CAC CAA GCC GUC^    GGC UGC A    3' (REV1 mRNA)
3'    U GUGGUU CGG CA        CCG ACG U    5' (Active Ribozyme)
                    A         C
                    A        U G
                     G              A
                      C=G  A G U
                      A=U
                      G=C
                      G=C
                    A         G
                      G U
```
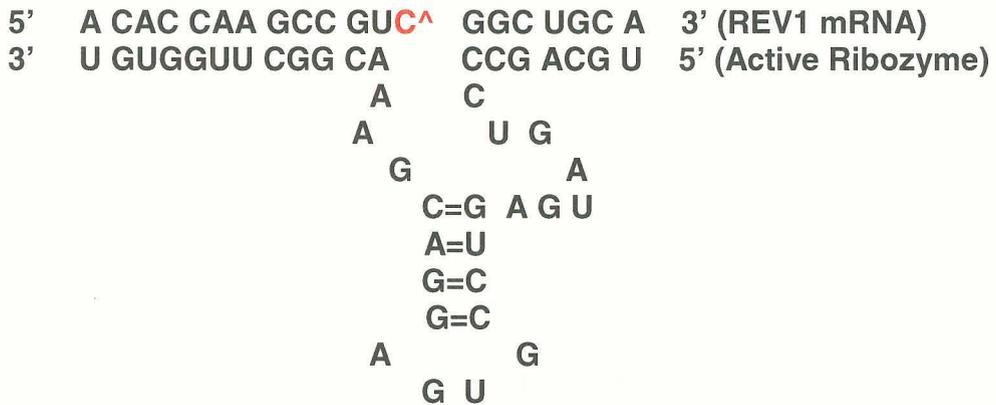
Figure 8. Structure of mouse REV1 ribozyme. Sequence of the target mRNA (top sequence) and the catalytically active ribozyme (bottom sequence) are shown. The two sequence recognition arms are shown base paired with the mouse REV1 target, surrounding the cleavage site at base 407, marked as C^. The central catalytic core is invariant.
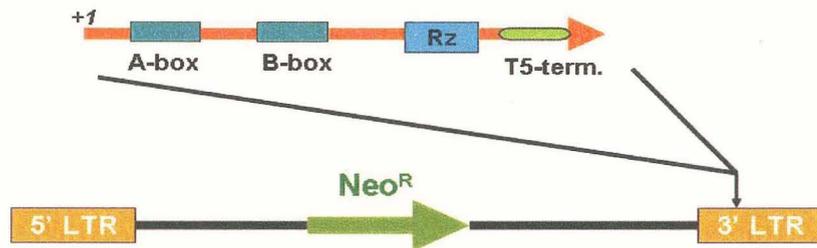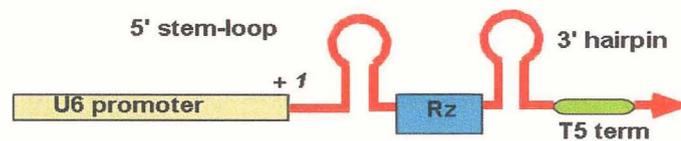
Figure 9. **Ribozyme expression cassettes designed to target REV1 mRNA .**
a. tRNA-Rz cassette for cytoplasmic localization, showing the human tRNA[Met]
gene with its A- and B-box internal promoters and the Pol III terminator region.
The ribozyme-coding sequence was inserted at the 3' end upstream of the
terminator; the entire cassette was inserted into the 3'-LTR of the pN2A retroviral
vector. **b.** U6-Rz cassette for nuclear localization, showing the human U6
promoter, the native 5' and 3' stem-loop structures and the Pol III terminator. The
ribozyme-coding sequence was inserted between the loop elements, replacing
the native U6 RNA coding region.

PEI-DNA FORMULATIONS

Polyethylenimine (PEI), high molecular weight (water free), was obtained from Sigma-Aldrich (CAS9002-98-6). Stock solutions were prepared at a concentration of 4.3 mg/mL in $3xdH_2O$. Experiments were performed to optimize the charge ratio expressed as PEI nitrogen:DNA phosphorous (N:P) for the Rz407pU6 plasmid. A ratio of 15:1 N:P results in a 1.94:1 (PEI:DNA weight) ratio and was used for all *in vivo* experiments. The desired amount of DNA (2 mg, endotoxin free) was mixed in 5 ml of $3xdH_2O$ per nebulization experiment. PEI was also mixed with 5 ml 3xdH2O. The DNA was slowly added to the PEI solution with vigorous vortexing after every 1 ml added. The solution was incubated at room temperature for 15 minutes prior to nebulization.

PEI/ DNA CELL TRANSFECTIONS

In vitro assays utilized Opti-MEM®I (GIBCO™) in lieu of H_2O in PEI/DNA complex preparation. Twenty minutes before transfection 2 µg of DNA in the forms of either gWiz™ luciferase [Aldeveron] or plasmid construct Rz407pN2A or Rz407pU6 was complexed with PEI as described above in the PEI-DNA formulations in 100µ Opti-MEM®I. NIH3T3 cells seeded at a density of $2x10^4$ cm^2 in six well plates had their growth media removed and the cells were rinsed in sterile PBS (pH 7.4). Appropriate dilutions of PEI/ DNA complexes was then added to each well to allow sufficient coverage. The cells were maintained at 37°C for at least 24 hours. Opti-MEM®I transfection media was then removed

and replaced with normal media for 24hrs before subsequent analysis with a luminometer (PharMingen Monolight™ 3010) or real-time RT- PCR.

JET-PEI/GFP COMPLEX TRANSFECTION

jetPEI™-FluoR is a tetramethyl rhodamine-conjugated linear polyethylenimine derivative (excitation at 555 nm; emission at 580 nm). jetPEI™-FluoR is useful for double labelling and colocalization experiments with green label using confocal microscopy (ie. green fluorescent protein). We utilized this rhodamine-conjugated PEI to deliver PCDNA3 GFP plasmid into NIH3T3 cells to visualize cellular uptake and location of PEI and GFP. NIH3T3 cells were plated in six well dishes at 5×10^5 cells per well. After cells attached ~24 hours the media was aspirated and cells washed with sterile PBS (pH 7.4). 4ug of PCDNA3 Green Fluorescent Protein (GFP) plasmid was combined with JetPEI™-FluoR (Polyplus transfections, France) at varying N:P ratios (ie 10:1, 20:1, and 30:1) diluted in enough Opti-MEM®I transfection media to cover wells (~2ml). Control wells received Opti-MEM®I transfection media only, GFP alone or JetPEI™. Transfection mixtures were allowed to saturate cells for 24 hours before visualization on fluorescent microscope outfitted with standard optical filter sets.

GENERAL ANIMAL

Fourteen week old, female A/J mice were used in these studies. Mice were obtained from Jackson Laboratories and housed within the Baxter building II animal research resource center (RRC). The animals were kept on 12 hr day/night cycles and fed normal chow.

IN VIVO NEBULIZATION

For exposure to nebulization procedures the mice were housed, five at a time, in a 22x9x10cm anesthesia chamber connected to Aero-Mist nebulizer (CIS-US Bedford, MA), (Figure 10). Normal air supplemented with 5% CO_2 at a 10 L/ min flow rate (as determined by a flow meter attached to the line connected between the air tank and nebulizer) was used to deliver 2 mg of DNA complexed with PEI via inhalation. Each treatment took approximately 30 minutes to complete. The mice tolerated the treatment well with no obvious signs of stress as determined by observing mouse behavior during nebulization.

CARCINOGENESIS PROCEDURES

Forty eight hours after first PEI treatment all mice were administered either a single bolus dose of 100 mg/ kg of B[a]P carcinogen or cornoil alone by intraperitioneal (IP) injection. All mice received by aerosol either, Rz407pU6/PEI or PEI (without DNA). Animals were sacrificed ~28 weeks post carcinogen injection.

Figure 10. Mouse nebulization chamber. For exposure to nebulization procedures the mice were housed, five at a time, in a 22x9x10cm anesthesia chamber connected to Aero-Mist nebulizer (blue top in picture (CIS-US Bedford, MA)) Normal air supplemented with 5% CO_2 was provided at a 10 L/min flow rate. Flow rate was determined by a flow meter attached to the line connected between the air tank and nebulizer (black rectangular box with knob). The nebulizer contained all PEI/DNA complex solutions.

HOMOGENATION OF WHOLE LUNG FOR LUCIFERASE AND REV1 EXPRESSION

Whole lung protein homogenates were obtained to analyze gWiz™ luciferase [Aldeveron] expression. For detecting potential strain differences PEI mediated transfection in Balb/c verses A/J mice, 2 mg of gWiz™ luciferase [Aldeveron] was complexed with PEI as indicated in PEI/DNA formulations section and delivered with a single treatment to three mice. Mice were sacrificed by overdose of ketamine/ xylazine. Mice received .5 ml of 8 mg/ ml ketamine/ 1.2 mg/ ml xylazine through IP injection. Lung were then dissected and rinsed in sterile PBS (pH 7.4) and immersed in RLB lysis solution provided in the *Renilla* Luciferase Assay System with Reporter Lysis Buffer Kit (Promega catalog# E4030). Samples were allowed one freeze/ thaw cycle to ensure complete lysis. Upon thawing an electric rotor/stator type tissue homogenizer (The Tissue-Tearor) was used to emulsify the sample. *Renilla* Luciferase substrate (provided in *Renilla* Luciferase Assay System Kit) was added to each sample and read using a luminometer (PharMingen Monolight™ 3010). For the REV1 real-time PCR analyses, lungs were dissected and mRNA was extracted using an Rneasy® Mini Kit (Qiagen Cat. No. 74104). Samples were disrupted in guanidine isothiocyanate lysis buffer (provided in the kit) and homogenized using an electric rotor/stator type tissue homogenizer (The Tissue-Tearor). Ethanol was added to the lysate and each sample was applied to the Rneasy® mini column before centrifugation. RNase-Free DNase Set (Cat. No. 79254) was added to each column to ensure complete DNA removal, as required for real-time PCR, before

total RNA was extracted in RNase free water. RNA was stored at -80° prior to real-time analysis.

LASER CAPTURE MICRODISSECTION (LCM)

RNA isolated from whole lung homogenates did not indicate a reduction in the levels of REV1 following ribozyme administration as determined by real-time RT-PCR. Data however indicates bronchial epithelial cells significantly express PEI/ DNA complexes[143]. To isolate these cells form the surrounding tissue we utilized Laser Capture Microdissection (LCM) technology. To measure REV1 levels post Rz407pU6 treatment, lungs were dissected 24hrs after animals received 2 mg of the plasmid. Animals were euthanized, lungs removed and flash frozen in O.C.T. Compound (Tissue-Tek, Sakura, Torrence, CA) using a 2-Methylbutane (Sigma-Aldrich CAS 78-78-4) bath suspended in liquid nitrogen. The frozen lungs were immediately transported to -80°C in dry ice and sectioned in RNase free conditions. Lung sections were stained with HistoGene™ LCM Frozen Section Staining Kit (Arcturus, Mt. View, CA) and ~3000 cells were captured on a Arcturus Pixcell® IIe Laser Capture Microdissection (LCM) System (Arcturus, Mt. View, CA) machine using CapSure™ HS LCM Caps (Arcturus, Mt. View, CA). RNA was isolated using PicoPure™ RNA Isolation Kit (Arcturus, Mt. View, CA) and stored at -80°C prior to performing real-time RT-PCR.

QUANTITATION OF LUNG REV1 MRNA USING REAL-TIME RT-PCR

Real-time quantitative RT-PCR was performed using ABI PRISM 7900 Sequence Detection System (Applied Biosystems AB, Foster City, CA) using TaqMan Universal PCR Mix (Applied Biosystems, Foster City, CA); a gene specific MGB TaqMan Probe (Applied Biosystems); mouse REV1 primers; TaqMan Rodent GAPDH Control reagents (Rodent GAPDH internal control Probe, forward and reverse primers; Applied Biosystems) The TaqMan gene-specific probe and primers were designed using the ABI Prism Primer Express Software Version 1.5 (Applied Biosystems, Foster City, CA) The sequence of the mouse REV1 primers are as follows:

mREV1Frt (forward) - 5'CCGGGAGTTGGACGTTCA3';

mREV1Rrt (reverse)- 5'GCAAATCTCCACAAGTCTTAATCC3';

The sequence of the mREV1 TaqMan Probe is as follows:

6FAM-AGCTTGCATCTTCG-MGBNFQ

Relative amounts of target RNA for duplicate sample runs were quantitated with the instrument software and normalized to the corresponding GAPDH values. Fold change values were calculated using the comparative C_T method (2^{-CT})[144].

MICRO-POSITRON EMISSION TOMOGRAPHY (MICROPET)

Micro-positron emission tomography (microPET) was used in these studies to visualize lung tumor development in mice. The microPET scans were performed at the James Graham Brown Cancer Center (JGBCC) utilizing a paid service. Mice were fasted for 16 hours prior to microPET. These animals were then transported from the Baxter II animal research resource center (RRC) to the JGBCC where the imaging took place. Mice were scanned at 12, 16, and 20 weeks, using the common tracer, [F-18]-fluorodeoxyglucose (FDG). Following scans mice were given normal chow and housed at the JGBCC for 24 hours before returning to the Baxter II animal facility.

TUMOR BURDEN/ HISTOLOGY

To determine tumor burden, lungs from sacrificed animals were placed in Tellyesniczky's Solution (90% ethanol, 5% formalin <10%>, and 5% acetic acid) for 24 hours followed by immersion in 70% ethanol for a minimum of 24 hours. Individual lobes of the lungs were separately dissected and gross tumors counts were performed on the surface of each lobe using a light box. Pathology was performed on paraffin embedded sections stained with haematoxylin and eosin (H&E) stain.

STATISTICS

Statistical analyses consisted of a negative binomial regression and planned post hoc comparisons between individual groups for tumor multiplicity count data. One-way ANOVA and t-tests between individual groups were used elsewhere when appropriate. Data with a trend p value of 0.05 or less were considered significant.

RESULTS

OPTIMIZATION OF PEI-REPORTER GENES AND PEI-RIBOZYME TRANSFECTION IN NIH3T3 CELLS.

The N:P ratio (PEI nitrogen:DNA phosphorous) has a significant impact on transfection efficiency and must be optimized. We used a reporter gene gWiz™ luciferase [Aldeveron] and the Rz407pU6 and Rz407pN2A constructs to verify expression of plasmids constructs, optimization of N:P (PEI nitrogen:DNA phosphorous) ratios, and verify inhibition of REV1 in both NIH3T3 cells and the murine lung.

The greatest expression was observed in NIH3T3 cells receiving PEI/gWiz™ luciferase (PEI/Luc) at a N:P ratio of 20:1 illustrated (Figure 11). However, when the same cell line was exposed to PEI-Rz407pU6 (2 μg of 2.9 kb plasmid) complex at varying N:P ratios (10:1, 20:1, 30:1) the largest reduction in REV1 mRNA was observed using a 10:1 N:P ratio (Figure 12). Delivery of both plasmids Rz407pU6 and Rz407pN2A in NIH 3T3 cells showed no additive effect. Rz407pN2A actually appear to inhibit REV1 reduction in these cells (Figure 13).
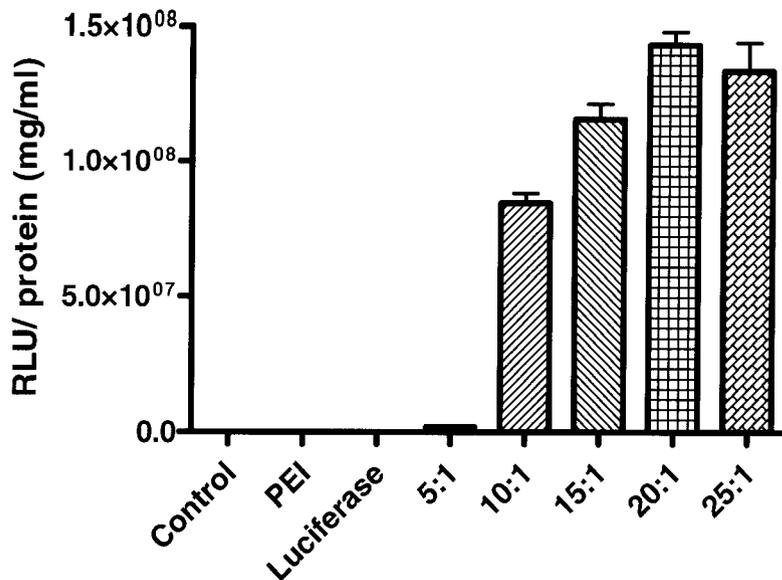
Figure 11. Luciferase expression in NIH3T3 cells following PEI/ LUC transfection. NIH3T3 cells seeded at a density of $2x10^4$ cm^2 in six well plates had their growth media removed and the cells were rinsed in sterile PBS (pH 7.4). Appropriate dilutions of PEI/ Luciferase complex was then added to each well to allow sufficient coverage. The cells were maintained at 37°C for at least 24 hours before lysis and analysis using a luminometer. Graph illustrates significant luciferse expression in NIH3T3 using 5-25:1 N:P ratios.

REV1 mRNA levels in NIH 3T3 cells
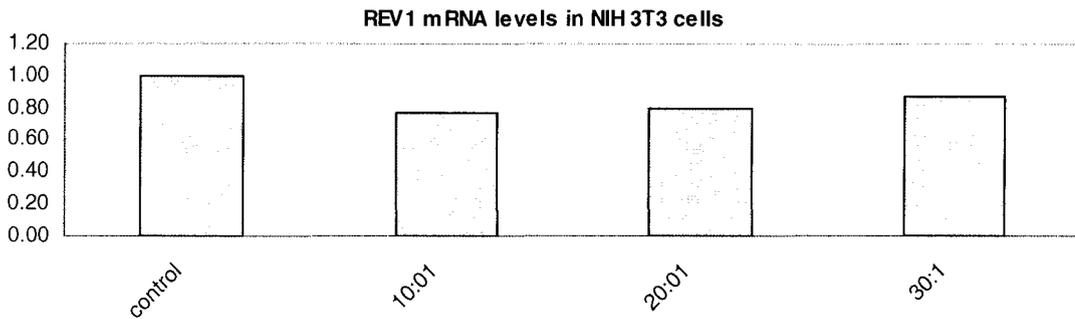
Figure 12. Analysis of REV1 mRNA inhibition in NIH 3T3 cells by real-time
RT PCR after PEI/ Rz407pU6 transfection. NIH3T3 cells seeded at a density of
$2x10^4$ cells/ cm^2 in six well plates had their growth media removed and the cells
were rinsed in sterile PBS (pH 7.4). Appropriate dilutions of PEI/ Rz407pU6
complex were added to each well. Real-time RT PCR analysis occurred after 24
hours. REV1 inhibition was most significant with the Rz407pU6 plasmid using a
10:1 ratio.

REV1mRNA levels in NIH3T3 cells
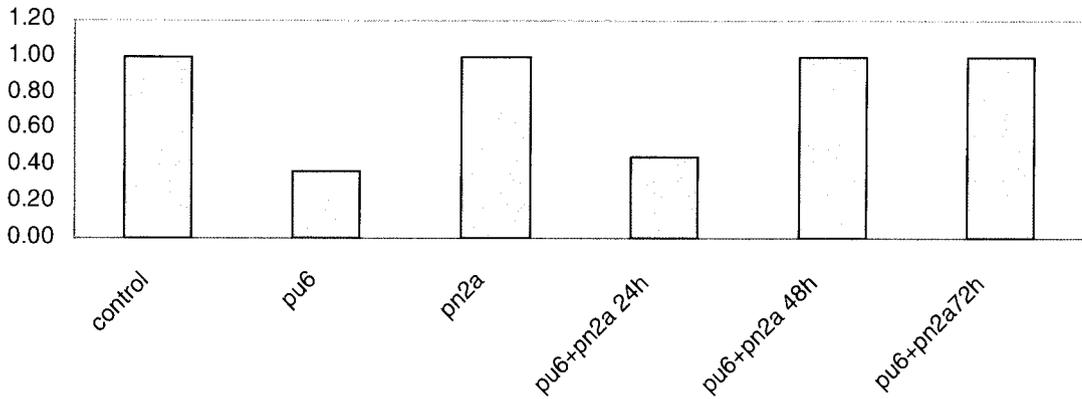
Figure 13. Analysis of REV1 mRNA inhibition in NIH 3T3 cells by real-time RT PCR after PEI/ Rz407pU6 and Rz407pN2A transfection. NIH3T3 cells seeded at a density of 2×10^4 cells/ cm^2 in six well plates had their growth media removed and the cells were rinsed in sterile PBS (pH 7.4). Appropriate dilutions of PEI/ Rz407pU6 complex were added to each well. Real-time PCR analysis occurred after 24 hours.

VISUALIZATION OF JET-PEI AND GREEN FLOURESCENT PROTEIN IN MURINE NIH3T3 CELLS.

NIH 3T3 cells were treated with jetPEI™-FluoR / PCDNA3 GFP complexes in six well dishes. Transfection mixtures were allowed to saturate cells for 24 hours before visualization on fluorescent microscope outfitted with standard optical filter sets. Control cells transfected with jetPEI™-FluoR only showed high cellular uptake of jetPEI™-FluoR (data not shown), while GFP only did not transfect. Cells treated with the jetPEI™-FluoR / PCDNA3 GFP complex showed broad cellular distribution of jetPEI™-FluoR (Figure 14, red) and expression of GFP reporter plasmid in smaller foci (Figure 14, green).
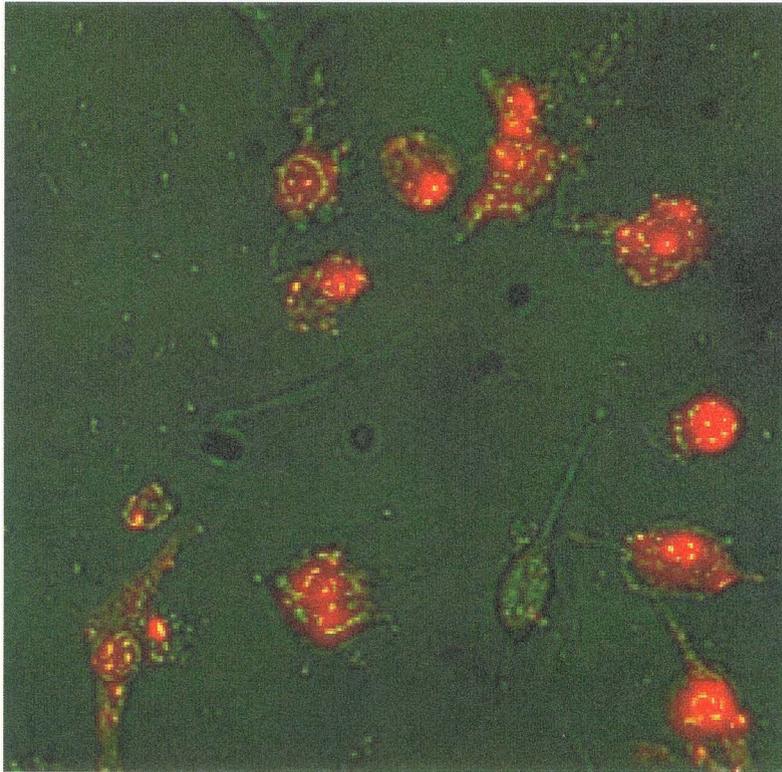
Figure 14. Visualization of jetPEI™-FluoR and PCDNA3-GFP in NIH3T3 cells. NIH 3T3 cells were treated with jetPEI™-FluoR / PCDNA3 GFP complexes in six well dishes. Transfection mixtures were allowed to saturate cells for 24 hours before visualization on fluorescent microscope outfitted with standard optical filter sets. Cells treated with the jetPEI™-FluoR / PCDNA3 GFP complex showed broad cellular distribution of jetPEI™-FluoR (red) and expression of GFP reporter plasmid in smaller foci plasmid (green).

OPTIMIZATION OF PEI/ LUC TRANSFECTION IN LUNG TISSUE.

In vivo delivery of luciferase reporter gene was used to detect possible strain differences in Balb/c versus A/J mice in PEI mediated gene delivery. PEI/Luc was administered (based on the PEI/Luc N:P ratios established in cell culture) at a N:P ratio of 15:1. 2mg of the reporter gene gWiz™ luciferase [Aldeveron] was delivered in thirty minutes. Lungs were dissected 24-48 hours later and analyzed for luciferase expression (Figure 15). The highest expression occurred in Balb/c mice though there was significant expression in both strains. Collagenase was added in an attempt to reduce the total sample homogenation time for one sample set. The additional treatment of lungs in the homogenation step with collagenase, adversely effected the overall detection of luciferase (Figure 15, column 3 and 4) and was discontinued. Based on these experiments a N:P ratio of 15:1 (1.92:1 w/w) ratio was used for all subsequent *in vivo* experiments.
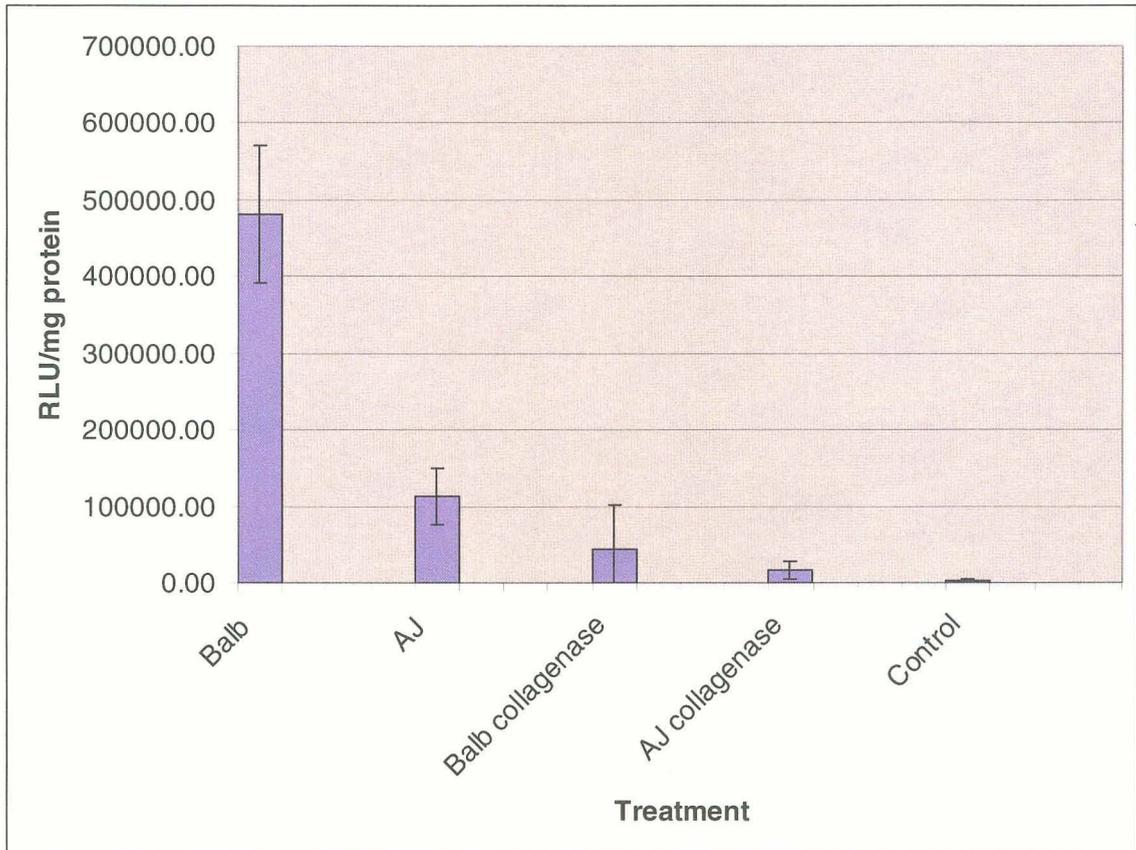
Figure 15. Luciferase expression in the lung. PEI/Luc was administered at a N:P ratio of 15:1 using 2 mg of the reporter gene gWiz™ luciferase [Aldeveron]. Graph represents relative light units (RLU)/ mg of lung protein 24-48 hours after transfection. Columns 3 and 4 show the decrease in RLU detection as result of the addition of collagenase before lysis.

LASER CAPTURE MICRODISSECTION

Mice were exposed twice to two milligram aerosolized doses of ribozyme plasmid Rz407pU6 complexed with PEI (15:1 N:P ratio) or PEI aerosol alone for 30 minutes in a whole body exposure chamber. Using laser capture micro-dissection it was possible to isolate only the bronchial epithelium in order to determine the expression of REV1. Figure 16 a shows a representative lung section as stained via Arcturus protocol before isolation. The subsequent picture Figure 16b shows the cap as it was isolated. The remaining photo Figure 16c shows the tissue after the cap was removed. LCM bronchial epithelium was examined after RNA isolation from ~3000 cells using real-time RT-PCR.

16a)   16b)   16c)

Figure 16a-c. Laser Capture Microdissection of Rz404pU6 treated lungs.
Lungs were dissected from the mice and flash frozen. Frozen lungs were
immediately transported to -80°C in dry ice and sectioned in RNase free
conditions. Lung sections were stained with HistoGene™ LCM Frozen Section
Staining Kit (Arcturus, Mt. View, CA) and cells captured on a Arcturus Pixcell® IIe
Laser Capture Microdissection (LCM) System (Arcturus, Mt. View, CA) machine
using CapSure™ HS LCM Caps (Arcturus, Mt. View, CA). RNA was isolated
using PicoPure™ RNA Isolation Kit (Arcturus, Mt. View, CA) and stored at -80°C
prior to performing real-time RT-PCR. 16a) 10x picture before capture. 16b) 10x
picture of cells captured on cap. 16c) 10x picture of tissue after removal of
capture cells.

REV1 EXPRESSION IN MOUSE LUNG FOLLOWING AEROSOL DELIVERY OF PEI/ RZ407PU6 COMPLEXES.

LCM allowed the isolation of bronchial epithelium tissue. This tissue was analyzed for REV1 transcript levels via real-time RT-PCR as described in the Materials and Methods section. These mice were taken in an unbiased manner 48 hours after treatment with Rz407pU6. Data in Figure 17 summarizes 3 independent real-Time RT-PCR experiments from two mice. Column 4 is the average of the two treated mice. The treatment of RZ407pU6 lead to an approximate 50% decrease in REV1 transcript (Figure 17).
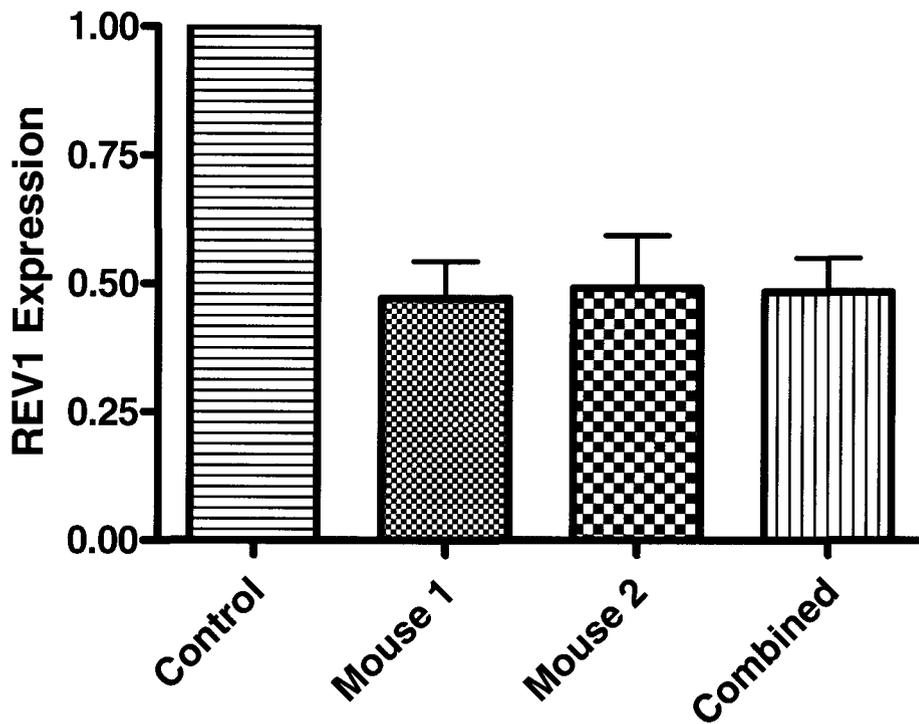
Figure 17. Inhibition of REV1 in the mouse lung. Graph represents a summary of 3 independent real-time RT-PCR experiments from two mice. Last bar is the average of the two treated mice. The treatment of RZ407pU6 lead to an approximate 50% decrease in REV1 transcript.

MICRO-POSITRON EMISSION TOMOGRAPHY (microPET)

The microPET scans of mice at 12, 16, and 20 weeks post-carcinogen injection were analyzed with the microPET manufacturers software. No lung tumors were visualized at any of the time points (12,16, or 20 weeks). During the 20 week scans, two B[a]P treated mice developed large site of injection tumors and had to be sacrificed. Upon visual inspection of the lungs, multiple >1mm tumors had arisen. MicroPET imaging was therefore determined inadequate in detecting B[a]P induced adenomas and was abandoned. Figure 18 illustrates a snap shot of a scan at 16 weeks.
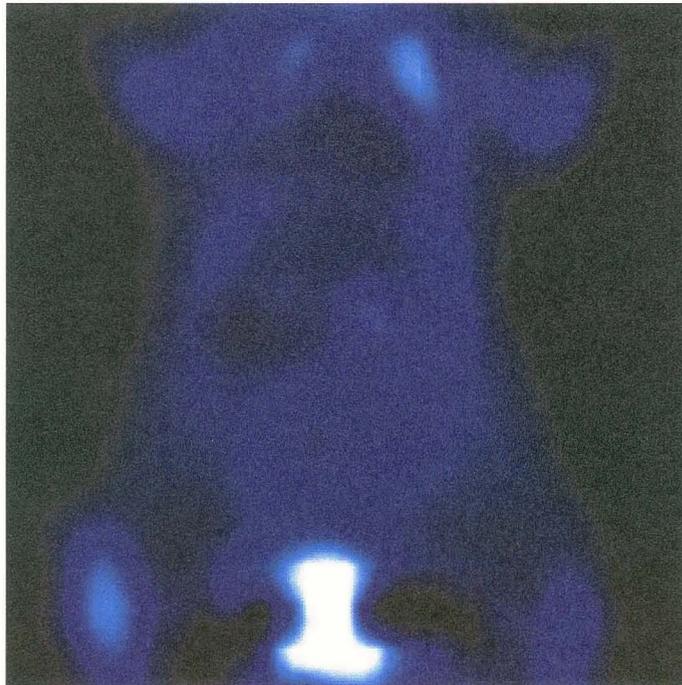
Figure 18. Micro-positron emission tomography (microPET). MicroPET scans were performed at the James Graham Brown Cancer Center (JGBCC) in collaboration with Dr. Chin Ng. Mouse pictured above was scanned at 16 weeks after B[a]P injection and PEI/Rz407pU6 complex inhalation using the common tracer, [F-18]-fluorodeoxyglucose (FDG). MicroPET imaging showed no indication of lung tumors.

INHIBITION OF LUNG TUMOR MULTIPLICITY AFTER AEROSOL DELIVERY OF PEI-RIBOZYME COMPLEXES.

We tested the efficacy of aerosol delivery of PEI- Rz407pU6 in the formation of B[a]P induced lung tumors in female A/J mice. Mice were exposed to 2mg of Rz407pU6 plasmid or control, 48 and 24hrs before treatment with 100mg/ kg B[a]P. After ~28 weeks post carcinogen the mice were sacrificed, lungs fixed, and tumor multiplicity and size recorded. Mice receiving B[a]P alone developed about 6.4 individual tumors per mouse (Figure 20, column 3). This was reduced to 3.4 tumors per lung (Figure 20, column 5) in mice receiving Rz407pU6. Statistical significance was reached using analysis that included negative binomial regression and planned post hoc comparisons between individual groups (p value <.02).

The female A/J mice used in these studies developed 0.5 spontaneous tumors per mouse (Figure 20, Column 1). Mice treated only with ribozyme developed .39 tumors per mouse (Figure 20, Column 2). The differences in spontaneous tumor burden between mice receiving PEI/corn oil alone and mice receiving cornoil plus Rz407pU6 did not reach statistical significance.

Treatment with PEI/ Rz407pU6 prevented the formation of tumors in 27% of the mice (Table 8, column 2). There was no apparent effect on which lobe tumors developed (Table 8). There was no increase or decrease in multiplicity or size when the PEI/ Rz407pU6 was given post carcinogen treatment when compared to carcinogen alone (Figure 19, compare columns 4 and 5). As expected, there remained a significant (p <.02) difference in tumor multiplicity

between treatment with PEI/ Rz407pU6 before B[a]P administration and PEI/ Rz407pU6 nebulization followed by B[a]P. Individual tumor sizes are plotted in Figure 20. There was no statistically significant difference between groups as determined by one-way ANOVA and t-tests.

Figure 19. Scatter plot of number of tumors that developed in female A/J mice. To determine tumor burden, lungs from sacrificed animals were placed in Tellyesniczky's Solution for 24 hours followed by emersion in 70% ethanol for a minimum of 24 hours. Individual lobes of the lungs were separately dissected and gross tumors counts were performed on the surface of each lobe using a light box. Graph represents the number of tumors per mouse for each group. B[a]P/ Ribozyme represents B[a]P injection before Rz407pU6 was administered (4 weeks post-carcinogen injection). Ribozyme/ B[a]P represents treatment with Rz407pU6 24 and 48 hours before B[a]P injection. Mice receiving B[a]P alone developed about 6.4 individual tumors per mouse (Table 20, column 3). This was reduced to 3.4 tumors per lung (Table 20, Column 5) in mice receiving Rz407pU6. Statistical significance (p value= .02) was reached using negative binomial regression and planned post hoc comparisons between individual groups.

Figure 20. Scatter plot of individual tumor size. To determine individual tumor size, lungs from sacrificed animals were placed in Tellyesniczky's Solution for 24 hours followed by emersion in 70% ethanol for a minimum of 24 hours. Individual lobes of the lungs were separately dissected and gross tumors counts were performed on the surface of each lobe using a light box. Graph represents the individual tumor size of all mice for each group. B[a]P/ Ribozyme represents B[a]P injection before Rz407pU6 was administerd (4 weeks post-carcinogen). Ribozyme/ B[a]P represents treatment with Rz407pU6 24 and 48 hours before B[a]P injection. There were no statistically significant differences between groups as determined by one-way ANOVA and t-tests between individual groups.

Table 8. Summary of tumor development			Total tumors in each lobe/ total tumors				
Group	No. of surviving mice	% of mice with tumors	Left Lung	Caudal Lobe	Cranial Lobe	Middle Lobe	Accessory Lobe
Control	12	42	50%	17%	0%	33%	0%
Rz407pU6	13	31	60%	20%	20%	0%	0%
B[a]P	12	100	38%	25%	17%	16%	4%
B[a]P+Rz407pU6	14	100	35%	28%	11%	14%	11%
Rz407pU6+B[a]P	15	73	43%	30%	11%	2%	15%

Table 8. Summary of lung tumor development. To determine tumor development, lungs from sacrificed animals were placed in Tellyesniczky's Solution for 24 hours followed by emersion in 70% ethanol for a minimum of 24 hours. Individual lobes of the lungs were separately dissected and gross tumors were measured on the surface of each lobe using a light box and ruler. Total tumors in each lobe for all groups reflected relative lobe size. The largest lobe is the left lung and contained the majority of tumors for each group. The caudal lobe second largest lobe and contained fewer tumors compared to the left lung but more than the remaining lobes. Relative tumor numbers in remaining lobes (cranial, middle, and accessory) were minimal.

TUMOR HISTOLOGY

Tumors from each treatment group were dissected from mice in each treatment group. Tumors were paraffin embedded and serial sectioned. Serial sections were treated with haematoxylin and eosin (H&E) stain. Sections were analyzed under a 10x microscope for differences in tumor histology. Mice in all five groups showed hyperplasia (Figure 21), and homogeneous spherical masses (Figure 21) that may or may not have compressed surrounding lung parenchyma, classified by A. Bennett Jenson, M.D. (Professor, Laboratory of Vaccinology, James Graham Brown Cancer Center) as adenoma (Figure 22). There was no histological evidence of metastasis (Figure 23).

Figure 21. Hyperplasia/ small adenoma formation in the murine lung. Lungs from sacrificed animals were placed in Tellyesniczky's Solution for 24 hours followed by emersion in 70% ethanol for a minimum of 24 hours. Lungs were paraffin embedded and sectioned at 8 μm. Sections were stained with haematoxylin and eosin (H&E) stain and analyzed on a microscope fitted with a camera. Tumors from all groups exhibited the same morphology. Pictured above is severe hyperplasia/ small adenoma formation as viewed at 10x.
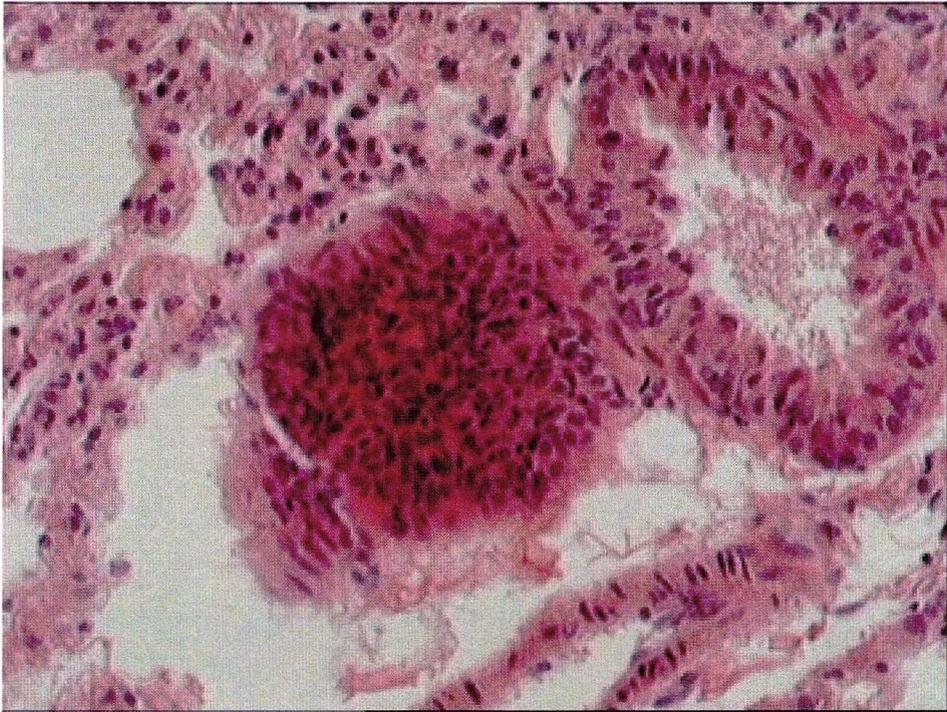
Figure 22. Adenoma formation in the murine lung. Lungs from sacrificed animals were placed in Tellyesniczky's Solution for 24 hours followed by emersion in 70% ethanol for a minimum of 24 hours. Lungs were paraffin embedded and sectioned at 8μm. Sections were stained with haematoxylin and eosin (H&E) stain and analyzed on a microscope fitted with a camera. Tumors from all groups exhibited the same morphology. Pictured above is an adenoma as viewed at 10x.
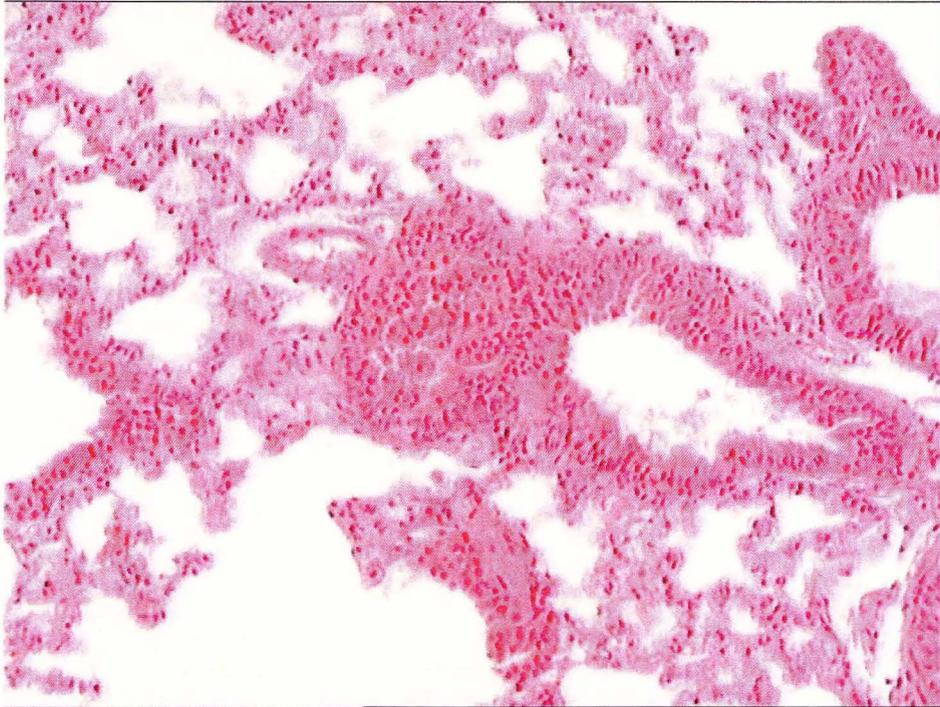
Figure 23. Massive adenoma formation in the murine lung.. Lungs from sacrificed animals were placed in Tellyesniczky's Solution for 24 hours followed by emersion in 70% ethanol for a minimum of 24 hours. Lungs were paraffin embedded and sectioned at 8μm. Sections were stained with haematoxylin and eosin (H&E) stain and analyzed on a microscope fitted with a camera. Tumors from all groups exhibited the same morphology. Pictured above is a massive adenoma as viewed at 10x.

DISCUSSION

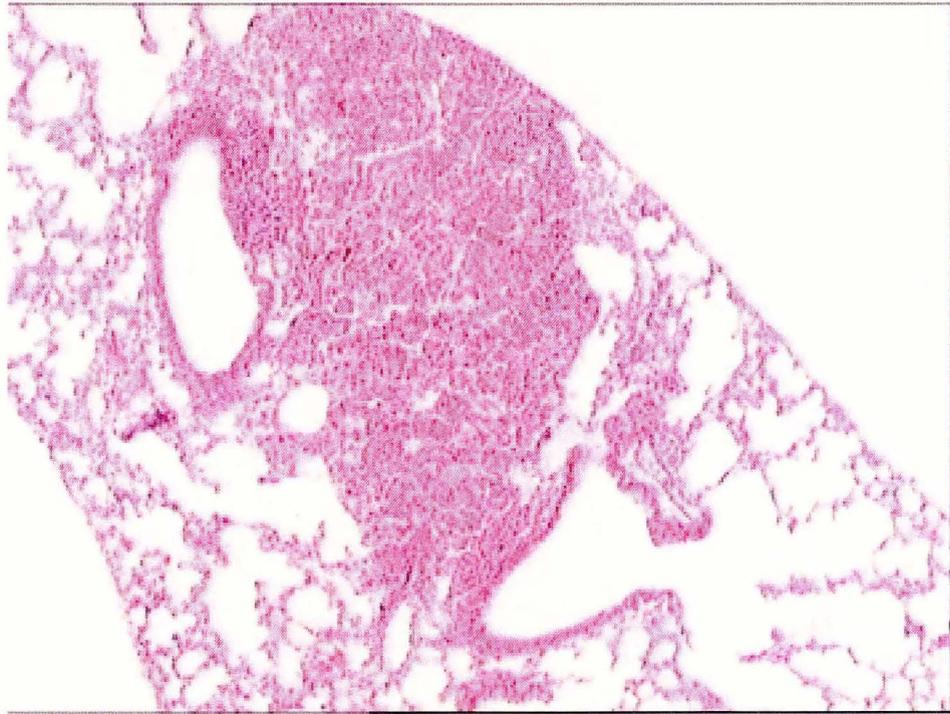REV1 is an integral component of the lesion bypass machinery required for bypass of replication blocking lesions. The metabolism of ubiquitous environmental carcinogen B[a]P (Figure 2a) leads to many DNA reactive intermediates that form such helix perturbing lesions.

Of particular historical importance, is the presumable ultimate carcinogen (±)- 7β, 8α- dihydroxy 9α, 10α -epoxy- 7, 8, 9, 10 tetrehyrobenzo[α]pyrene (BPDE) which is implicated as the primary metabolite responsible for the majority of mutations induced by TLS[145] (Figure 2b).The specific effect of targeting certain TLS polymerases, including REV1, to reduce error prone bypass of lesions such as that produced by B[a]P, is currently a topic of great research interest.

We hypothesize that by selectively inhibiting REV1 in the murine lung we would reduce the formation of mutations resulting from B[a]P exposure. This would effectively inhibit or reduce the initiation phase of carcinogenesis leading to tumor development. Although knock out mice exist for REV1, the genotype results in strain-specific effects on embryonic lethality. Survivable strains exhibit transiently reduced weight with no other obvious abnormalities. These data suggest that REV1 may function in a strain-dependant fashion in regards to endogenous DNA damage[146]. It currently unknown is unknown if REV1 has additional functions in addition to its role in TLS. Based on the similarity between data derived from yeast and higher eukaryotes, we hypothesized REV1 reduction would inhibit mutagenesis and effectively be observable as a reduction in tumor formation.

GENE DELIVERY VIA PEI/DNA AEROSOL INHALATION

Polyethylenimine (PEI) mediate gene therapy is an attractive means to deliver a variety of transgene products to the lung[147,148]. One major use of the cationic polymer PEI is to complex it with DNA and aerosolizing the mixture to deliver transgenes to the lung[149]. PEI gene delivery is noted for not inducing many cellular protective responses[150,151] that are seen with transgenes delivered via viruses. PEI holds therapeutic promise in many pulmonary diseases that are sensitive to exogenous particles and viruses. One important consideration supporting PEI gene therapy in carcinogen-induced mouse models is that it does not appear to be inflammatory to the murine lung[152,153]. This feature is noteworthy since inflammation promotion using BHT has been shown to increase both tumor multiplicity and size in B[a]P induced tumors[154]. PEI based gene delivery to the lung has been shown to be successful in multiple animal models of human disease and recently used to re-establishing p53 status and eradicating metastasis of lung cancers in mice[155-158]. Because of these studies, the use of non-viral gene delivery is currently gaining promise in the fields of gene therapy[159] and was used in these studies to aid in the delivery of the REV1 targeting ribozyme plasmid Rz406Pu6.

We utilized the whole body exposure approach to deliver aerosolized PEI/DNA complexes to the murine lung. This exposure method remains a fast reliable method to deliver and sustain transgene expression in the lung[160]. REV1 levels are cell-cycle dependant and speculate that REV1 inhibition through PEI delivery

would be present weeks after inhalation[161]. We found significant *in vivo* and *in vitro* luciferase expression with PEI/luc 48 hours after treatment using the whole animal approach with varying N:P ratios (Figure 11). The ratio of N:P is critical and has a significant effect on transfection efficiency and must be optimized. While the importance of N:P optimization to get transgenes into the cytoplasm cannot be understated, it is notable that the plasmid compaction of DNA rather than the N:P ratio is primarily responsible for transgene trafficking to the nucleus[162]. Significant expression using PEI/ luc *in vitro* occurred when using a range from 15:1 to 25:1 N:P ratio (Figure 11). When the same techniques were applied *in vivo* with Rz107pU6 a ratio of 10:1 was optimal (Figure 15). Based on these differences a 15:1 ratio was used for nubilization experiments and was found to be effective. Our studies confirm PEI/DNA treatment was well tolerated in the mouse and is not cytotoxic at the dose and exposure time used cell culture.

Initial experiments (data not shown), using electroporation, indicated both Rz407pU6 and Rz407pN2A as very effective antiREV1 constructs, consistently lowering transcript up to ~80% *in vitro*. However when complexed with PEI transfected into NIH 3T3 cells, Rz407pU6 and not Rz407pN2A was found to reduce REV1 mRNA transcript (Figure 13). Rz407pN2A did not lower REV1 mRNA transcript (Figure 13). Rz407pN2A is a much larger plasmid (10.1 kb) compared to Rz407pU6 (2.9 kb) perhaps explaining lack of REV1 inhibition and its use in subsequent experiments was discontinued.

REV1 INHIBITION IN THE MURINE LUNG

To determine reduction of REV1 mRNA in the murine lung we treated mice with aerosolized PEI/Rz407pU6 and analyzed whole lung homogenate for REV1 expression via real-time PCR. Not surprisingly, due to the vast size and diverse cell types, we observed no reduction in REV1 when analyzing total lung mRNA. We demeaned this methodology inappropriate since PEI has been shown to mediate significant expression of plasmids across certain regions but not necessarily the entire lung. However using LCM we were able to obtain cells from the bronchial epithelium and analyze REV1 (Figures 16 and 17). This tissue has been reported to not only significantly express plasmids delivered with aerosolized PEI/DNA but has also been elucidated as the region harboring bronchioalveolar stem cells (BASC) responsible for adenocarcinomas[143,163]. The studies here report here a reduction in REV1 mRNA transcript by 50%, using 4 µg of Rz407pU6 delivered over 2 x 30min exposures (Figure 17). Together these data support the use of PEI/ DNA based aerosol therapy as a safe and effective method to deliver genes to bronchial epithelium. The reduction in REV1 mRNA after Rz407pU6 transgene expression in the lung also supports the use of hammerhead ribozymes as an effective method to consistently knockdown REV1.

MICRO-POSITRON EMISSION TOMOGRAPHY (MICROPET)

Mice were scanned at 12, 16, and 20 weeks, using the common tracer, [F-18]-fluorodeoxyglucose (FDG). Scans were analyzed with micro PET

manufacturers software (Figure 18). Unfortunately, no tumors were visible at any of the time points. The most logical reason as to why lung tumors not were visualized may be explained by either lack of resolution in the microPET pet imaging system or lack of FDG uptake by the tumors. While the microPet imaging personnel indicated that tumors approximately 0.8mm in diameter are visible by microPET, the actual uptake of FDG by the tumor and surrounding tissue may impact this resolution. The background levels of FDG in the lung appeared to be relatively minor. Thus, either the resolution of microPET is less than indicated or the tumors in the lung absorbed FDG at approximately the same levels as the surrounding tissue.

REV1 REDUCTION DECREASES TUMOR MULTIPLICITY IN THE MURINE LUNG

Effects of targeting certain translesion synthesis polymerases to inhibit cancer formation remains unclear, particularly as shown in Chapter II with the inhibition of pol iota[164]. TLS however is recognized as an important mechanism of action in the formation of mutations that eventually lead to tumor development[164]. This hypothesis of inhibiting cancer by lowering the cells ability to erroneously bypass DNA lesions is supported in these studies.

We report here that the use of plasmid encoding a ribozyme inhibitory RNA (Rz407pU6) complexed with PEI and delivered to the lung before B[a]P injection decreased lung tumor multiplicity from an average of 6.4 tumors/ mouse to 3.7 tumors/ mouse (p value=.02) (Figure 19). There was also a reduction in the

total number of mice that developed tumors from 100% to 73% (Table 8). Our data suggests tumor inhibition by REV1 is primarily due to the reduction in mutations formed through the TLS pathway. Thus, tumor inhibition by these mechanisms is chemopreventive and requires the therapy to be initiated before DNA adducts are replicated. These data presented here are consistent with inhibition of initiation rather than a delay in progression. This conclusion is supported by observations that there were no significant differences in tumor size, the tumors were histologically similar (Figures 21-23), and 4 of 15 surviving mice did not develop tumors (Table 8).

The question remained what effect, if any, on tumor development would be observed when this REV1 inhibition occurred after the majority of adducts were cleared. To address this we included one treatment group given Rz407pU6 ~4weeks post carcinogen. As expected, there were no differences in mouse mortality or tumor development and morphology. These data suggest noninvasive REV1 inhibition may still be used in tissue previously exposed to a carcinogen with no ill effects and support REV1 inhibition as a useful strategy in the chemoprevention of lung cancer.

TUMOR HISTOLOGY

Tumors from each treatment group were dissected from mice in each treatment. Tumors were paraffin embedded and serial sectioned. Serial sections were treated with haematoxylin and eosin (H&E) stain. Sections were analyzed under a 10x microscope for differences in tumor morphology. Mice in all five groups showed hyperplasia occurring around the bronchial epithelium (Figure 21). Homogeneous spherical masses were also observed in all groups and these masses may or may not have compressed surrounding lung parenchyma, classified as adenoma (Figure 22). Additionally, extremely large adenomas with no apparent loss of border or metastasis were observed in all groups (Figure 23). These results indicated that Rz406pU6 had no observable effects the types of tumors formed and suggest that inhibition occurred during the initiation phase of carcinogenesis.

CHAPTER IV

DISCUSSION

The data presented in this dissertation provide insights into the
mechanisms used by higher eukaryotic cells to complete the replication of
genomes that enter S-phase with residual, unrepaired DNA damage. These
mechanisms have been conserved from prokaryotes to eukaryotes, including
plants and post-mitotic organisms such as *D. melanogater* and *C. elegans.* The
ubiquitous nature of DNA damage tolerance pathways attests to their importance
in genome maintenance. The molecular details surrounding these pathways are
only now being elucidated, and the most intensively studied organisms are *E. coli*
amongst the prokaryotes and *S. cerevisiae* amongst the eukaryotes. The
increased complexity of damage tolerance pathways in higher eukaryotes, in
particular the presence of a number of polymerases that are not found in lower
organisms, has obscured the molecular mechanisms involved. Of particular
interest in this regard are the events surrounding the switch from replicative to Y-
family DNA polymerases and the factors that govern which of the universe of
polymerases is to be employed when the replicative complex is stalled at a
particular lesion. One notion in the literature supposes that polymerases are

specialized for bypass of particular lesions. This arose from *in vitro* data using purified polymerases in the absence of accessory proteins, such as PCNA. These data indicate that pol eta bypasses T-T CPD with the preferential insertion of A-A across form the lesion, thereby being error-free. Teleologically, this specialization is supported by the fact that the UV component of sunlight is the most ubiquitous carcinogen to which organisms are exposed, and T-T CPD are the most common photoproduct. If true, then are other polymerases specialized for other adducts, such as those induced by chemical carcinogens? It is difficult to imagine how a stalled polymerase complex would differentiate between one helix-distorting lesion and another. An alternative possibility, which is not necessarily mutually exclusive with the lesion-specific idea, is that there is a hierarchy of polymerases. My approach to begin to address the issue of the events surrounding polymerase switching in higher eukaryotic cells was to examine the mutagenic phenotype of cells derived from mice with combinatorial deficiencies in pol eta and/or pol iota. Importantly, the development of these mouse models allows us to examine the relationship between mutagenesis and carcinogenesis in a detailed manner.

The discovery in 1999 of DNA polymerase eta and its deficiency as the molecular defect underlying the skin cancer-prone XP variant syndrome was a major development on the field of mutagenesis. This immediately led to an intensive international effort to develop a knockout mouse. However, many attempts to accomplish this resulted in embryonic lethality, a result that remains puzzling even now since lethality does not accompany biallelic deficiency in

human cells. Parenthetically, it is speculated that disruption of a large genomic region surrounding the pol eta gene disrupts another gene required for development. Fortunately, Dr. Kunkel and Dr. Kucherlapati were able to devise a strategy to ablate the polymerase domain with minimal disruption to the genomic structure surrounding the gene. The mutagenesis studies reported in this dissertation were derived, in part, from these mice. I found that these cells recapitulate the UV sensitivity of human XP variant cells to a remarkable extent. For instance, the D_{37} of murine cells deficient in pol eta is ~ 3 J/m^2, which compares favorably with the reported value of 3.8 J/ m^2 in XP variant cells. More importantly, the murine cells are extraordinarily hypermutable with respect to UV. The frequency of mutations at every UV fluence examined was several fold higher than that observed in wild-type cells. Further, examination of the spectrum of mutations indicated that most of the mutations arose from putative photoproducts in the leading strand template, and there was a very high proportion of CG to AT transversions, all of which arose from this strand. This spectrum is very similar to that found in XP variant cells, and confirm the hypothesis that pol eta preferentially acts on the leading strand template. In its absence, another, more error-prone enzyme assumes this function resulting in hypermutability. Carcinogenesis studies with these mice resulted in an accelerated UV-induced skin cancer phenotype, as expected from the hypermutability of the cells derived from these mice and in accord with the clinical observations in XP variant patients.

In contrast to the phenotype of the pol eta-deficient mice, pol iota deficiency resulted in greatly *reduced* mutant frequency compared to wild-type cells. Examination of the mutation spectrum derived from these mice showed that there were no differences in the kinds of mutations induced by UV, but the frequency of mutations arising from photoproducts in the lagging strand template was greatly reduced. The importance of these findings is that this is the first clear demonstration that pol iota has a biological function, performing error-prone bypass of UV photoproducts *in vivo*. Further, data support a model in which pol eta primarily acts on the leading strand template at the same time that pol iota acts on the lagging strand. The function of pol iota becomes even more apparent when pol eta is also absent, as in the double knockout. In this case, the extreme hypermutability resulting from the pol eta deficiency is reduced essentially to wild type levels. The pol iota deficiency in this background reduces mutations arising from photoproducts in both strands, but has a proportionally greater effect on those in the lagging strand template. These data support the conclusion that pol iota is the principal TLS polymerase in the absence of pol eta. Further, a third polymerase is able to conduct mutagenic photoproduct bypass, since the mutant frequency in the double knockout is reduced but not to zero. It can be speculated that this polymerase may be pol kappa, and suggests that the preferred hierarchy is pol eta > pol iota > pol kappa, at least for UV photoproducts.

There is a large body of data to support the hypothesis that cancer results from the accumulation of mutations in critical growth-control genes.

Therefore, the greatly reduced frequency of mutations in the cells derived form the double knockout mice would predict that these mice would develop skin cancer with a much greater latency than the pol eta (XP variant) mice. Unexpectedly, however, the former mice developed squamous cell skin cancer with a greatly decreased latency, which was highly statistically significant. The reasons for this are speculative and form the basis of future studies.

The simplest of explanations would be that mutagenesis at the *Hprt* locus in primary fibroblasts does not reflect mutations in the cell types and/or genes most relevant to development of skin tumors in mice. Opposition to this hypothesis is supported by measurements of mutagenesis at the *Hprt* locus in pol eta-deficient XP variant fibroblasts that do correlate with elevated susceptibility to skin cancer. Despite this evidence, it would be possible to further test against *Hprt* criticism through the isolation of keratinocytes, the cell type of tumor origin, and comparatively sequence key genes such as p53 and check for mutation spectrum differences.

Another possibility is that pol iota may play an important role in the development of normal immunity, such that a deficiency in pol iota would compromise immune suppression of skin cancer and lead to increased susceptibility. This possibility is unlikely due to reports of normal class switch recombination and somatic hypermutation of immunoglobulin genes in 129-derived strains of mice, many substrains of which have a naturally occurring deficiency of pol iota. However these studies were not completed during UV-irradiation and may not rule out the possibility that difference in immune

suppression may remain. Thus, inflammation may still play a large part in the observed difference in tumor formation and would have to be tested as the animals were being exposed to UV-light.

Another possibility, and the one I favor, is the idea that pol iota has multiple cellular roles and modulates cancer susceptibility. One role that can be experimentally tested is that pol iota is involved in cell cycle checkpoint responses to DNA damage. For instance, it has been known for some time that the mouse *pol iota* gene is on chromosome 18 and within the *Par2* (pulmonary adenoma resistance 2) locus. This is a major determinant of susceptibility to urethane-induced pulmonary adenomas. A defective pol iota allele in the 129X1/Sv mouse strain has been shown to be associated with increased susceptibility to urethane-induced lung tumors. The possibility of additional roles for pol iota remains and is currently under active investigation.

In Chapter III the well-established TLS polymerase REV1 was targeted in an attempt to lower the incidence of B[a]P induced murine lung tumors. These studies were based on earlier observations from the McGregor laboratory that ribozyme-mediated REV1 inhibition reduced BPDE-induced mutation in cell culture. In these studies endogenous REV1 mRNA in the lung was effectively lowered with the use of novel treatments. These treatments included the use of a REV1 mRNA targeting hammerhead ribozyme by delivery through PEI mediated aerosolized therapy. This reduction was found to effectively decrease the multiplicity of B[a]P induced tumors in the murine lung. This reduction did not affect the size or types of tumors induced suggesting that pure inhibition of

cancer formation at the initiation step was attained and not just a progressive delay. These studies support the use of targeting TLS as a chemoprotective measure. The question remains as to why inhibiting certain TLS polymerase has such a diverse impact on cancer formation as shown by the end result of cancer formation.

The provocative question regarding TLS implications in cancer is highlighted by comparisons between the end cancer results of Chapter II and III. In Chapter II the tumors appeared faster with TLS polymerase inhibition but TLS polymerase inhibition in Chapter III reduced tumor formation. The differences between these studies are supportive evidence that for a true decrease in cancer formation to occur TLS may have to be inhibited completely. If TLS is completely inhibited, cells are forced to resolve blocked DNA replication forks either by error-free recombination or to undergo apoptosis. If TLS inhibition occurs at only the level of the specific polymerases responsible for bypass other polymerases may assume the bypass. This bypass could occur in either an error-prone or error-free manner presumably dependent on both the type of lesion and specific polymerase performing the bypass. This multi-polymerase bypass is supported in Chapter II with pol iota assuming a larger role on both the leading and lagging strands in the absence of pol eta. Additionally, because there were residual mutations in the double knockouts, at least one other polymerase is capable of lesion bypass. This indicates TLS in Chapter II was not stopped but was rather merely altered. In contrast, REV1 inhibition appears to reduce the incidence of cancer. REV1 function in TLS is not considered to be catalytic, rather may be

structural acting to tether all of the polymerases that actually perform the bypass. Thus, REV1 inhibition abolishes TLS complex formation and drastically reduces the ability of cells to insert nucleotides across from lesions through TLS. With TLS completely shut down the logical system to assume function would be damage avoidance pathways. This pathway would appear to assume the role of TLS in an error free manner using undamaged templates to replicate the DNA. These data suggest that the most clinically useful approach in chemoprevention would be to shut down TLS completely, rather than attempting selective polymerase inhibition.

REFERENCES

1. Clingen,P.H. *et al.* Correlation of UVC and UVB cytotoxicity with the induction of specific photoproducts in T-lymphocytes and fibroblasts from normal human donors. *Photochem. Photobiol.* **61**, 163-170 (1995).

2. Sundaram,C., Koster,W. & Schallreuter,K.U. The effect of UV radiation and sun blockers on free radical defence in human and guinea pig epidermis. *Arch. Dermatol. Res.* **282**, 526-531 (1990).

3. Goodsell,D.S. The molecular perspective: ultraviolet light and pyrimidine dimers. *Oncologist.* **6**, 298-299 (2001).

4. Cordeiro-Stone,M. *et al.* DNA damage responses protect xeroderma pigmentosum variant from UVC-induced clastogenesis. *Carcinogenesis* **23**, 959-965 (2002).

5. Dixon,A.J. & Dixon,B.F. Ultraviolet radiation from welding and possible risk of skin and ocular malignancy. *Med. J. Aust.* **181**, 155-157 (2004).

6. Mitchell,D.L. The relative cytotoxicity of (6-4) photoproducts and cyclobutane dimers in mammalian cells. *Photochem. Photobiol.* **48**, 51-57 (1988).

7. Setlow,R.B. The photochemistry, photobiology, and repair of polynucleotides. *Prog. Nucleic Acid Res. Mol. Biol.* **8**, 257-295 (1968).

8. Mitchell,D.L. & Nairn,R.S. The biology of the (6-4) photoproduct. *Photochem. Photobiol.* **49**, 805-819 (1989).

9. Parris,C.N. & Kraemer,K.H. Ultraviolet-induced mutations in Cockayne syndrome cells are primarily caused by cyclobutane dimer photoproducts while repair of other photoproducts is normal. *Proc. Natl. Acad. Sci. U. S. A* **90**, 7260-7264 (1993).

10. Bissonauth,V. *et al.* The efficacy of a broad-spectrum sunscreen to protect engineered human skin from tissue and DNA damage induced by solar ultraviolet exposure. *Clin. Cancer Res.* **6**, 4128-4135 (2000).

11. Autrup,H. & Seremet,T. Excretion of benzo[a]pyrene-Gua adduct in the urine of benzo[a]pyrene-treated rats. *Chem. Biol. Interact.* **60**, 217-226 (1986).

12. Roberts,A.E., Bogdanffy,M.S., Brown,D.R. & Schatz,R.A. Lung metabolism of benzo[a]pyrene in rats treated with p-xylene and/or ethanol. *J. Toxicol. Environ. Health* **18**, 257-266 (1986).

13. Daubeze,M. *et al.* [Metabolic activation of benzo(a)pyrene by human amniotic fluid]. *C. R. Acad. Sci. III* **302**, 625-628 (1986).

14. Kondraganti,S.R. *et al.* Polycyclic aromatic hydrocarbon-inducible DNA adducts: evidence by 32P-postlabeling and use of knockout mice for Ah receptor-independent mechanisms of metabolic activation in vivo. *Int. J. Cancer* **103**, 5-11 (2003).

15. Seo,K.Y., Nagalingam,A., Tiffany,M. & Loechler,E.L. Mutagenesis studies with four stereoisomeric N2-dG benzo[a]pyrene adducts in the identical 5'-CGC sequence used in NMR studies: G->T mutations dominate in each case. *Mutagenesis* **20**, 441-448 (2005).

16. Cheng,S.C., Hilton,B.D., Roman,J.M. & Dipple,A. DNA adducts from carcinogenic and noncarcinogenic enantiomers of benzo[a]pyrene dihydrodiol epoxide. *Chem. Res. Toxicol.* **2**, 334-340 (1989).

17. Adimoolam,S. & Ford,J.M. p53 and regulation of DNA damage recognition during nucleotide excision repair. *DNA Repair (Amst)* **2**, 947-954 (2003).

18. Evan,G.I. & Vousden,K.H. Proliferation, cell cycle and apoptosis in cancer. *Nature* **411**, 342-348 (2001).

19. van Oosten,M. *et al.* Differential role of transcription-coupled repair in UVB-induced G2 arrest and apoptosis in mouse epidermis. *Proc. Natl. Acad. Sci. U. S. A* **97**, 11268-11273 (2000).

20. Jentsch,S., McGrath,J.P. & Varshavsky,A. The yeast DNA repair gene RAD6 encodes a ubiquitin-conjugating enzyme. *Nature* **329**, 131-134 (1987).

21. Sung,P., Prakash,S. & Prakash,L. Mutation of cysteine-88 in the Saccharomyces cerevisiae RAD6 protein abolishes its ubiquitin-conjugating activity and its various biological functions. *Proc. Natl. Acad. Sci. U. S. A* **87**, 2695-2699 (1990).

22. Ulrich,H.D. & Jentsch,S. Two RING finger proteins mediate cooperation between ubiquitin-conjugating enzymes in DNA repair. *EMBO J.* **19**, 3388-3397 (2000).

23. Hoege,C., Pfander,B., Moldovan,G.L., Pyrowolakis,G. & Jentsch,S. RAD6-dependent DNA repair is linked to modification of PCNA by ubiquitin and SUMO. *Nature* **419**, 135-141 (2002).

24. Torres-Ramos,C.A., Prakash,S. & Prakash,L. Requirement of RAD5 and MMS2 for postreplication repair of UV-damaged DNA in Saccharomyces cerevisiae. *Mol. Cell Biol.* **22**, 2419-2426 (2002).

25. Li,Z., Xiao,W., McCormick,J.J. & Maher,V.M. Identification of a protein essential for a major pathway used by human cells to avoid UV- induced DNA damage. *Proc. Natl. Acad. Sci. U. S. A* **99**, 4459-4464 (2002).

26. Sonoda,E., Takata,M., Yamashita,Y.M., Morrison,C. & Takeda,S. Homologous DNA recombination in vertebrate cells. *Proc. Natl. Acad. Sci. U. S. A* **98**, 8388-8394 (2001).

27. Sonoda,E. *et al.* Sister chromatid exchanges are mediated by homologous recombination in vertebrate cells. *Mol. Cell Biol.* **19**, 5166-5169 (1999).

28. Ulrich,H.D. The srs2 suppressor of UV sensitivity acts specifically on the. *Nucleic Acids Res.* **29**, 3487-3494 (2001).

29. Chiu,R.K. *et al.* Lysine 63-polyubiquitination guards against translesion synthesis-induced mutations. *PLoS. Genet.* **2**, e116 (2006).

30. Watts,F.Z. Sumoylation of PCNA: Wrestling with recombination at stalled replication forks. *DNA Repair (Amst)* **5**, 399-403 (2006).

31. Pfander,B., Moldovan,G.L., Sacher,M., Hoege,C. & Jentsch,S. SUMO-modified PCNA recruits Srs2 to prevent recombination during S phase. *Nature* **436**, 428-433 (2005).

32. Watts,F.Z. Sumoylation of PCNA: Wrestling with recombination at stalled replication forks. *DNA Repair (Amst)* **5**, 399-403 (2006).

33. Pfander,B., Moldovan,G.L., Sacher,M., Hoege,C. & Jentsch,S. SUMO-modified PCNA recruits Srs2 to prevent recombination during S phase. *Nature* **436**, 428-433 (2005).

34. Ohmori,H. *et al.* The Y-family of DNA polymerases. *Mol. Cell* **8**, 7-8 (2001).

35. Kunkel,T.A. & Bebenek,K. DNA replication fidelity. *Annu. Rev. Biochem.* **69**, 497-529 (2000).

36. Masutani,C. *et al.* The XPV (xeroderma pigmentosum variant) gene encodes human DNA polymerase eta. *Nature* **399**, 700-704 (1999).

37. Rattray,A.J. & Strathern,J.N. Error-prone DNA polymerases: when making a mistake is the only way to get ahead. *Annu. Rev. Genet.* **37**, 31-66 (2003).

38. Murakumo,Y. *et al.* A human REV7 homolog that interacts with the polymerase zeta catalytic subunit hREV3 and the spindle assembly checkpoint protein hMAD2. *J. Biol. Chem.* **275**, 4391-4397 (2000).

39. Diaz,M. *et al.* Decreased frequency and highly aberrant spectrum of ultraviolet-induced mutations in the hprt gene of mouse fibroblasts expressing antisense RNA to DNA polymerase zeta. *Mol. Cancer Res.* **1**, 836-847 (2003).

40. Bemark,M., Khamlichi,A.A., Davies,S.L. & Neuberger,M.S. Disruption of mouse polymerase zeta (Rev3) leads to embryonic lethality and impairs blastocyst development in vitro. *Curr. Biol.* **10**, 1213-1216 (2000).

41. Diaz,M., Verkoczy,L.K., Flajnik,M.F. & Klinman,N.R. Decreased frequency of somatic hypermutation and impaired affinity maturation but intact germinal center formation in mice expressing antisense RNA to DNA polymerase zeta. *J. Immunol.* **167**, 327-335 (2001).

42. Zan,H. *et al.* The translesion DNA polymerase zeta plays a major role in Ig and bcl-6 somatic hypermutation. *Immunity.* **14**, 643-653 (2001).

43. Haracska,L., Prakash,S. & Prakash,L. Yeast DNA polymerase zeta is an efficient extender of primer ends opposite from 7,8-dihydro-8-Oxoguanine and O6-methylguanine. *Mol. Cell Biol.* **23**, 1453-1459 (2003).

44. Li,Z. *et al.* hREV3 is essential for error-prone translesion synthesis past UV or benzo[a]pyrene diol epoxide-induced DNA lesions in human fibroblasts. *Mutat. Res.* **510**, 71-80 (2002).

45. Acharya,N., Johnson,R.E., Prakash,S. & Prakash,L. Complex formation with Rev1 enhances the proficiency of Saccharomyces cerevisiae DNA polymerase zeta for mismatch extension and for extension opposite from DNA lesions. *Mol. Cell Biol.* **26**, 9555-9563 (2006).

46. Hubscher,U., Nasheuer,H.P. & Syvaoja,J.E. Eukaryotic DNA polymerases, a growing family. *Trends Biochem. Sci.* **25**, 143-147 (2000).

47. Maher,V.M., Ouellette,L.M., Curren,R.D. & McCormick,J.J. Frequency of ultraviolet light-induced mutations is higher in xeroderma pigmentosum variant cells than in normal human cells. *Nature* **261**, 593-595 (1976).

48. McCormick,J.J., Kateley-Kohler,S., Watanabe,M. & Maher,V.M. Abnormal sensitivity of human fibroblasts from xeroderma pigmentosum variants to transformation to anchorage independence by ultraviolet radiation. *Cancer Res.* **46**, 489-492 (1986).

49. Masutani,C. *et al.* The XPV (xeroderma pigmentosum variant) gene encodes human DNA polymerase eta. *Nature* **399**, 700-704 (1999).

50. Johnson,R.E., Kondratick,C.M., Prakash,S. & Prakash,L. hRAD30 mutations in the variant form of xeroderma pigmentosum. *Science* **285**, 263-265 (1999).

51. McGregor,W.G., Wei,D., Maher,V.M. & McCormick,J.J. Abnormal, error-prone bypass of photoproducts by xeroderma pigmentosum variant cell extracts results in extreme strand bias for the kinds of mutations induced by UV light. *Mol. Cell Biol.* **19**, 147-154 (1999).

52. Wang,Y.C., Maher,V.M., Mitchell,D.L. & McCormick,J.J. Evidence from mutation spectra that the UV hypermutability of xeroderma pigmentosum variant cells reflects abnormal, error-prone replication on a template containing photoproducts. *Mol. Cell Biol.* **13**, 4276-4283 (1993).

53. Washington,M.T., Johnson,R.E., Prakash,S. & Prakash,L. Accuracy of thymine-thymine dimer bypass by Saccharomyces cerevisiae DNA polymerase eta. *Proc. Natl. Acad. Sci. U. S. A* **97**, 3094-3099 (2000).

54. Sun,L. *et al.* Yeast pol eta holds a cis-syn thymine dimer loosely in the active site during elongation opposite the 3'-T of the dimer, but tightly opposite the 5'-T. *Biochemistry* **42**, 9431-9437 (2003).

55. Johnson,R.E., Prakash,S. & Prakash,L. Efficient bypass of a thymine-thymine dimer by yeast DNA polymerase, Poleta. *Science* **283**, 1001-1004 (1999).

56. Watanabe,M., Maher,V.M. & McCormick,J.J. Excision repair of UV- or benzo[a]pyrene diol epoxide-induced lesions in xeroderma pigmentosum variant cells is 'error free'. *Mutat. Res.* **146**, 285-294 (1985).

57. Choi,J.H., Besaratinia,A., Lee,D.H., Lee,C.S. & Pfeifer,G.P. The role of DNA polymerase iota in UV mutational spectra. *Mutat. Res.* **599**, 58-65 (2006).

58. Mitchell,D.L., Haipek,C.A. & Clarkson,J.M. (6-4)Photoproducts are removed from the DNA of UV-irradiated mammalian cells more efficiently than cyclobutane pyrimidine dimers. *Mutat. Res.* **143**, 109-112 (1985).

59. Armstrong,J.D. & Kunz,B.A. Site and strand specificity of UVB mutagenesis in the SUP4-o gene of yeast. *Proc. Natl. Acad. Sci. U. S. A* **87**, 9005-9009 (1990).

60. Brash,D.E. & Haseltine,W.A. UV-induced mutation hotspots occur at DNA damage hotspots. *Nature* **298**, 189-192 (1982).

61. Haracska,L., Yu,S.L., Johnson,R.E., Prakash,L. & Prakash,S. Efficient and accurate replication in the presence of 7,8-dihydro-8-oxoguanine by DNA polymerase eta. *Nat. Genet.* **25**, 458-461 (2000).

62. Garg,P., Stith,C.M., Majka,J. & Burgers,P.M. Proliferating cell nuclear antigen promotes translesion synthesis by DNA polymerase zeta. *J. Biol. Chem.* **280**, 23446-23450 (2005).

63. Kannouche,P. *et al.* Localization of DNA polymerases eta and iota to the replication machinery is tightly co-ordinated in human cells. *EMBO J.* **21**, 6246-6256 (2002).

64. Zhang,Y., Yuan,F., Wu,X., Taylor,J.S. & Wang,Z. Response of human DNA polymerase iota to DNA lesions. *Nucleic Acids Res.* **29**, 928-935 (2001).

65. Vaisman,A., Frank,E.G., McDonald,J.P., Tissier,A. & Woodgate,R. poliota-dependent lesion bypass in vitro. *Mutat. Res.* **510**, 9-22 (2002).

66. Vaisman,A. *et al.* Sequence context-dependent replication of DNA templates containing UV-induced lesions by human DNA polymerase iota. *DNA Repair (Amst)* **2**, 991-1006 (2003).

67. Johnson,R.E., Washington,M.T., Haracska,L., Prakash,S. & Prakash,L. Eukaryotic polymerases iota and zeta act sequentially to bypass DNA lesions. *Nature* **406**, 1015-1019 (2000).

68. Tissier,A. *et al.* Misinsertion and bypass of thymine-thymine dimers by human DNA polymerase iota. *EMBO J.* **19**, 5259-5266 (2000).

69. Tissier,A., McDonald,J.P., Frank,E.G. & Woodgate,R. poliota, a remarkably error-prone human DNA polymerase. *Genes Dev.* **14**, 1642-1650 (2000).

70. Bebenek,K. *et al.* 5'-Deoxyribose phosphate lyase activity of human DNA polymerase iota in vitro. *Science* **291**, 2156-2159 (2001).

71. Celewicz,L., Mayer,M. & Shetlar,M.D. The photochemistry of thymidylyl-(3'-5')-5-methyl-2'-deoxycytidine in aqueous solution. *Photochem. Photobiol.* **81**, 404-418 (2005).

72. Vaisman,A., Takasawa,K., Iwai,S. & Woodgate,R. DNA polymerase iota-dependent translesion replication of uracil containing cyclobutane pyrimidine dimers. *DNA Repair (Amst)* **5**, 210-218 (2006).

73. McDonald,J.P. *et al.* 129-derived strains of mice are deficient in DNA polymerase iota and have normal immunoglobulin hypermutation. *J. Exp. Med.* **198**, 635-643 (2003).

74. Frank,E.G. *et al.* Altered nucleotide misinsertion fidelity associated with poliota-dependent replication at the end of a DNA template. *EMBO J.* **20**, 2914-2922 (2001).

75. Wang,M. *et al.* Pol iota is a candidate for the mouse pulmonary adenoma resistance 2 locus, a major modifier of chemically induced lung neoplasia. *Cancer Res.* **64**, 1924-1931 (2004).

76. Lee,G.H. & Matsushita,H. Genetic linkage between Pol iota deficiency and increased susceptibility to lung tumors in mice. *Cancer Sci.* **96**, 256-259 (2005).

77. Lawrence,C.W. Cellular roles of DNA polymerase zeta and Rev1 protein. *DNA Repair (Amst)* **1**, 425-435 (2002).

78. Acharya,N. *et al.* Complex formation of yeast Rev1 and Rev7 proteins: a novel role for the polymerase-associated domain. *Mol. Cell Biol.* **25**, 9734-9740 (2005).

79. Lawrence,C.W., Das,G. & Christensen,R.B. REV7, a new gene concerned with UV mutagenesis in yeast. *Mol. Gen. Genet.* **200**, 80-85 (1985).

80. Nair,D.T., Johnson,R.E., Prakash,L., Prakash,S. & Aggarwal,A.K. Rev1 employs a novel mechanism of DNA synthesis using a protein template. *Science* **309**, 2219-2222 (2005).

81. Zhang,Y. *et al.* Response of human REV1 to different DNA damage: preferential dCMP insertion opposite the lesion. *Nucleic Acids Res.* **30**, 1630-1638 (2002).

82. Nelson,J.R., Lawrence,C.W. & Hinkle,D.C. Deoxycytidyl transferase activity of yeast REV1 protein. *Nature* **382**, 729-731 (1996).

83. Nelson,J.R., Gibbs,P.E., Nowicka,A.M., Hinkle,D.C. & Lawrence,C.W. Evidence for a second function for Saccharomyces cerevisiae Rev1p. *Mol. Microbiol.* **37**, 549-554 (2000).

84. Lin,W. *et al.* The human REV1 gene codes for a DNA template-dependent dCMP transferase. *Nucleic Acids Res.* **27**, 4468-4475 (1999).

85. Prakash,S., Johnson,R.E. & Prakash,L. EUKARYOTIC TRANSLESION SYNTHESIS DNA POLYMERASES: Specificity of Structure and Function. *Annu. Rev. Biochem.* **74**, 317-353 (2005).

86. Guo,C. *et al.* REV1 protein interacts with PCNA: significance of the REV1 BRCT domain in vitro and in vivo. *Mol. Cell* **23**, 265-271 (2006).

87. D'Souza,S. & Walker,G.C. Novel role for the C terminus of Saccharomyces cerevisiae Rev1 in mediating protein-protein interactions. *Mol. Cell Biol.* **26**, 8173-8182 (2006).

88. Larimer,F.W., Perry,J.R. & Hardigree,A.A. The REV1 gene of Saccharomyces cerevisiae: isolation, sequence, and functional analysis. *J. Bacteriol.* **171**, 230-237 (1989).

89. Lemontt,J.F. Mutants of Yeast Defective in Mutation Induced by Ultraviolet Light. *Genetics* **68**, 21-33 (1971).

90. Gibbs,P.E., McGregor,W.G., Maher,V.M., Nisson,P. & Lawrence,C.W. A human homolog of the Saccharomyces cerevisiae REV3 gene, which encodes the catalytic subunit of DNA polymerase zeta. *Proc. Natl. Acad. Sci. U. S. A* **95**, 6876-6880 (1998).

91. Murakumo,Y. *et al.* A human REV7 homolog that interacts with the polymerase zeta catalytic subunit hREV3 and the spindle assembly checkpoint protein hMAD2. *J. Biol. Chem.* **275**, 4391-4397 (2000).

92. Zhang,Y. *et al.* Response of human REV1 to different DNA damage: preferential dCMP insertion opposite the lesion. *Nucleic Acids Res.* **30**, 1630-1638 (2002).

93. Guo,C. *et al.* Mouse Rev1 protein interacts with multiple DNA polymerases involved in translesion DNA synthesis. *EMBO J.* **22**, 6621-6630 (2003).

94. Garg,P. & Burgers,P.M. Ubiquitinated proliferating cell nuclear antigen activates translesion DNA polymerases eta and REV1. *Proc. Natl. Acad. Sci. U. S. A* **102**, 18361-18366 (2005).

95. Guo,C. *et al.* Ubiquitin-binding motifs in REV1 protein are required for its role in the tolerance of DNA damage. *Mol. Cell Biol.* **26**, 8892-8900 (2006).

96. Guo,C. *et al.* Mouse Rev1 protein interacts with multiple DNA polymerases involved in translesion DNA synthesis. *EMBO J.* **22**, 6621-6630 (2003).

97. Broomfield,S., Hryciw,T. & Xiao,W. DNA postreplication repair and mutagenesis in Saccharomyces cerevisiae. *Mutat. Res.* **486**, 167-184 (2001).

98. Prakash,S. & Prakash,L. Translesion DNA synthesis in eukaryotes: a one- or two-polymerase affair. *Genes Dev.* **16**, 1872-1883 (2002).

99. Lin,Q. *et al.* Increased susceptibility to UV-induced skin carcinogenesis in polymerase eta-deficient mice. *Cancer Res.* **66**, 87-94 (2006).

100. Parrinello,S. *et al.* Oxygen sensitivity severely limits the replicative lifespan of murine fibroblasts. *Nat. Cell Biol.* **5**, 741-747 (2003).

101. Yang,J.L., Maher,V.M. & McCormick,J.J. Amplification and Direct Nucleotide Sequencing of Cdna from the Lysate of Low Numbers of Diploid Human-Cells. *Gene* **83**, 347-354 (1989).

102. Nicklas,J.A., Hunter,T.C., O'Neill,J.P. & Albertini,R.J. Fine structure mapping of the hypoxanthine-guanine phosphoribosyltransferase (HPRT) gene region of the human X chromosome (Xq26). *Am. J. Hum. Genet.* **49**, 267-278 (1991).

103. Mahowald,A.P. & Hardy,P.A. Genetics of Drosophila embryogenesis. *Annu. Rev. Genet.* **19**, 149-177 (1985).

104. Elion,G.B. Symposium on immunosuppressive drugs. Biochemistry and pharmacology of purine analogues. *Fed. Proc.* **26**, 898-904 (1967).

105. Albertini,R.J. HPRT mutations in humans: biomarkers for mechanistic studies. *Mutat. Res.* **489**, 1-16 (2001).

106. Knaap,A.G. & Simons,J.W. A mutational assay system for L5178Y mouse lymphoma cells, using hypoxanthine-guanine-phosphoribosyl-transferase (HGPRT) -deficiency as marker. The occurrence of a long expression time for mutations induced by X-rays and EMS. *Mutat. Res.* **30**, 97-110 (1975).

107. McGregor,W.G., Chen,R.H., Lukash,L., Maher,V.M. & McCormick,J.J. Cell cycle-dependent strand bias for UV-induced mutations in the transcribed strand of excision repair-proficient human fibroblasts but not in repair-deficient cells. *Mol. Cell Biol.* **11**, 1927-1934 (1991).

108. Maher,V.M., Ouellette,L.M., Curren,R.D. & McCormick,J.J. Frequency of ultraviolet light-induced mutations is higher in xeroderma pigmentosum variant cells than in normal human cells. *Nature* **261**, 593-595 (1976).

109. Lopes,M., Foiani,M. & Sogo,J.M. Multiple mechanisms control chromosome integrity after replication fork uncoupling and restart at irreparable UV lesions. *Mol. Cell* **21**, 15-27 (2006).

110. Kannouche,P. *et al.* Localization of DNA polymerases eta and iota to the replication machinery is tightly co-ordinated in human cells. *EMBO J.* **22**, 1223-1233 (2003).

111. Garinis,G.A., Jans,J. & van der Horst,G.T. Photolyases: capturing the light to battle skin cancer. *Future. Oncol.* **2**, 191-199 (2006).

112. Celewicz,L., Mayer,M. & Shetlar,M.D. The photochemistry of thymidylyl-(3'-5')-5-methyl-2'-deoxycytidine in aqueous solution. *Photochem. Photobiol.* **81**, 404-418 (2005).

113. Vaisman,A., Takasawa,K., Iwai,S. & Woodgate,R. DNA polymerase iota-dependent translesion replication of uracil containing cyclobutane pyrimidine dimers. *DNA Repair (Amst)* **5**, 210-218 (2006).

114. Vrieling,H. *et al.* DNA strand specificity for UV-induced mutations in mammalian cells. *Mol. Cell Biol.* **9**, 1277-1283 (1989).

115. Cohen,S.M., Brylawski,B.P., Cordeiro-Stone,M. & Kaufman,D.G. Mapping of an origin of DNA replication near the transcriptional promoter of the human HPRT gene. *J. Cell Biochem.* **85**, 346-356 (2002).

116. Mitchell,D.L., Jen,J. & Cleaver,J.E. Relative induction of cyclobutane dimers and cytosine photohydrates in DNA irradiated in vitro and in vivo with ultraviolet-C and ultraviolet-B light. *Photochem. Photobiol.* **54**, 741-746 (1991).

117. Garg,P., Stith,C.M., Majka,J. & Burgers,P.M. Proliferating cell nuclear antigen promotes translesion synthesis by DNA polymerase zeta. *J. Biol. Chem.* **280**, 23446-23450 (2005).

118. Zhong,X. *et al.* The fidelity of DNA synthesis by yeast DNA polymerase zeta alone and with accessory proteins. *Nucleic Acids Res.* **34**, 4731-4742 (2006).

119. Loeb,L.A. A mutator phenotype in cancer. *Cancer Res.* **61**, 3230-3239 (2001).

120. McIlwraith,M.J. *et al.* Human DNA polymerase eta promotes DNA synthesis from strand invasion intermediates of homologous recombination. *Mol. Cell* **20**, 783-792 (2005).

121. Kawamoto,T. *et al.* Dual roles for DNA polymerase eta in homologous DNA recombination and translesion DNA synthesis. *Mol. Cell* **20**, 793-799 (2005).

122. Ogi,T. & Lehmann,A.R. The Y-family DNA polymerase kappa (pol kappa) functions in mammalian nucleotide-excision repair. *Nat. Cell Biol.* **8**, 640-642 (2006).

123. Opperman,T., Murli,S., Smith,B.T. & Walker,G.C. A model for a umuDC-dependent prokaryotic DNA damage checkpoint. *Proc. Natl. Acad. Sci. U. S. A* **96**, 9218-9223 (1999).

124. Stamato,T.D., Richardson,E. & Perez,M.L. UV-light induces delayed mutations in Chinese hamster cells. *Mutat. Res.* **328**, 175-181 (1995).

125. Stamato,T.D. & Perez,M.L. EMS and UV-light-induced colony sectoring and delayed mutation in Chinese hamster cells. *Int. J. Radiat. Biol.* **74**, 739-745 (1998).

126. Martomo,S.A. *et al.* Normal hypermutation in antibody genes from congenic mice defective for DNA polymerase iota. *DNA Repair (Amst)* **5**, 392-398 (2006).

127. Gening,L.V., Makarova,A.V., Malashenko,A.M. & Tarantul,V.Z. A false note of DNA polymerase iota in the choir of genome caretakers in mammals. *Biochemistry (Mosc.)* **71**, 155-159 (2006).

128. Wang,M. *et al.* Pol iota is a candidate for the mouse pulmonary adenoma resistance 2 locus, a major modifier of chemically induced lung neoplasia. *Cancer Res.* **64**, 1924-1931 (2004).

129. Lee,G.H. & Matsushita,H. Genetic linkage between Pol iota deficiency and increased susceptibility to lung tumors in mice. *Cancer Sci.* **96**, 256-259 (2005).

130. Clark,D.R., Zacharias,W., Panaitescu,L. & McGregor,W.G. Ribozyme-mediated REV1 inhibition reduces the frequency of UV-induced mutations in the human HPRT gene. *Nucleic Acids Res.* **31**, 4981-4988 (2003).

131. Wattenberg,L.W. *et al.* Chemoprevention of pulmonary carcinogenesis by aerosolized budesonide in female A/J mice. *Cancer Res.* **57**, 5489-5492 (1997).

132. Wattenberg,L.W. & Estensen,R.D. Studies of chemopreventive effects of budenoside on benzo[a]pyrene-induced neoplasia of the lung of female A/J mice. *Carcinogenesis* **18**, 2015-2017 (1997).

133. Clark,D.R., Zacharias,W., Panaitescu,L. & McGregor,W.G. Ribozyme-mediated REV1 inhibition reduces the frequency of UV-induced mutations in the human HPRT gene. *Nucleic Acids Res.* **31**, 4981-4988 (2003).

134. Rutkauskaite,E. *et al.* Ribozymes that inhibit the production of matrix metalloproteinase 1 reduce the invasiveness of rheumatoid arthritis synovial fibroblasts. *Arthritis Rheum.* **50**, 1448-1456 (2004).

135. Schedel,J. *et al.* Targeting cathepsin L (CL) by specific ribozymes decreases CL protein synthesis and cartilage destruction in rheumatoid arthritis. *Gene Ther.* (2004).

136. Zuker,M. & Jacobson,A.B. "Well-determined" regions in RNA secondary structure prediction: analysis of small subunit ribosomal RNA. *Nucleic Acids Res.* **23**, 2791-2798 (1995).

137. Bertrand,E. *et al.* The expression cassette determines the functional activity of ribozymes in mammalian cells by controlling their intracellular localization. *RNA.* **3**, 75-88 (1997).

138. Thompson,J.D. *et al*. Improved accumulation and activity of ribozymes expressed from a tRNA-based RNA polymerase III promoter. *Nucleic Acids Res.* **23**, 2259-2268 (1995).

139. Ilves,H., Barske,C., Junker,U., Bohnlein,E. & Veres,G. Retroviral vectors designed for targeted expression of RNA polymerase III-driven transcripts: a comparative study. *Gene* **171**, 203-208 (1996).

140. Good,P.D. *et al*. Expression of small, therapeutic RNAs in human cell nuclei. *Gene Ther.* **4**, 45-54 (1997).

141. Lee,N.S. *et al*. Functional colocalization of ribozymes and target mRNAs in Drosophila oocytes. *FASEB J.* **15**, 2390-2400 (2001).

142. Good,P.D. *et al*. Expression of small, therapeutic RNAs in human cell nuclei. *Gene Ther.* **4**, 45-54 (1997).

143. Rudolph,C. *et al*. Aerosolized nanogram quantities of plasmid DNA mediate highly efficient gene delivery to mouse airway epithelium. *Mol. Ther.* **12**, 493-501 (2005).

144. Livak,K.J. & Schmittgen,T.D. Analysis of relative gene expression data using real-time quantitative PCR and the 2(-Delta Delta C(T)) Method. *Methods* **25**, 402-408 (2001).

145. Mukhopadhyay,S., Clark,D.R., Watson,N.B., Zacharias,W. & McGregor,W.G. REV1 accumulates in DNA damage-induced nuclear foci in human cells and is implicated in mutagenesis by benzo[a]pyrenediolepoxide. *Nucleic Acids Res.* **32**, 5820-5826 (2004).

146. Jansen,J.G. *et al*. Strand-biased defect in C/G transversions in hypermutating immunoglobulin genes in Rev1-deficient mice. *J. Exp. Med.* **203**, 319-323 (2006).

147. Densmore,C.L. Polyethyleneimine-based gene therapy by inhalation. *Expert. Opin. Biol. Ther.* **3**, 1083-1092 (2003).

148. Densmore,C.L. Advances in noninvasive pulmonary gene therapy. *Curr. Drug Deliv.* **3**, 55-63 (2006).

149. Gautam,A., Densmore,C.L., Xu,B. & Waldrep,J.C. Enhanced gene expression in mouse lung after PEI-DNA aerosol delivery. *Mol. Ther.* **2**, 63-70 (2000).

150. Schwiebert,L.M. Cystic fibrosis, gene therapy, and lung inflammation: for better or worse? *Am. J. Physiol Lung Cell Mol. Physiol* **286**, L715-L716 (2004).

151. Klink,D. *et al.* Gene delivery systems--gene therapy vectors for cystic fibrosis. *J. Cyst. Fibros.* **3 Suppl 2**, 203-212 (2004).

152. Gautam,A., Densmore,C.L. & Waldrep,J.C. Pulmonary cytokine responses associated with PEI-DNA aerosol gene therapy. *Gene Ther.* **8**, 254-257 (2001).

153. Ziady,A.G., Davis,P.B. & Konstan,M.W. Non-viral gene transfer therapy for cystic fibrosis. *Expert. Opin. Biol. Ther.* **3**, 449-458 (2003).

154. Bauer,A.K., Dwyer-Nield,L.D., Keil,K., Koski,K. & Malkinson,A.M. Butylated hydroxytoluene (BHT) induction of pulmonary inflammation: a role in tumor promotion. *Exp. Lung Res.* **27**, 197-216 (2001).

155. Jia,S.F. *et al.* Aerosol gene therapy with PEI: IL-12 eradicates osteosarcoma lung metastases. *Clin. Cancer Res.* **9**, 3462-3468 (2003).

156. Gautam,A. *et al.* Aerosol gene therapy for metastatic lung cancer using PEI-p53 complexes. *Methods Mol. Med.* **75**, 607-618 (2003).

157. Gautam,A., Densmore,C.L. & Waldrep,J.C. Inhibition of experimental lung metastasis by aerosol delivery of PEI-p53 complexes. *Mol. Ther.* **2**, 318-323 (2000).

158. Gautam,A., Densmore,C.L. & Waldrep,J.C. Inhibition of experimental lung metastasis by aerosol delivery of PEI-p53 complexes. *Mol. Ther.* **2**, 318-323 (2000).

159. Densmore,C.L. Advances in noninvasive pulmonary gene therapy. *Curr. Drug Deliv.* **3**, 55-63 (2006).

160. Rudolph,C. *et al.* Methodological optimization of polyethylenimine (PEI)-based gene delivery to the lungs of mice via aerosol application. *J. Gene Med.* **7**, 59-66 (2005).

161. Densmore,C.L. Advances in noninvasive pulmonary gene therapy. *Curr. Drug Deliv.* **3**, 55-63 (2006).

162. Pollard,H. *et al.* Polyethylenimine but not cationic lipids promotes transgene delivery to the nucleus in mammalian cells. *J. Biol. Chem.* **273**, 7507-7511 (1998).

163. Kim,C.F. *et al.* Identification of bronchioalveolar stem cells in normal lung and lung cancer. *Cell* **121**, 823-835 (2005).

164. Dumstorf,C.A. *et al.* Participation of mouse DNA polymerase {iota} in strand-biased mutagenic bypass of UV photoproducts and suppression of skin cancer. *Proc. Natl. Acad. Sci. U. S. A* **103**, 18083-18088 (2006).

CURRICULM VITAE

Chad Aaron Dumstorf

Mailing Address:
3111 Lighthouse Dr.
Jeffersonville, IN 47130

Tel: (812) 284-4918
Mobile: (812) 989-5567
Email: Cadums01@louisville.edu

QUALIFICATIONS

- Expert in mammalian based molecular genetics and toxicology after environmental carcinogen exposure.
- Strong knowledge and environmental polycyclic hydrocarbon initiated mutagenesis (HPRT mutagenesis, cytotoxicity assays, and DNA sequence analysis).
- Expertise in skin and lung tumor models and *in vivo* gene delivery associated with UV light and environmental carcinogens.
- Experienced in biochemical, analytical, and molecular biological techniques data gathering, statistics, and analysis (real-time RT-PCR; Western-Blot; SDS-PAGE, gel electrophoresis; molecular cloning strategies; RNA/ DNA extraction, purification, and analysis; cellular transfections; reporter assays, laser capture microdissection, SV40 cell immortalization).
- Knowledgeable in Arcturus LCM to Affymetrix Microarray; PET Imaging; flow cytometry.
- Management of personnel, funds, and equipment associated with NIH, Center for Genetics and Molecular Medicine, and Kentucky Lung Cancer Research Board grants.
- Excellent ability to form relationships and collaboration between diverse individuals.
- Superb public speaking and presentation ability.

EDUCATION

2004-Present	University of Louisville, School of Medicine
	Degree: Doctor of Philosophy
	Major: Pharmacology and Toxicology
	Thesis: Participation of mouse dna polymerases Iota, Eta, and Rev1 in translesion synthesis of carcinogen induced DNA adducts and carcinogenesis

2002-2004	University of Louisville, School of Medicine
	Degree: Master of Science
	Major: Pharmacology and Toxicology
	Thesis: Mutagenesis of induced tumors in the murine lung

2001-2002	Indiana University
	Degree: Bachelor of General Studies
	Major: General Studies

1998-2001	Chaminade University
	Degree: Associate in Arts
	Major: Liberal Arts

WORK EXPERIENCE

| 2002-Present | University of Louisville |
| | • Graduate Research Fellow |

1996-2000	United States Navy
	• Petty Officer Third Class
	• Torpedo Man's Class A school

RESEARCH ACTIVITIES

Publications:

Chad A. Dumstorf, Alan Clark, Qingcong Lin, Grace E. Kissling, Tao Yuan, Raju Kucherlapati, W.Glenn McGregor, Tom Kunkle; Participation of Mouse DNA Polymerase Iota in Strand-biased Mutagenic Bypass of UV Photoproducts and Suppression of Skin Cancer. Proc. Nat. Acad. Sci. (USA) 103: 18083-18088, 2006

Elangovan Krishnan, Chad A. Dumstorf, Alfred B Jenson, William Glenn McGregor and Bodduluri Haribabu; Role of Leukotriene B4 Receptor-1 in Inflammation Promoted Lung Tumorigenesis. Manuscript in progress; Submission Cancer Research April, 2007

Chad A. Dumstorf, Suparna Mukhopadhyay, W. Glenn McGregor; Inhibition of lung tumorigenesis in A/J mice by REV1 inhibition. Manuscript in progress; Submission Cancer Research April, 2007

Oral presentations:

Chad A. Dumstorf; Mutagenesis: The Good, The Bad, and Polymerase Iota. Pharmacology and Toxicology Department Seminar, 2003

Chad A. Dumstorf; Alan Clark; Lin Qingcong; Tom Burke; Raju Kucherlapati; Tom Kunkel; Glenn McGregor; Participation of Mouse DNA polymerase Iota in Strand-biased Mutagenic Bypass of UV Photoproducts and Suppression of Skin Cancer. Midwest DNA Repair Symposium, Indianapolis, IN

Poster presentations:

Chad A. Dumstorf, Elangovan Krishnan, Haribabu Bodduluri, W. Glenn McGregor; Inflammation Enhances the Carcinogenic Potential of Mutagens in Murine Pulmonary Adenomas. Midwest DNA Repair Symposium, Lexington, KY, 2004

Chad A. Dumstorf, Elangovan Krishnan, Haribabu Bodduluri, W. Glenn McGregor; Inflammation Enhances Mutagenesis and Carcinogenesis in Murine Lungs. Research Louisville, 2004

Elangovan Krishnan, Chad A. Dumstorf, Alfred Bennet Jenson, William Glenn McGregor, Bodduluri Haribabu; Role of Leukotriene B4 Receptor Mediated Pulmonary Inflammation in Lung Cancer. James Graham Brown Cancer Retreat, 2005; Louisville, KY

Chad A. Dumstorf, Alan Clark, Lin Qingcong, Tom Burke, Raju Kucherlapati, Tom Kunkel, Glenn McGregor; Multiple DNA Polymerases are involved in Mutagenic Translesion Synthesis past UV Photoproducts In Vivo. Research Louisville, Louisville, KY 2005; Ohio Valley Society Of Toxicology 2005; Louisville, KY

Lyndsey Stallons, Chad A. Dumstorf, Elangovan Krishnan, Sabine Weigel, Wolfgang Zacharias, Bodduluri Hairababu, W. G. McGregor; Chronic inflammation Does not Alter Patterns of gene expression in Carcinogen-Initiated Lung Cancer. Research Louisville, Louisville, KY, 2005

Elangovan Krishnan, Chad A. Dumstorf, Alfred Jenson, W. Glenn McGregor, Haribabu Bodduluri; Leukotriene B4: At the Crossroads of Chronic Inflammation and Cancer. Research Louisville; 2005; Louisville, KY

Chad A. Dumstorf, Alan Clark, Lin Qingcong, Tom Burke, Raju Kucherlapati, Tom Kunkel, W. Glenn McGregor; Participation of Mouse DNA polymerase Iota in Strand-biased Mutagenic Bypass of UV Photoproducts and Suppression of Skin Cancer. Research Louisville;

Midwest DNA Repair Symposium, Indianapolis, IN; James Graham Brown Cancer Center Retreat, 2006

Elangovan Krishnan, Chad A. Dumstorf, Mian Mushtaq, Paramahamsa Maturu, Alfred Bennett Jenson, William Glenn McGregor, Haribabu Bodduluri, Role of Leukotriene B4 and its High Affinity Receptor BLT1 in Inflammation Promoted Lung Cancer. Research Louisville, 2006

W. Glenn McGregor, Tom Burke, Isacc Miller Chad Dumstorf; Cells from Skin Cancer-Prone Xeroderma Pigmentosum Variant Patients Have Greatly Reduced Mutant Frequencies Induced by the Environmental Carcinogen BPDE. Research Louisville; James Graham Brown Cancer Center Retreat, 2006

Elangovan Krishnan, Mian Mushtaq, Chad A. Dumstorf, Alfred Jenson, W.Glenn McGregor, Bodduluri Haribabu; Targeting Inflammation to Treat Cancers: Role of Leukotriene B4 Receptor-1 in Mouse Models of "Inflammation Promoted Cancers" and Familial Adenomatous Polyposis. James Graham Brown Cancer Center Retreat, 2006

HONORS AND ACHIEVMENTS

University of Louisville
- 1st Place Poster James Graham Brown Cancer Center Retreat, 2005
- 3rd Place Poster Research Louisville, 2006
- Honorable Mention Research Louisville, 2006

United States Navy
- Weapons Department Sailor of the Year
- Command Assessment Team
- Navy Achievement Medal
- Good Conduct Medal
- Honorable Discharge

Miscellaneous
- Eagle Scout, 1994
- PADI Divemaster, 1999

ADDITIONAL SKILLS

Computer knowledge:
    MS Office: Word, Excel, PowerPoint
    Adobe: Illustrator, Photoshop, Acrobat
    Data analysis software: Vector NTI, Chromas, Summit
    Statistical software: GraphPad Prism 4

Languages:
    English: fluent

REFERENCES

W. Glenn McGregor, M.D.
    Professor, Pharmacology and Toxicology, University of Louisville
    570 S. Preston St.
    Baxter Bldg. 1 Rm. 221A
    Louisville, KY 40212
    Tel: (502) 727-8270
    Email: wgmcgregor@louisville.edu

Haribabu Bodduluri, Ph.D.
    Professor of Microbiology
    University of Louisville
    570 S. Preston St.
    Baxter Bldg. 2 Rm. 119B
    Louisville, KY 40212
    Tel: (502) 852-7503
    Email: h0bodd01@louisville.edu

Victoria B. Kyle, D.V.M., M.S.
    Associate Professor, Research Resource Center
    511 S. Floyd St. Suite 120
    Louisville, KY 40202
    Tel: (502) 852-7051
    Email: victoria.kyle@louisville.edu